NASA TECHNICAL NOTE

NASA TN D-2465

NASA TN D-2465

C. 1

LOAN COPY: I
AFWL (V
KIRTLAND AI

0079554

TECH LIBRARY KAFB, NM

EFFECTS OF CONFIGURATION GEOMETRY ON THE TRANSONIC AERODYNAMIC CHARACTERISTICS OF CANARD AIRPLANE CONFIGURATIONS

by James A. Blackwell, Jr., and Thomas C. Kelly

Langley Research Center
Langley Station, Hampton, Va.

NATIONAL AERONAUTICS AND SPACE ADMINISTRATION • WASHINGTON, D. C. • SEPTEMBER 1964

TECH LIBRARY KAFB, NM

0079554

EFFECTS OF CONFIGURATION GEOMETRY ON THE TRANSONIC AERODYNAMIC CHARACTERISTICS OF CANARD AIRPLANE CONFIGURATIONS

By James A. Blackwell, Jr., and Thomas C. Kelly

Langley Research Center
Langley Station, Hampton, Va.

NATIONAL AERONAUTICS AND SPACE ADMINISTRATION

For sale by the Office of Technical Services, Department of Commerce,
Washington, D.C. 20230 -- Price $2.00

EFFECTS OF CONFIGURATION GEOMETRY

ON THE TRANSONIC AERODYNAMIC CHARACTERISTICS

OF CANARD AIRPLANE CONFIGURATIONS

By James A. Blackwell, Jr., and Thomas C. Kelly
Langley Research Center

SUMMARY

An investigation was conducted in the Langley 8-foot transonic pressure tunnel over a Mach number range of 0.40 to 1.20 to determine the effects of geometric variations on the aerodynamic characteristics of a canard airplane configuration. The geometric variations investigated were the effects of wing planform and vertical location, forebody deflection and length, and canard planform, deflection, and dihedral. The Reynolds number per foot of the tests varied with Mach number over a range of 1.69×10^6 to 3.11×10^6.

The results indicate that the trapezoidal-wing configuration exhibited higher lift-curve slopes, reduced drag due to lift, and increased lift-drag ratios relative to the delta-wing configuration throughout the Mach number range of the investigation; however, the delta-wing configuration exhibited a much lower transonic drag rise. At low Mach numbers, the trapezoidal-wing configuration experienced wing stall at lift coefficients for which no indication of stall was evident for the delta-wing configuration. Variations in vertical location of the trapezoidal-wing planform had little effect on the low-lift longitudinal aerodynamic characteristics. At large angles of attack, movement of the wing from the low to the high position was accompanied by an improvement in subsonic longitudinal aerodynamic characteristics, particularly a delay in the onset of wing stall.

Deflections of the fuselage forebody with the canards on or off provided significant increases in the zero-lift pitching moment with little or no increase in drag. Increasing the forebody length resulted in a decrease in static stability level and an increase in canard pitching effectiveness as a result of the increase in canard moment-arm length.

The trapezoidal canard exhibited a higher pitching effectiveness compared with the delta canard at low lift coefficients, but experienced earlier stall at the lower Mach numbers with an attendant loss in effectiveness.

Increases in the dihedral of the trapezoidal canard resulted in significant increases in longitudinal stability and a notable loss in directional stability.

INTRODUCTION

In current supersonic aircraft design, such as the commercial air transport, increased design Mach numbers have dictated the use of high wing sweep and rearward engine placement. These design concepts have had an effect in bringing about renewed interest in the use of a canard as a longitudinal control device. This interest stems largely from the fact that highly swept wings and rearward engine placement result in a rearward movement of the airplane center-of-gravity position which reduces the trim effectiveness of an aft-mounted horizontal tail and improves the canard trim effectiveness.

Extensive investigations (summarized in refs. 1 and 2) conducted at Langley and Ames Research Centers have added considerably to the information available on the effects of variations in canard, wing, and body arrangement. As a continuation of these studies, an investigation was conducted at transonic speeds to show the effects of wing planform and vertical location, forebody deflection and length, and canard planform, deflection, and dihedral. Many of the configurations used in this investigation are identical to those for which results at supersonic speeds are reported in reference 1.

The present investigation was performed in the Langley 8-foot transonic pressure tunnel over a Mach number range of 0.40 to 1.20. The Reynolds numbers per foot of the tests varied with Mach number over a range of 1.69×10^6 to 3.11×10^6. The angle-of-attack range varied from about -2° to 20°.

SYMBOLS

The results are presented as force and moment coefficients with the longitudinal aerodynamic data referred to the stability-axis system and the lateral aerodynamic data referred to the body-axis system. The reference center of moments was on the center line of the body at a point 12 inches forward of the base for all configurations. The symbols are defined as follows:

b	wing span, in.
$\bar{c}$	wing mean geometric chord, in.
HL	hinge line
$(L/D)_{max}$	maximum lift-drag ratio
M	free-stream Mach number
q	free-stream dynamic pressure, lb/sq ft
R	Reynolds number per foot
S	wing area, including fuselage intercept, sq ft

C_L	lift coefficient, $\frac{\text{Lift}}{qS}$
C_D	drag coefficient, $\frac{\text{Drag}}{qS}$
C_m	pitching-moment coefficient, $\frac{\text{Pitching moment}}{qS\bar{c}}$
C_l	rolling-moment coefficient, $\frac{\text{Rolling moment}}{qSb}$
C_n	yawing-moment coefficient, $\frac{\text{Yawing moment}}{qSb}$
C_Y	side-force coefficient, $\frac{\text{Side force}}{qS}$
α	angle of attack, measured relative to center line of rear of body, deg
β	angle of sideslip, measured relative to center line of body, deg
Γ_c	angle of canard dihedral, measured relative to horizontal plane containing center line of forebody, deg
δ_c	angle of canard deflection, measured relative to forebody center line, positive when trailing edge down, deg
δ_n	angle of forebody deflection, deg (see fig. 1(a))
$C_{D,o}$	drag coefficient at zero lift
$C_{m,o}$	pitching-moment coefficient at zero lift
C_{L_α}	lift-curve slope, measured at $C_L \approx 0$, $\frac{\partial C_L}{\partial \alpha}$ per deg
$C_{m_{C_L}}$	longitudinal-stability parameter, measured at $C_L \approx 0$, $\frac{\partial C_m}{\partial C_L}$ per deg
$C_{m_{\delta_c}}$	canard pitching effectiveness parameter, measured at $C_L \approx 0$ using $\delta_c = 0^\circ$ and 10°, $\frac{\partial C_m}{\partial \delta_c}$ per deg
C_{n_β}	directional-stability parameter, measured at $\beta \approx 0^\circ$, $\frac{\partial C_n}{\partial \beta}$ per deg
C_{l_β}	effective-dihedral parameter, measured at $\beta \approx 0^\circ$, $\frac{\partial C_l}{\partial \beta}$ per deg

C_{Y_β}	side-force parameter, measured at $\beta \approx 0^\circ$, $\frac{\partial C_Y}{\partial \beta}$ per deg	

Component designations:

B_4	basic forebody
B_5	extended forebody
W_3	trapezoidal wing
W_4	delta wing
C_2	trapezoidal canard
C_5	delta canard
V_2	vertical tail

MODELS AND APPARATUS

Details of the models are shown in figure 1, and the geometric characteristics are presented in table I. Coordinates of the bodies are given in table II. Photographs of the model are shown in figure 2. It should be noted that since many of the configuration components tested in this investigation were identical to those discussed in reference 1, the same nomenclature is used in this investigation. Variations in wing vertical position were possible as shown in figure 1(a). The various body lengths and forebody deflections (see fig. 1(a)) were obtained by using the same forebody and afterbody with cylindrical center-body adapters having different lengths or different angles. The canard hinge-line location was fixed with respect to the forebody and hence the canards moved with the forebody as the forebody deflection or body length varied. The canards were motor driven and the canard deflections were set by remote control. The dihedral angle of the canards was varied (fig. 1(d)) by interchanging sets of canards having different dihedral angles.

Force and moment measurements were made through the use of a six-component internal strain-gage balance. The model was mounted in the wind tunnel on a remote-controlled center-line sting.

TECHNIQUES AND TEST CONDITIONS

Range of Investigation

This investigation was conducted in the Langley 8-foot transonic pressure tunnel over a Mach number range of 0.40 to 1.20. The angle of attack varied generally from about -2° to 20° at zero sideslip. In addition, tests were conducted through a range of sideslip angles from about -2° to 10° for an angle of attack of 0° for the configuration used to determine the effects of canard dihedral. The variation of the test Reynolds number per foot with Mach number is shown in figure 3.

Corrections

The angles of attack and sideslip of the model have been corrected for deflection of the balance and sting under load and for tunnel flow angularity. Drag results have been adjusted to correspond to the condition of free-stream static pressure acting at the model base.

Transition Strips

The investigation was conducted with boundary-layer transition fixed. The transition strips were 0.10 inch wide and composed of No. 60 carborundum grains set in a plastic adhesive. The transition strips were located with the forward edges of the strips at 10 percent of the local chord behind the leading edge of the wings, canards, and vertical tail and 1.5 inches aft of the body nose.

PRESENTATION OF RESULTS

The results of this investigation have been reduced to coefficient and parameter form. The basic longitudinal aerodynamic data for all configurations are presented in figures 4 to 11 and summarized in figures 12 to 19. The basic lateral aerodynamic data for the configuration showing the effect of canard dihedral are presented in figure 20 and summarized in figure 21. To aid in the location of data, the following list is given:

	Figure
Effects of trapezoidal canard C_2 and trapezoidal-canard deflection on the longitudinal aerodynamic characteristics of $B_4W_3V_2$ midwing configuration. $\delta_n = 0^{\circ}$; $\Gamma_c = 0^{\circ}$	4
Effects of trapezoidal canard C_2 and trapezoidal-canard deflection on the longitudinal aerodynamic characteristics of $B_4W_4V_2$ midwing configuration. $\delta_n = 0^{\circ}$; $\Gamma_c = 0^{\circ}$	5
Effects of delta canard C_5 and delta-canard deflection on the longitudinal aerodynamic characteristics of $B_4W_4V_2$ midwing configuration. $\delta_n = 0^{\circ}$; $\Gamma_c = 0^{\circ}$	6
Effects of wing vertical location on the longitudinal aerodynamic characteristics of $B_4W_3C_2V_2$ configuration for canard deflection angles of 0° and 10°. $\delta_n = 0^{\circ}$; $\Gamma_c = 0^{\circ}$	7

DISCUSSION

Effects of Wing

Planform.- Some effects of wing planform on the longitudinal aerodynamic characteristics with canards on and off are summarized in figure 12 from data presented in figures 4 and 5 for midwing configurations having wings of equal area. A comparison of the effects of wing planform, canards on or off, indicates that the trapezoidal-wing configuration has considerably higher values of C_{L_α}, lower drag due to lift, and resultant higher values of $(L/D)_{max}$ than the delta-wing configuration throughout the Mach number range of the investigation. Similar results have been shown in references 3 and 4 on similar configurations up to a Mach number of approximately 2.2. Variations with Mach number of the drag coefficient at zero lift for the trapezoidal- and delta-wing configurations (fig. 12(b)) show little change at subsonic speeds, but above a Mach number of 0.90 there is a noticeable reduction in drag rise for the delta-wing configuration, a result of the combined favorable effects of higher wing sweep and lower wing thickness.

The trapezoidal- and delta-wing configurations, with canards on or off, are longitudinally stable throughout the Mach number range, for the chosen moment reference, as shown in figure 12. The larger change in $C_{m_{C_L}}$ with Mach number for the trapezoidal-wing configuration than for the delta-wing configuration results primarily from the differences in $\bar{c}$ for the two configurations. The actual physical variation in aerodynamic-center position is very nearly the same for both wing planforms; for example, between Mach numbers of 0.40 and 1.20 the aerodynamic-center shift amounted to approximately 1.70 inches and 1.68 inches for the trapezoidal- and delta-wing configurations with canards on, respectively.

In comparing lift curves for the configurations with the two wing planforms for canards off (figs. 4(a) and 5(a)), it is interesting to note the occurrence of wing stall for the trapezoidal-wing planform at Mach numbers of 0.40 to 0.90, at a lift coefficient of approximately 0.7; however, the lift curve for the delta-wing planform shows no indication of stalling up to the highest test angle of attack over the entire Mach number range. Addition of the canard ahead of the wing resulted in a slight improvement in the high-lift characteristics of the trapezoidal-wing configuration, but had little or no effect on the lift characteristics of the delta-wing configuration. (See figs. 4(a) and 5(a).) These variations are a probable result of the effects of the canard-induced downwash field noted for similar configurations in reference 5. Considerable improvement in the stall characteristics of the trapezoidal-wing planform may be realized, however, from use of leading-edge devices as indicated in references 6 and 7.

Vertical location.- The effects of wing vertical location on the longitudinal aerodynamic characteristics of a trapezoidal-wing configuration are presented in figure 7 and summarized in figure 13. The effects of wing vertical location on C_{L_α}, $C_{m_{C_L}}$, and $C_{m_{\delta_c}}$ are relatively small. The slightly higher $(L/D)_{max}$ obtained for the midwing configuration is due primarily to the lower minimum drag (fig. 7(c)) of the midwing configuration.

In figure 7, a comparison of the data for the three wing vertical locations shows that as the wing is moved from the low position to the high position there is a substantial improvement in the longitudinal aerodynamic characteristics at the higher angles of attack at subsonic speeds. This improvement is shown by an increase in lift, a decrease in drag, and an increase in linearity of the pitching-moment characteristics.

Effects of Forebody

Length.- The effects of forebody length on the longitudinal aerodynamic characteristics of a trapezoidal midwing configuration with canards on are shown in figure 8 and summarized in figure 14. Varying the forebody length had little effect on C_{L_α}; however, an increase in forebody length decreased the static stability level and increased the canard pitching effectiveness as a result of the increase in canard moment-arm length. The maximum value of lift-drag ratio is reduced (fig. 14(b)) as the body length is increased, primarily because of an increase in drag associated with the increase in wetted area and skin friction.

Deflection.- The effects of forebody deflection on the longitudinal aerodynamic characteristics of a trapezoidal-planform high-wing configuration with canards off are presented in figure 9 and summarized in figure 15. From figure 15 it can be seen that deflecting the forebody of this configuration has generally slight effects. The primary effect of forebody deflection appears in the pitching-moment coefficient at zero lift (fig. 15) where increases in forebody deflection are accompanied by slight increases in $C_{m,o}$.

Results for deflecting the forebody of the same high-wing configuration with canards on are presented in figure 10 and summarized in figure 16. It should be noted again that since canard deflection angles are measured relative to the forebody center line, increases in forebody deflection result in increases in canard angle relative to the free stream. The increases in canard angle, in turn, are the primary cause of the variations shown in figure 16. The increases in $C_{m,o}$ resulting from deflection of the forebody with canards on (where the canards are at an angle of 0° relative to the forebody center line) compared with the sum of the independent values of $C_{m,o}$ obtained by deflecting the forebody with canards off and by deflecting the canards (on an undeflected forebody) indicate that somewhat higher values of $C_{m,o}$ are obtained by deflecting the forebody with canards on. For example, at a Mach number of 1.20, deflecting the forebody 2° with the canards on results in a $C_{m,o}$ of 0.0390 (from $C_{m,o}$ plotted against M, fig. 16(b)) compared with 0.0296, a value which is the sum of the independent values obtained by deflecting the forebody 2° with canards off ($C_{m,o} = 0.0110$ from $C_{m,o}$ plotted against M, fig. 15) and by deflecting the canards 2^{o} for $\delta_n = 0^{o}$ $\left(\Delta C_m = 0.0186\right.$ from $C_{m_{\delta_c}}$ plotted against M, fig. 16(b)$\left.\right)$. The higher values of $C_{m,o}$ obtained by deflecting the forebody with canards on is a probable result of increased upwash over the forebody with increased forebody deflection and its effect upon canard lift.

Canard

Planform.- Some effects of canard planform on the longitudinal aerodynamic characteristics of delta midwing configurations having canards with either trapezoidal or delta planforms are summarized in figure 17 from data presented in figures 5 and 6. Addition of the trapezoidal or delta canards to the midwing $B_4W_4V_2$ configuration had a negligible effect on the lift-curve slope (fig. 17). The negligible effect of the canards on C_{L_α} is an apparent result of any increase in lift generated by the canards being canceled by a reduction in lift on the wing caused by flow interference from the canards. (See ref. 5.) The static stability level for the trapezoidal-canard configuration is lower than for the delta-canard configuration as a result of the relatively higher lift-curve slope of the trapezoidal canard surface. The effects of canard planform on the drag characteristics (fig. 17(b)) are generally slight.

Control effectiveness.- The pitching effectiveness of the trapezoidal and delta canards is presented in figures 4, 5, and 6 and summarized in figure 18. A comparison of the pitching effectiveness of the trapezoidal and delta canards on the delta-wing configuration (fig. 18) indicates that the trapezoidal canard has a notably higher $C_{m_{\delta_c}}$ as a result of its higher C_{L_α} at low lift coefficients; however, at the lower Mach numbers, the delta canard exhibits better pitching-moment characteristics at higher lift coefficients (compare figs. 5(c) and 6(c)) because of the trapezoidal canard stalling at relatively low combined deflections and angles of attack. Improvement in the use of the trapezoidal canard as a longitudinal-control device at subsonic speeds may be realized by the use of leading- and trailing-edge devices. (See refs. 6 and 7.)

If interference effects are neglected, the canard for a given angular deflection should be expected to provide equal incremental pitching moments for both the delta- and trapezoidal-wing planforms. The greater apparent pitching effectiveness of the trapezoidal canard for the trapezoidal-wing configuration than for the delta-wing configuration (fig. 18) is primarily a result of the variations in $\bar{c}$ as noted in the discussion of wing planform; however, some of the difference in canard pitching effectiveness for the two configurations undoubtedly is due to variations in canard-wing interference effects. These effects are probably similar to those discussed in references 5 and 8.

A comparison of the pitching-moment curves (figs. 4(c) and 5(c)) for configurations with canards on shows that at low subsonic speeds the trapezoidal canard stalls at a much lower lift coefficient for the delta-wing configuration than for the trapezoidal-wing configuration. This is due to the trapezoidal canard being at a higher angle of attack for the delta-wing configuration than for the trapezoidal-wing configuration at a given lift coefficient.

Dihedral.- The use of folding canard surfaces has been proposed as a means to control aerodynamic-center travel over the range from subsonic to supersonic flight speeds. In order to explore the effects of canard dihedral, the trapezoidal midwing configuration was tested with the dihedral angles of the trapezoidal canard at 0°, 30°, 60°, and 90°. (See fig. 1(d).) The effects of canard dihedral on the longitudinal aerodynamic characteristics are presented in figure 11 and summarized in figure 19. From figure 19 it is apparent that the effects of canard dihedral on C_{L_α}, $(L/D)_{max}$, and $C_{D,o}$ are generally small and involve slight decreases in C_{L_α} and $(L/D)_{max}$ and a slight increase in $C_{D,o}$ as canard dihedral increases. The main effect of increasing canard dihedral angle is to increase the stability level, as would be expected, by an amount that remains fairly constant over the Mach number range.

The lateral and directional aerodynamic characteristics of trapezoidal midwing configurations with trapezoidal-canard dihedral angles of 0° and 90° are presented in figure 20 and summarized in figure 21. Both configurations possess positive effective dihedral $\left(-C_{l_\beta}\right)$ and are directionally stable throughout the Mach number range at $\alpha = 0^\circ$. Comparing the results for the configuration with the canard dihedral angle of 90° with those for the configuration with the canard dihedral angle of 0° indicates that there is a substantial decrease in the lateral stability, a slight increase in C_{Y_β} (more negative), and a notable reduction in C_{n_β} (approximately 40 percent) for the canard dihedral angle of 90° as would be expected.

CONCLUSIONS

An investigation has been conducted at transonic speeds to determine the effects on the aerodynamic characteristics of canard airplane configurations of variations in wing planform and vertical location, forebody deflection and length, and canard planform, deflection, and dihedral. The results of the investigation indicate the following conclusions:

1. Throughout the Mach number range of the investigation, the trapezoidal-wing configuration exhibited higher lift-curve slopes, reduced drag due to lift, and increased lift-drag ratios in comparison with the delta-wing configuration; however, the delta-wing configuration exhibited a much lower transonic drag rise. At low Mach numbers, the trapezoidal-wing configuration experienced wing stall at lift coefficients for which no indication of stall was evident for the delta-wing configuration.

2. Variations in vertical location of the trapezoidal planform-wing had little effect on the low-lift longitudinal aerodynamic characteristics. At large angles of attack, movement of the wing from the low to high position was accompanied by an improvement in subsonic longitudinal aerodynamic characteristics, particularly a delay in the onset of wing stall.

3. Deflections of the fuselage forebody with canards on or off for the trapezoidal-wing configuration provided increases in the zero-lift pitching moment with little or no increase in drag. Increasing the forebody length of the trapezoidal-wing configuration resulted in a decrease in static stability level and an increase in canard pitching effectiveness as a result of the increase in canard moment-arm length.

4. The trapezoidal canard exhibited a higher pitching effectiveness compared with the delta canard on the delta-wing configuration at low lift coefficients, but experienced earlier stall at the lower Mach numbers with attendant loss in effectiveness.

5. Increases in the dihedral of the trapezoidal canard on the trapezoidal-wing configuration resulted in significant increases in longitudinal stability and a notable loss in directional stability.

Langley Research Center,
National Aeronautics and Space Administration,
Langley Station, Hampton, Va., June 25, 1964.

REFERENCES

1. Spearman, M. Leroy, and Driver, Cornelius: Some Factors Affecting the Stability and Performance Characteristics of Canard Aircraft Configurations. NACA RM L58D16, 1958.

2. Hall, Charles F., and Boyd, John W.: Effects of Canards on Airplane Performance and Stability. NACA RM A58D24, 1958.

3. Peterson, Victor L., and Boyd, John W.: Static Stability and Control of Canard Configurations at Mach Numbers From 0.70 to 2.22 - Longitudinal Characteristics of an Unswept Wing and Canard. NACA RM A57K27, 1958.

4. Boyd, John W., and Peterson, Victor L.: Static Stability and Control of Canard Configurations at Mach Numbers From 0.70 to 2.22 - Triangular Wing and Canard on an Extended Body. NACA RM A57K14, 1958.

5. Spencer, Bernard, Jr., and Sleeman, William C., Jr.: Low-Speed Longitudinal Characteristics of an Airplane Configuration Including Effects of Canard and Wing Trailing-Edge Flap Controls in Combination. NASA TN D-1397, 1962. (Supersedes NASA MEMO 4-22-59L.)

6. Spencer, Bernard, Jr.: Effects of Canard Planform and Wing-Leading-Edge Modification on Low-Speed Longitudinal Aerodynamic Characteristics of a Canard Airplane Configuration. NASA TN D-958, 1961.

7. Spencer, Bernard, Jr.: Low-Speed Aerodynamic Characteristics of a Canard Airplane Configuration Having Split Flaps Located Ahead of the Wing Trailing Edge and Leading- and Trailing-Edge Flaps on the Canard Control. NASA TN D-1245, 1962.

8. Driver, Cornelius: Longitudinal and Lateral Stability and Control Characteristics of Various Combinations of the Component Parts of Two Canard Airplane Configurations at Mach Numbers of 1.41 and 2.01. NASA MEMO 10-1-58L, 1958.

TABLE I.- GEOMETRIC CHARACTERISTICS OF MODEL

	B_4	B_5
Body:		
Maximum diameter, in.	3.33	3.33
Length, in.	37.00	41.50
Base area, sq in.	8.71	8.71
Fineness ratio	11.10	12.50

	W_3	W_4
Wing:		
Span, in.	24.00	16.72
Root chord at body center line, in.	12.80	22.97
Tip chord, in.	3.20	0
Area, including intercept, sq in.	192.00	192.00
Aspect ratio	3.00	1.46
Taper ratio	0.25	0.00
Mean geometric chord, in.	8.96	15.31
Sweepback angle of leading edge	$30^{\circ}58'$	70°
Thickness, percent chord	4.0	2.5
Airfoil section	Circular arc	Hexagonal

	C_2	C_5
Canard:		
Area, exposed, sq in.	13.59	14.44
Ratio of exposed area to wing area	0.071	0.075
Area, including intercept, sq in.	24.90	31.20
Airfoil section	Hexagonal	Hexagonal
Maximum thickness, in.	0.188	0.313
Sweepback angle of leading edge	38.6°	70°
Span, in.	6.60	6.74
Mean geometric chord, in.	4.02	6.17
Hinge-line location, percent chord	50.70	42.20

	V_2
Vertical tail:	
Area, exposed, sq in.	23.46
Airfoil section	Wedge plate
Maximum thickness, in.	0.188
Sweepback angle of leading edge	60°
Span, exposed, in.	5.10
Aspect ratio	1.11
Taper ratio	0.314

TABLE II.- COORDINATES FOR BODIES B_4 AND B_5

Body station, in.	Radius, in.
Parabolic forebodies, B_4 and B_5	
0	0
.297	.076
.627	.156
.956	.233
1.285	.307
1.615	.378
1.945	.445
2.275	.509
2.605	.573
2.936	.627
3.267	.682
3.598	.732
3.929	.780
4.260	.824
4.592	.865
4.923	.903
5.255	.940
5.587	.968
5.920	.996
6.252	1.020
6.583	1.042
Conical frustum forebodies, B_4 and B_5	
6.583	1.042
17.750	1.667
Cylindrical afterbody, B_4	
17.750	1.667
37.000	1.667
Cylindrical afterbody, B_5	
17.750	1.667
41.500	1.667

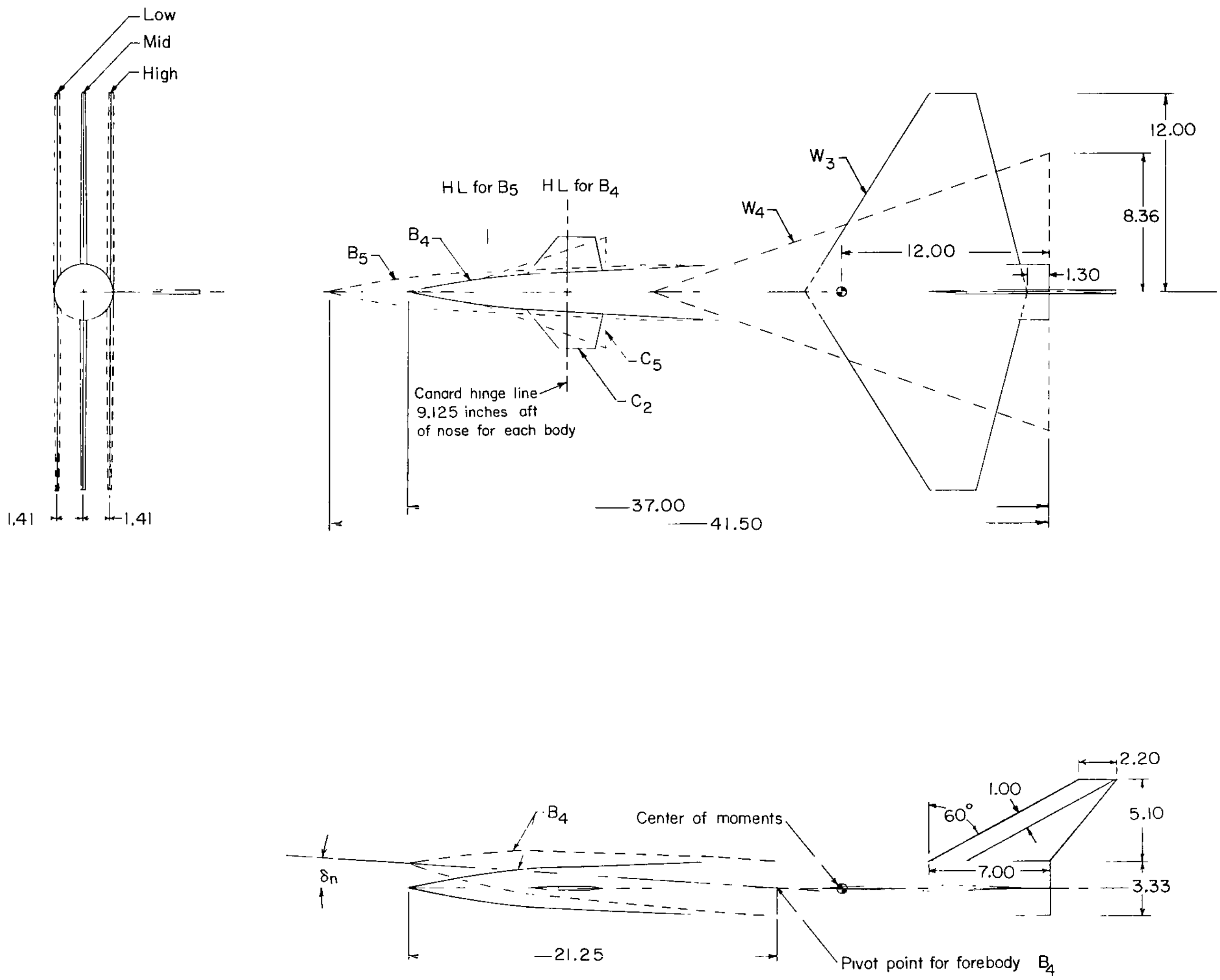

(a) Three-view drawing of general arrangement.

Figure 1.- Details of model. All dimensions are in inches unless otherwise noted.

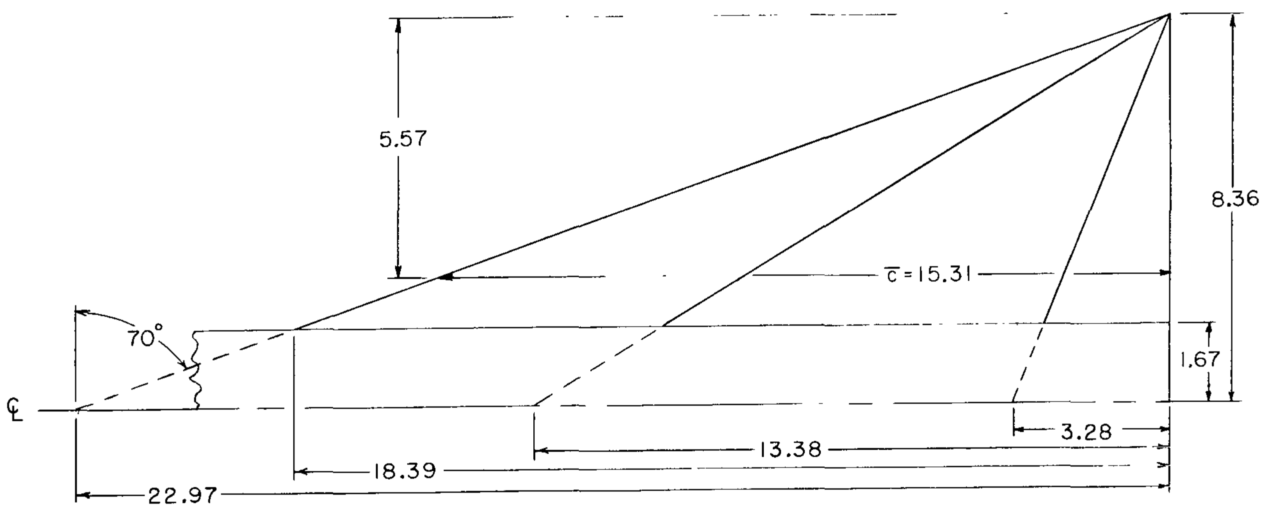

Delta wing W_4

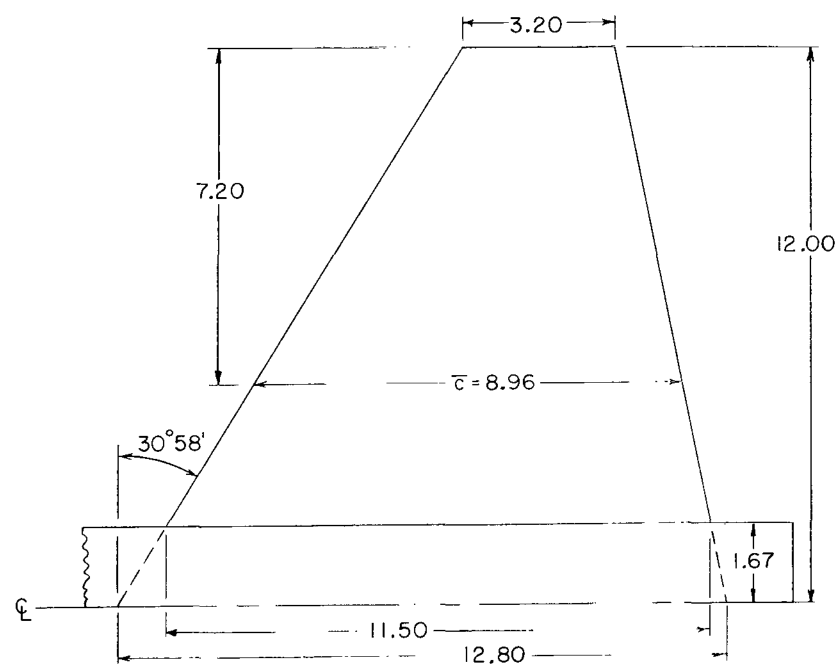

Trapezoidal wing W_3

(b) Details of wings.

Figure 1.- Continued.

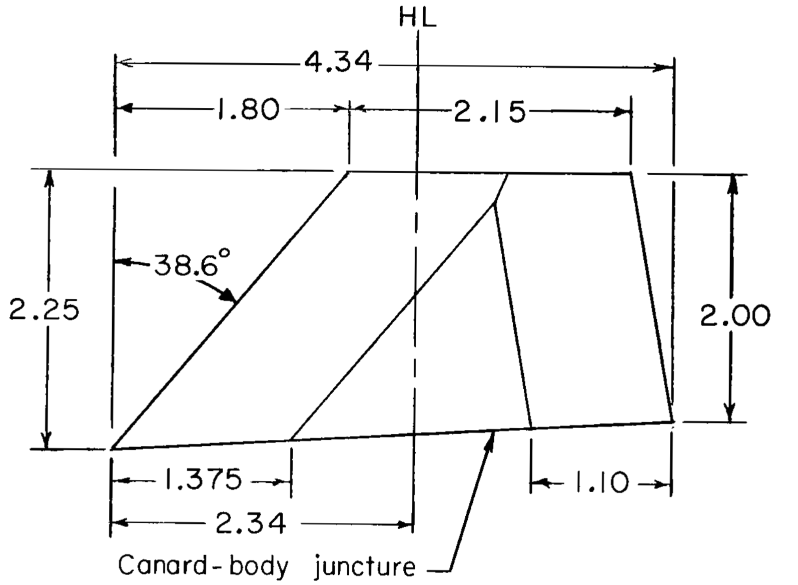

Trapezoidal canard C_2

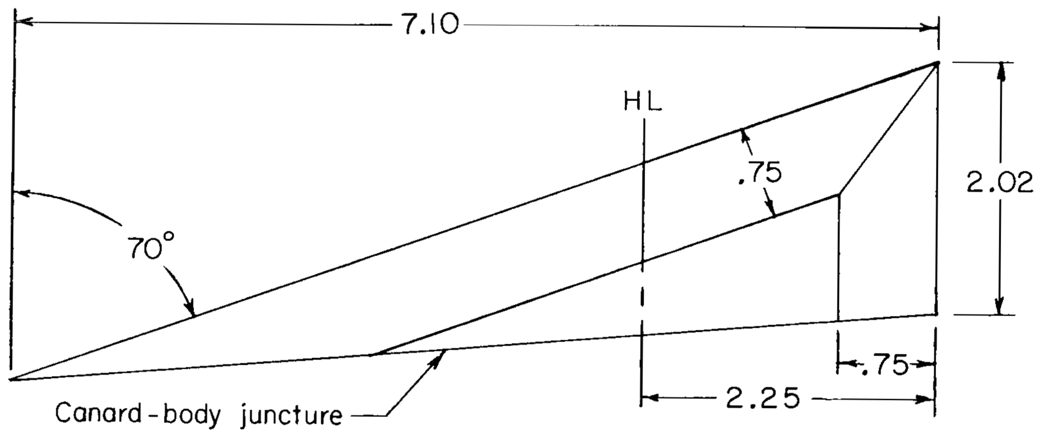

Delta canard C_5

(c) Details of canard planforms.

Figure 1.- Continued.

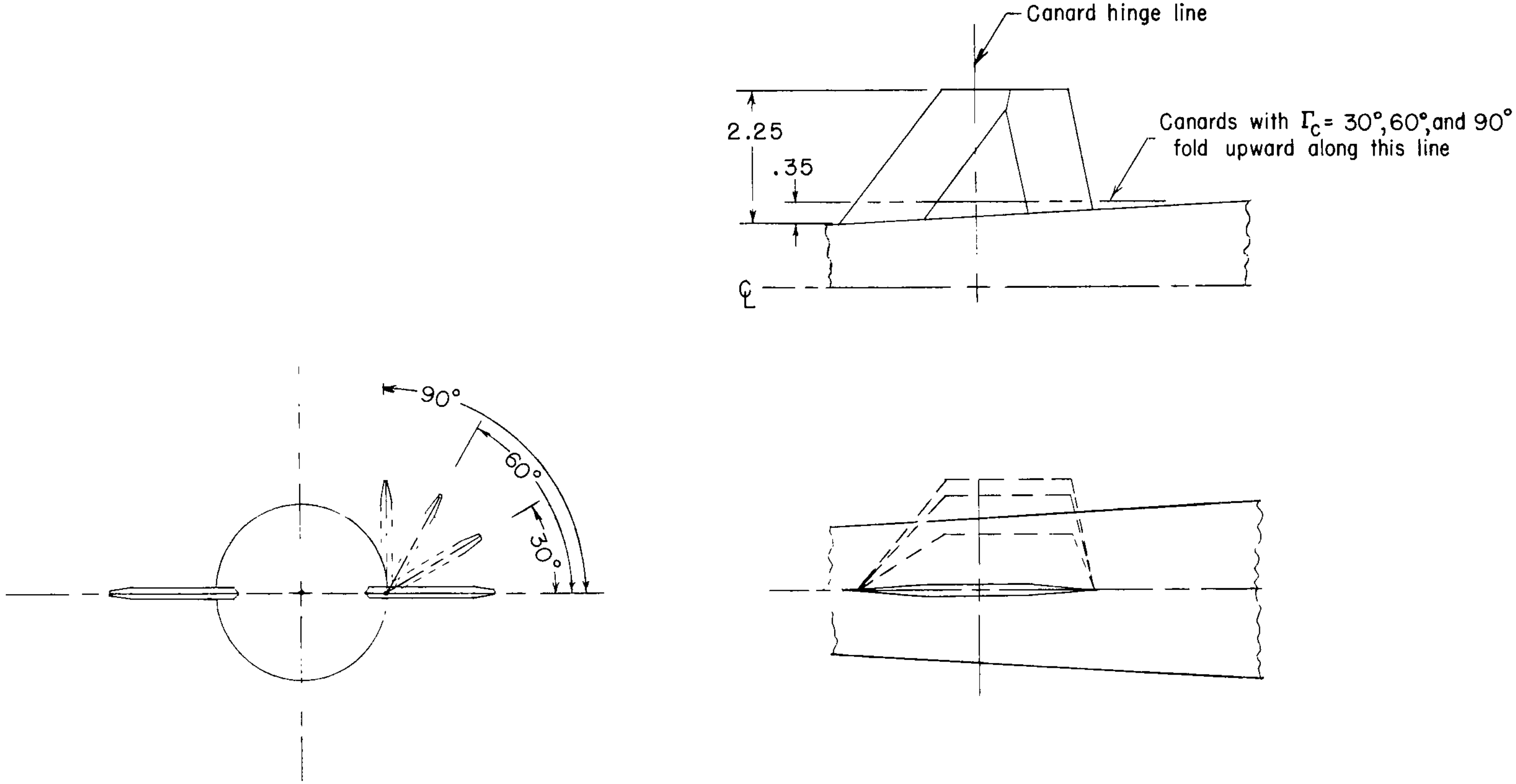

(d) Dihedral of canard.

Figure 1.- Concluded.

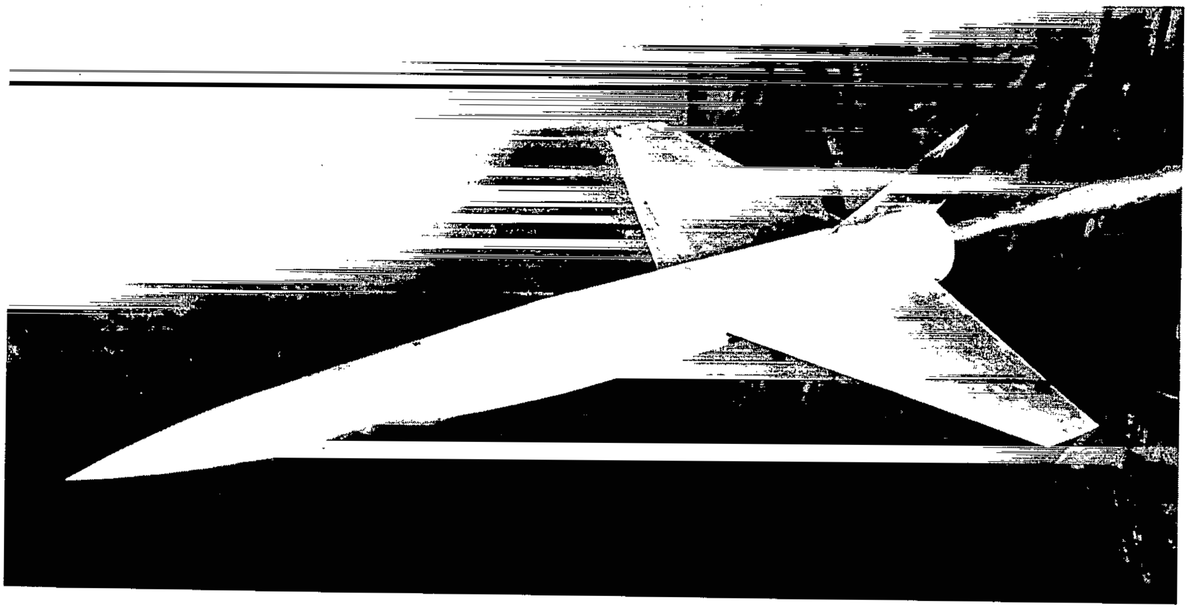

(a) Configuration $B_4W_3C_2V_2$ with midwing. L-58-323a

(b) Configuration $B_4W_4C_2V_2$ with midwing. L-58-325a

Figure 2.- Photographs of model.

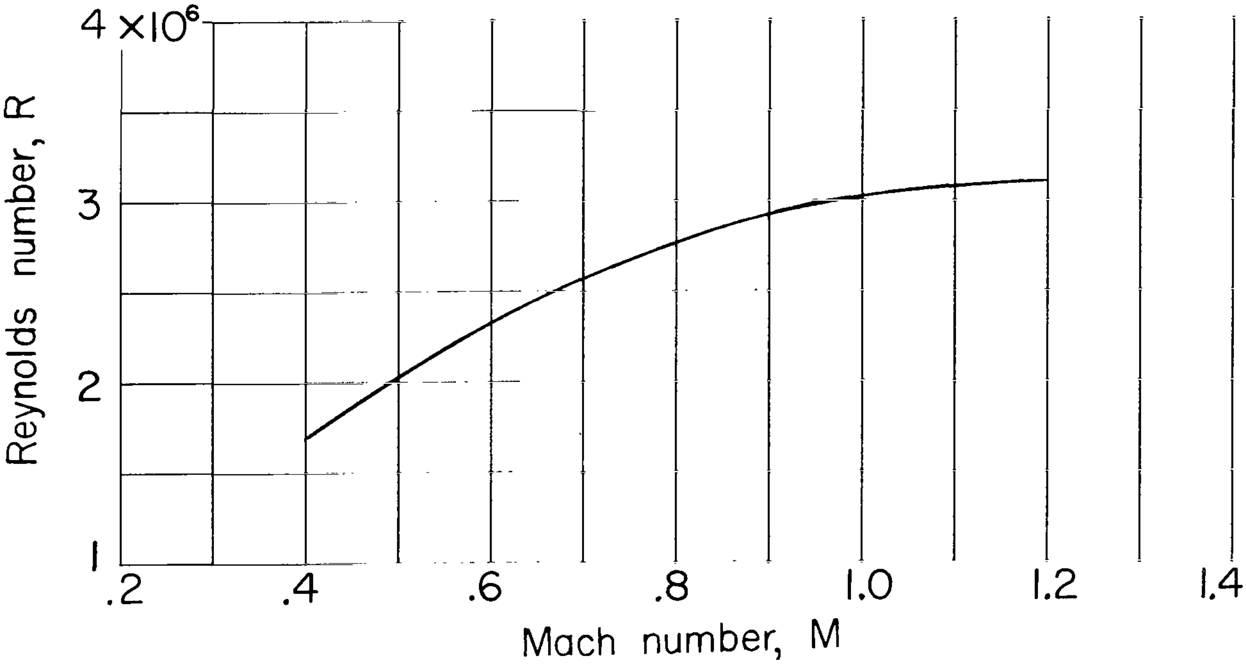

Figure 3.- Variation with Mach number of test Reynolds number per foot.

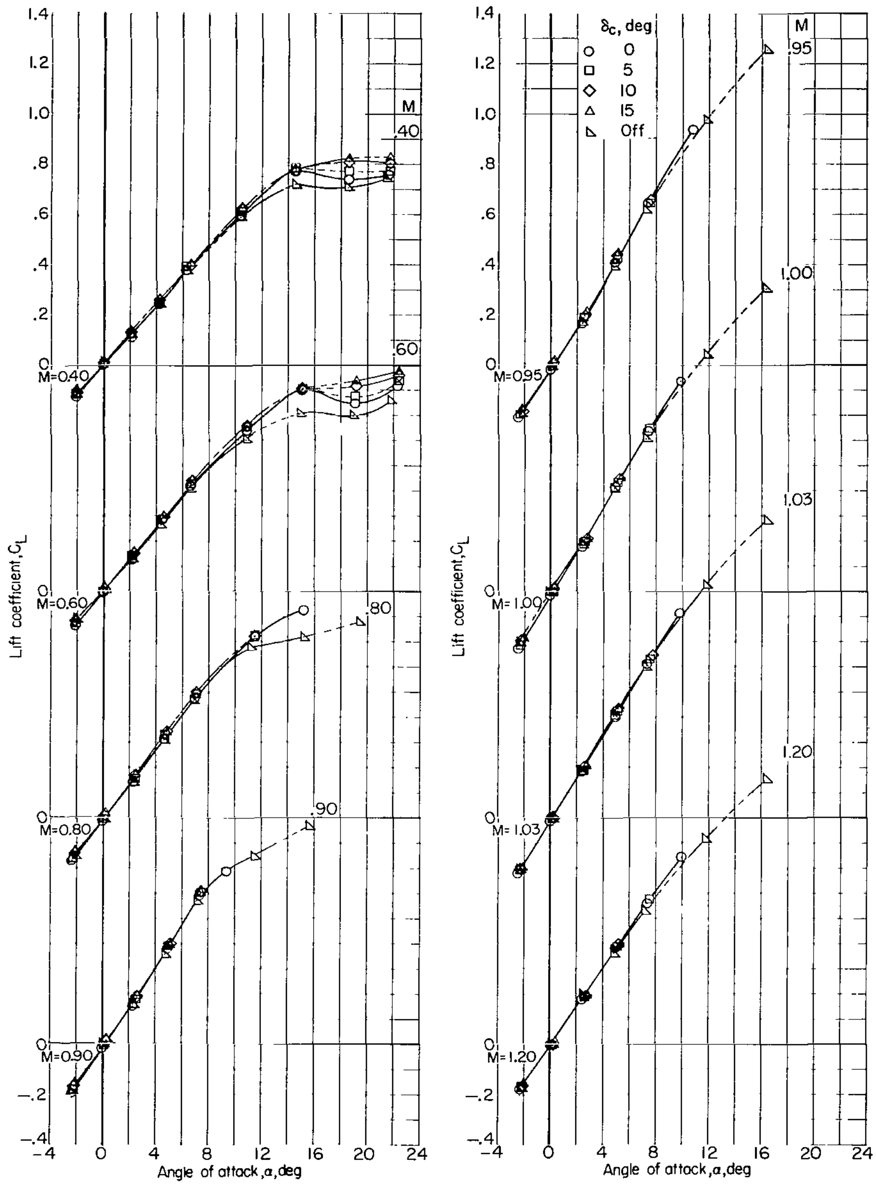

(a) Lift coefficient plotted against angle of attack.

Figure 4.- Effects of trapezoidal canard C_2 and trapezoidal-canard deflection on the longitudinal aerodynamic characteristics of $B_4W_3V_2$ midwing configuration. $\delta_n = 0^{\circ}$; $\Gamma_c = 0^{\circ}$.

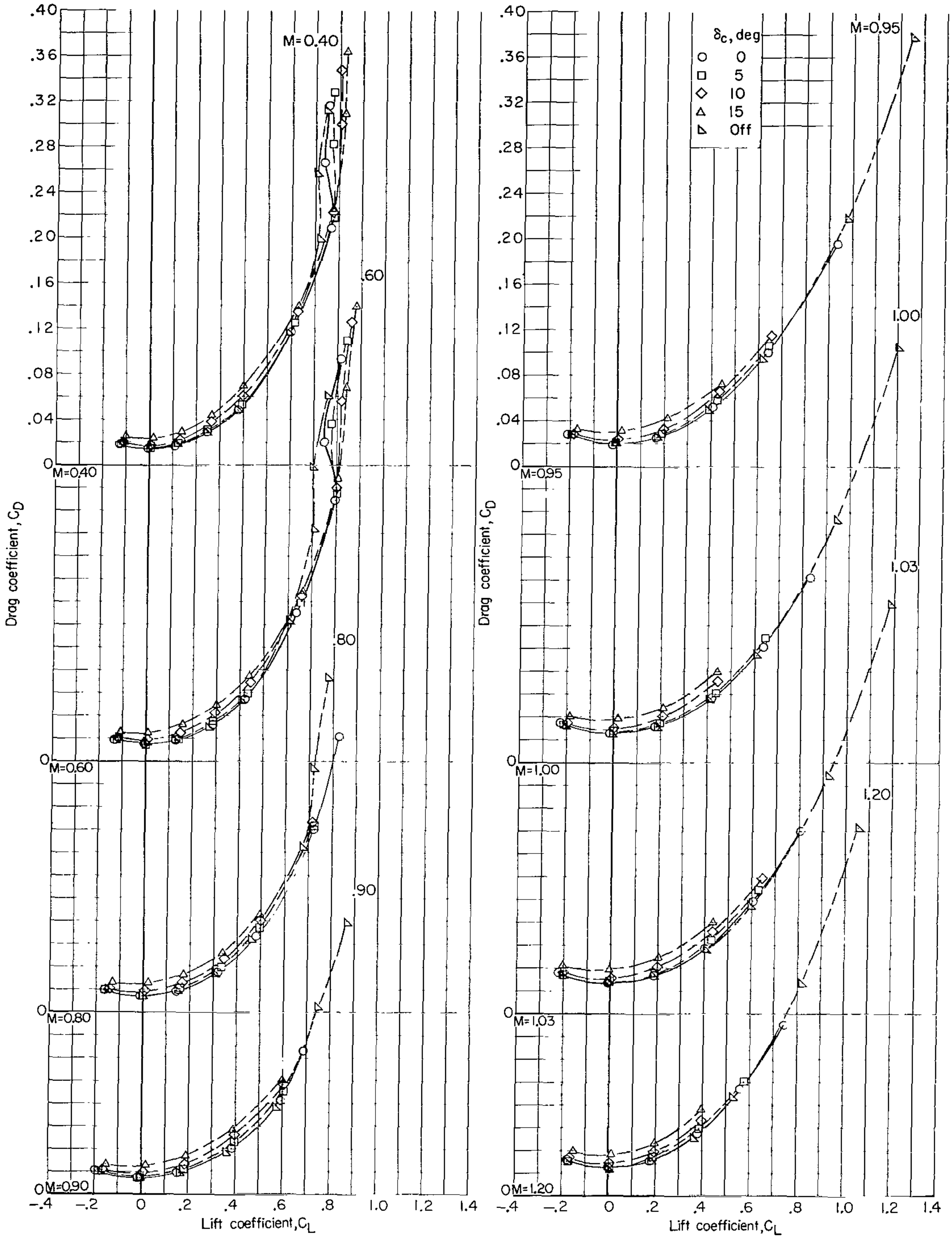

(b) Drag coefficient plotted against lift coefficient.

Figure 4.- Continued.

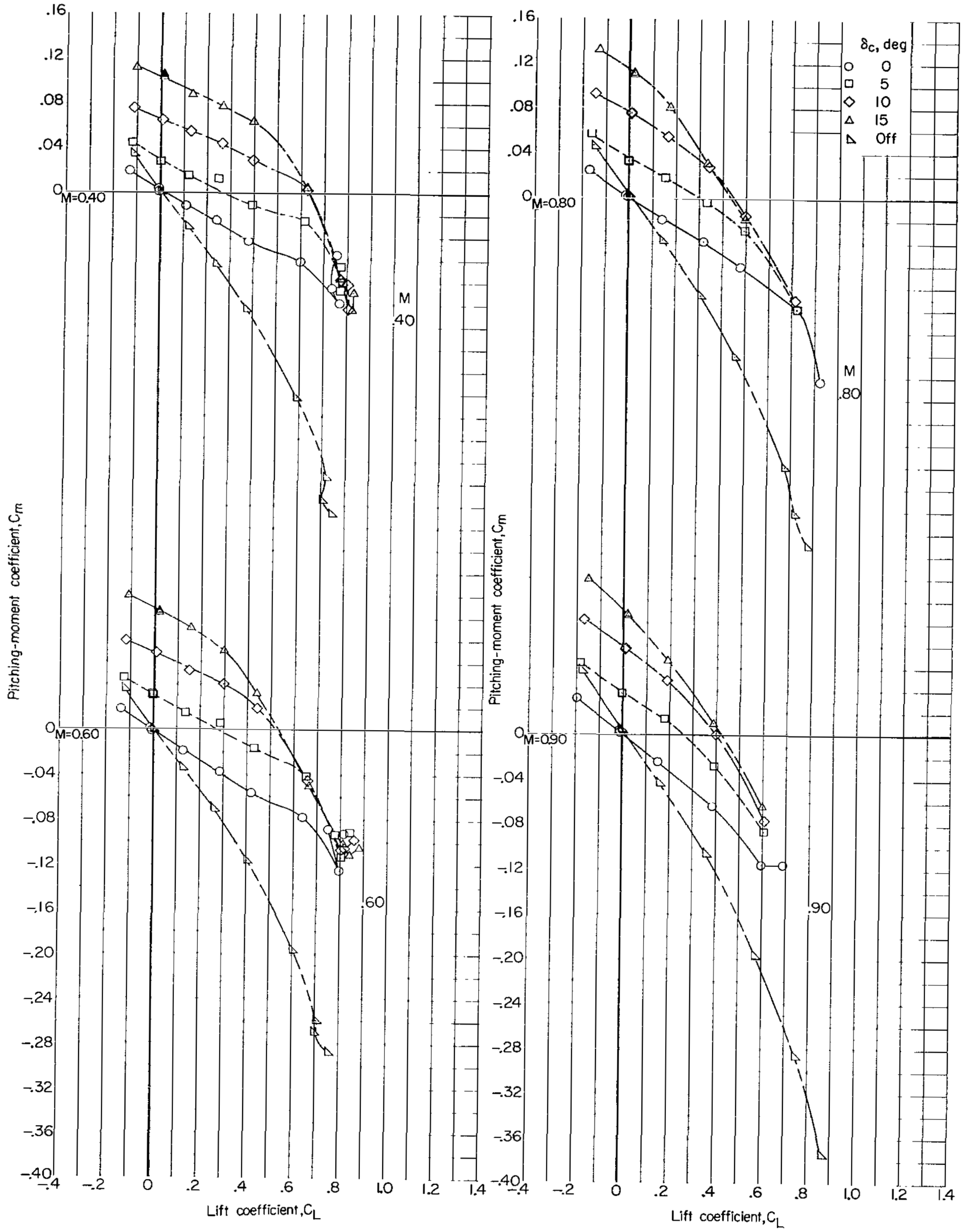

(c) Pitching-moment coefficient plotted against lift coefficient.

Figure 4.- Continued.

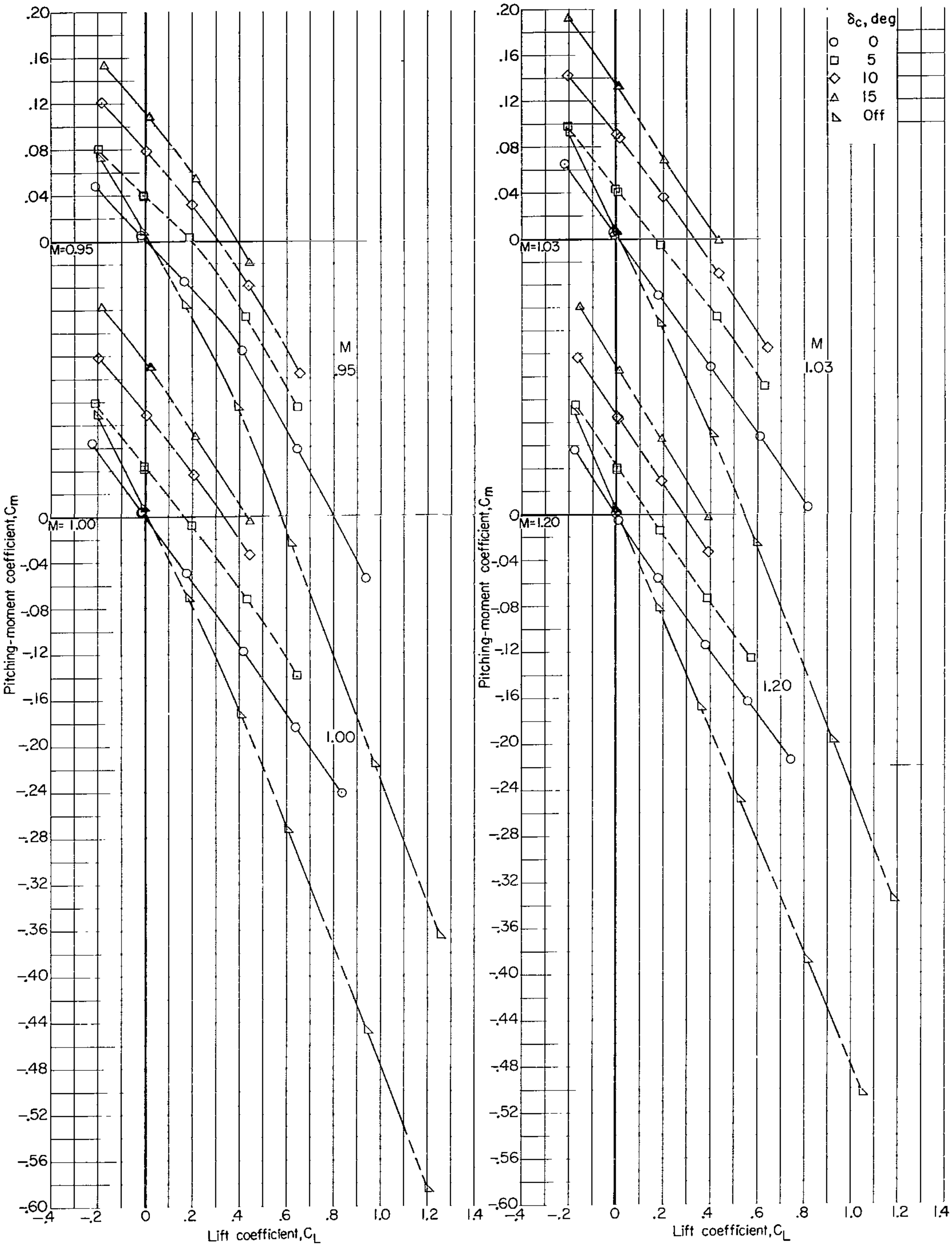

(c) Pitching-moment coefficient plotted against lift coefficient. Concluded.

Figure 4.- Concluded.

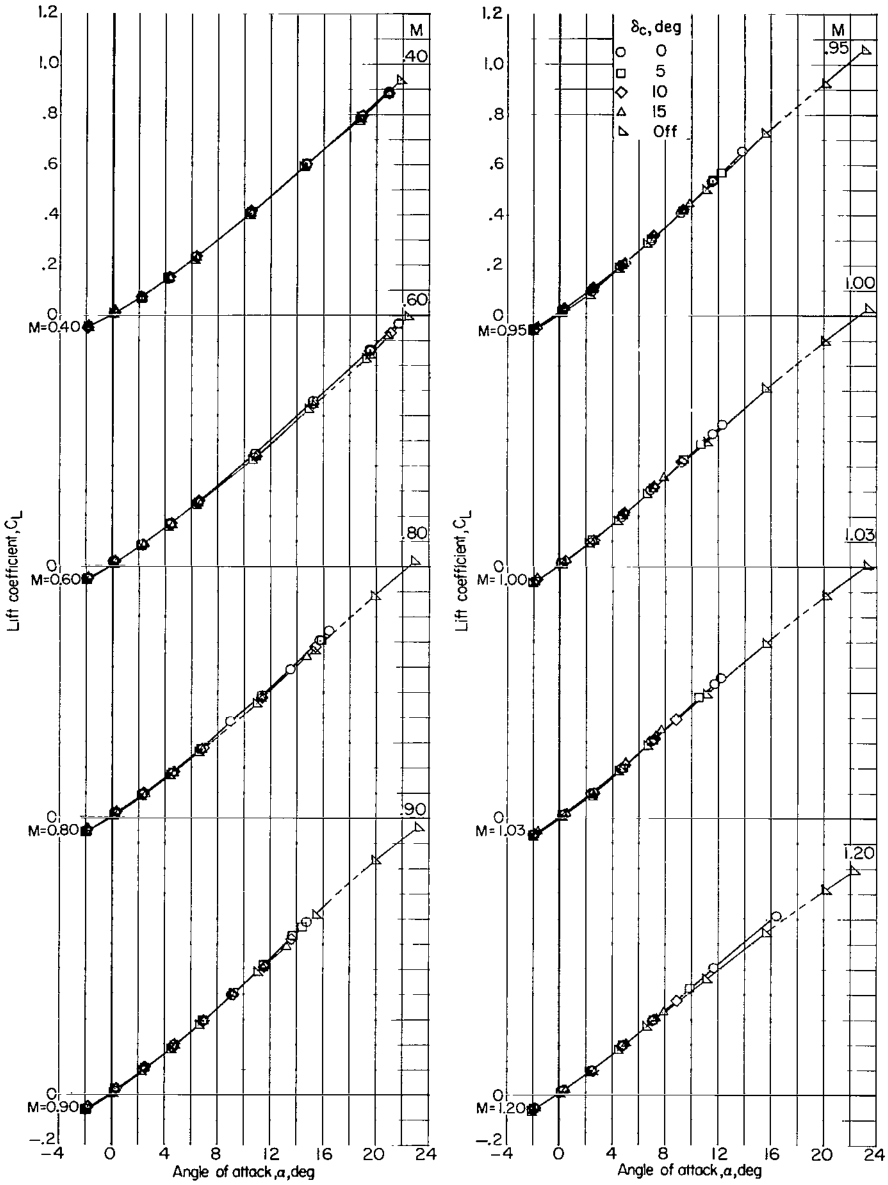

(a) Lift coefficient plotted against angle of attack.

Figure 5.- Effects of trapezoidal canard C_2 and trapezoidal-canard deflection on the longitudinal aerodynamic characteristics of $B_4W_4V_2$ midwing configuration. $\delta_n = 0^{\circ}$; $\Gamma_c = 0^{\circ}$.

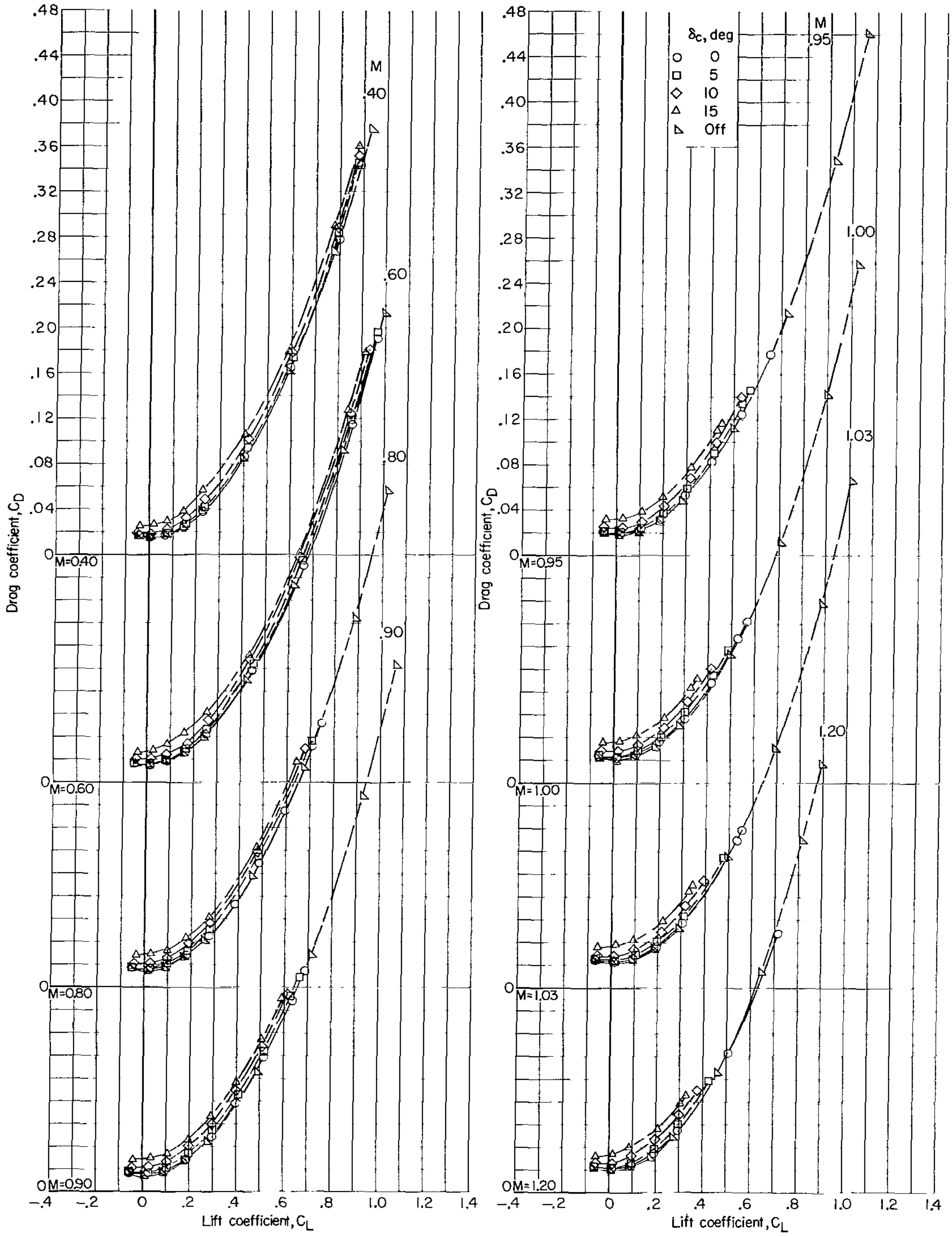

(b) Drag coefficient plotted against lift coefficient.

Figure 5.- Continued.

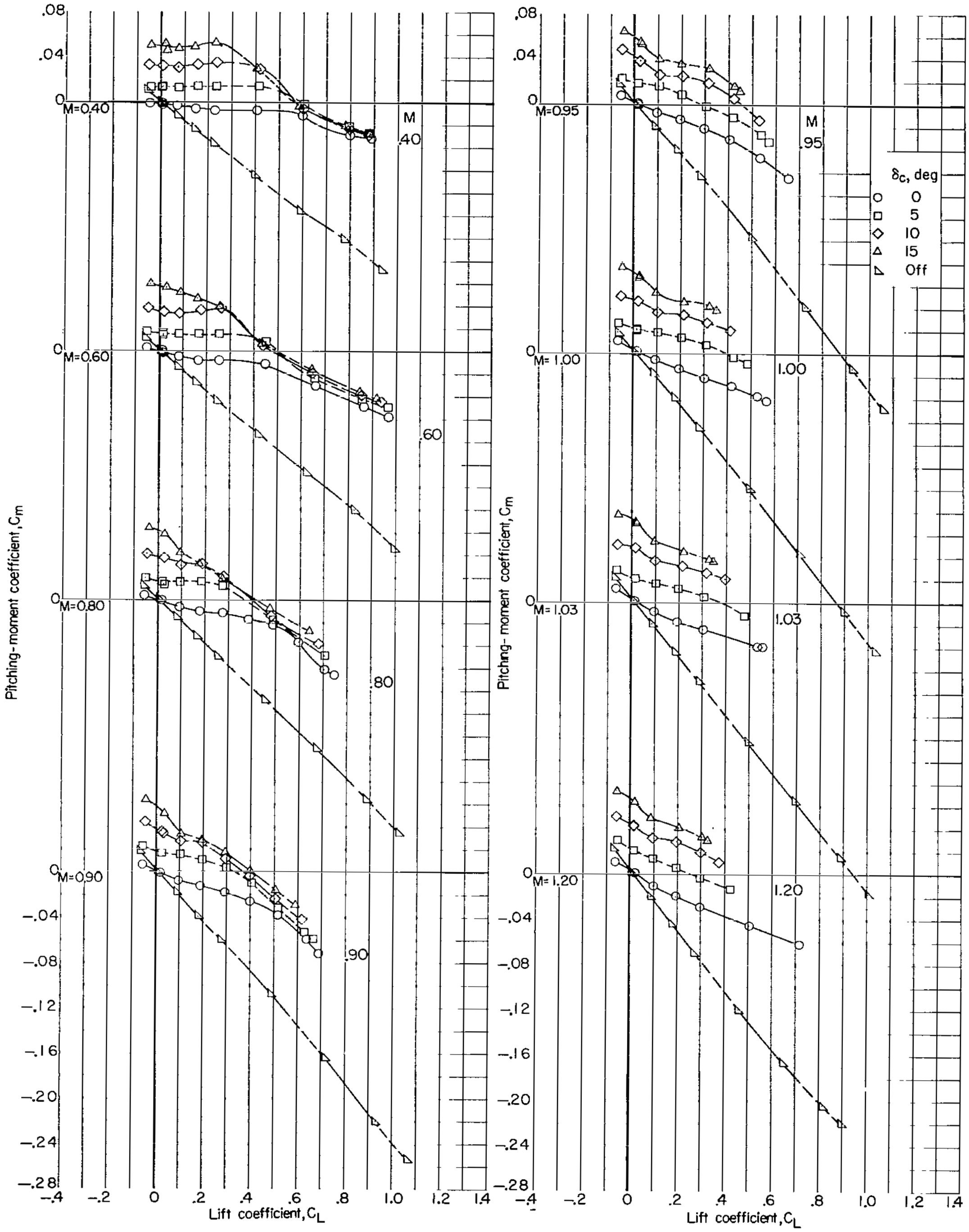

(c) Pitching-moment coefficient plotted against lift coefficient.

Figure 5.- Concluded.

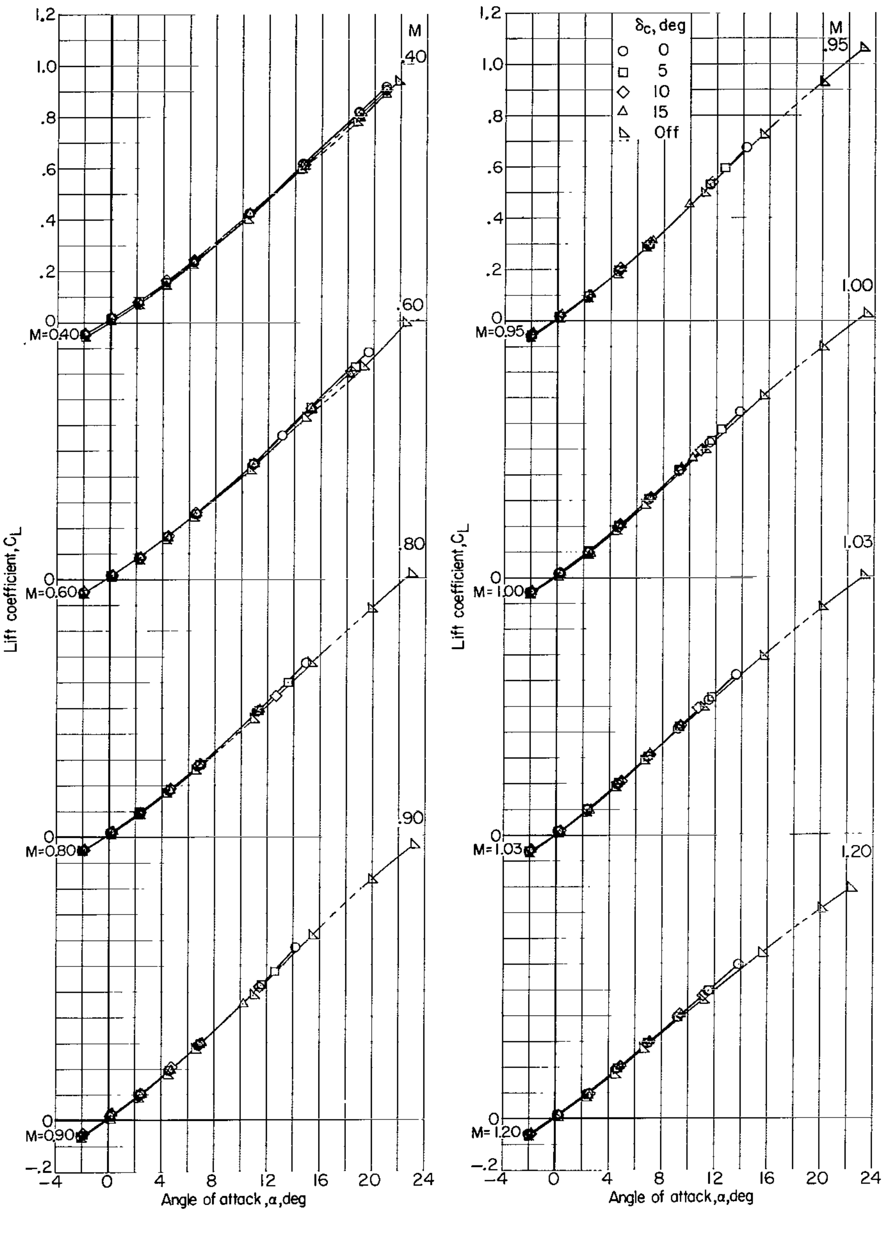

(a) Lift coefficient plotted against angle of attack.

Figure 6.- Effects of delta canard C_5 and delta-canard deflection on the longitudinal aerodynamic characteristics of $B_4W_4V_2$ midwing configuration. $\delta_n = 0^{\circ}$; $\Gamma_c = 0^{\circ}$.

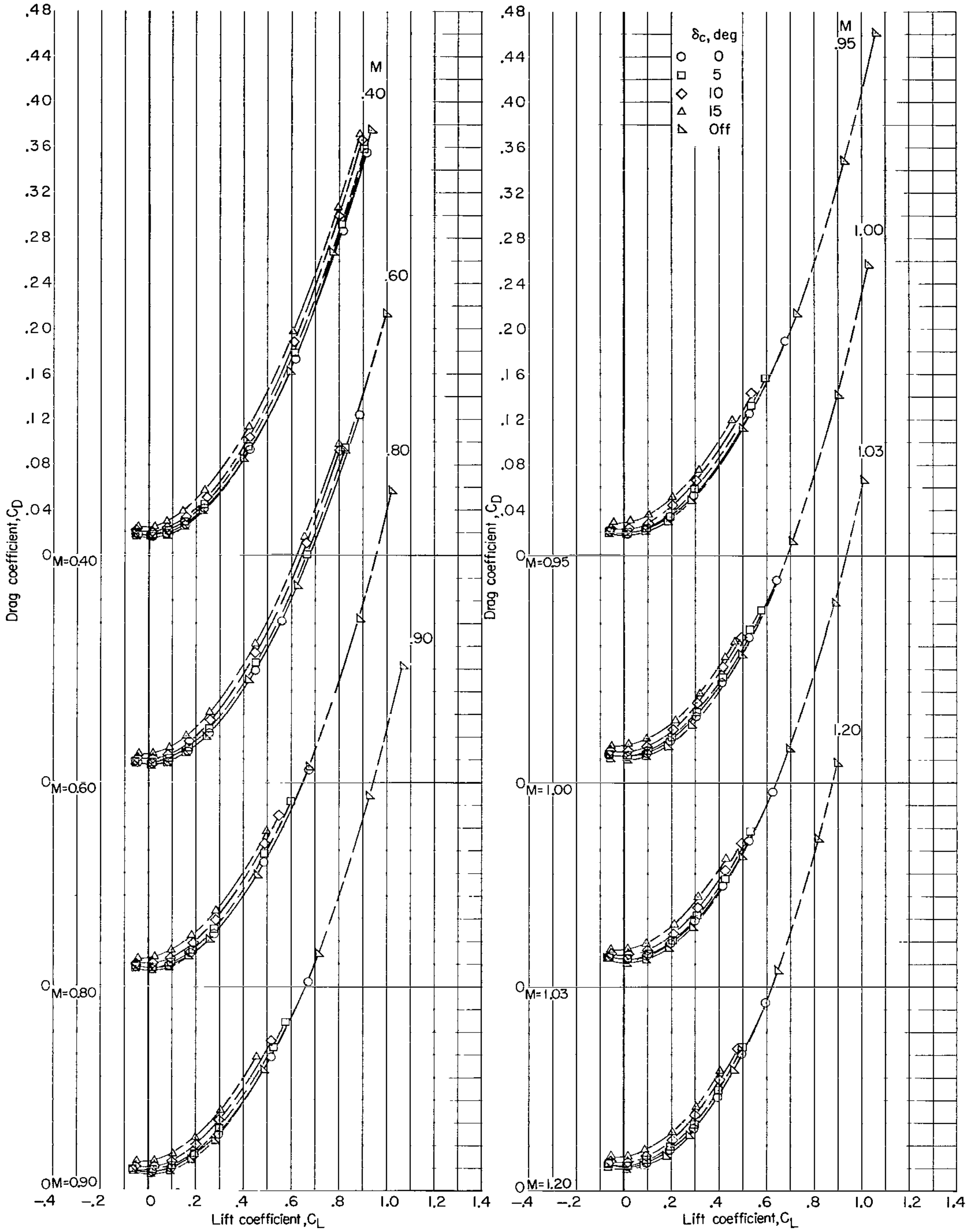

(b) Drag coefficient plotted against lift coefficient.

Figure 6.- Continued.

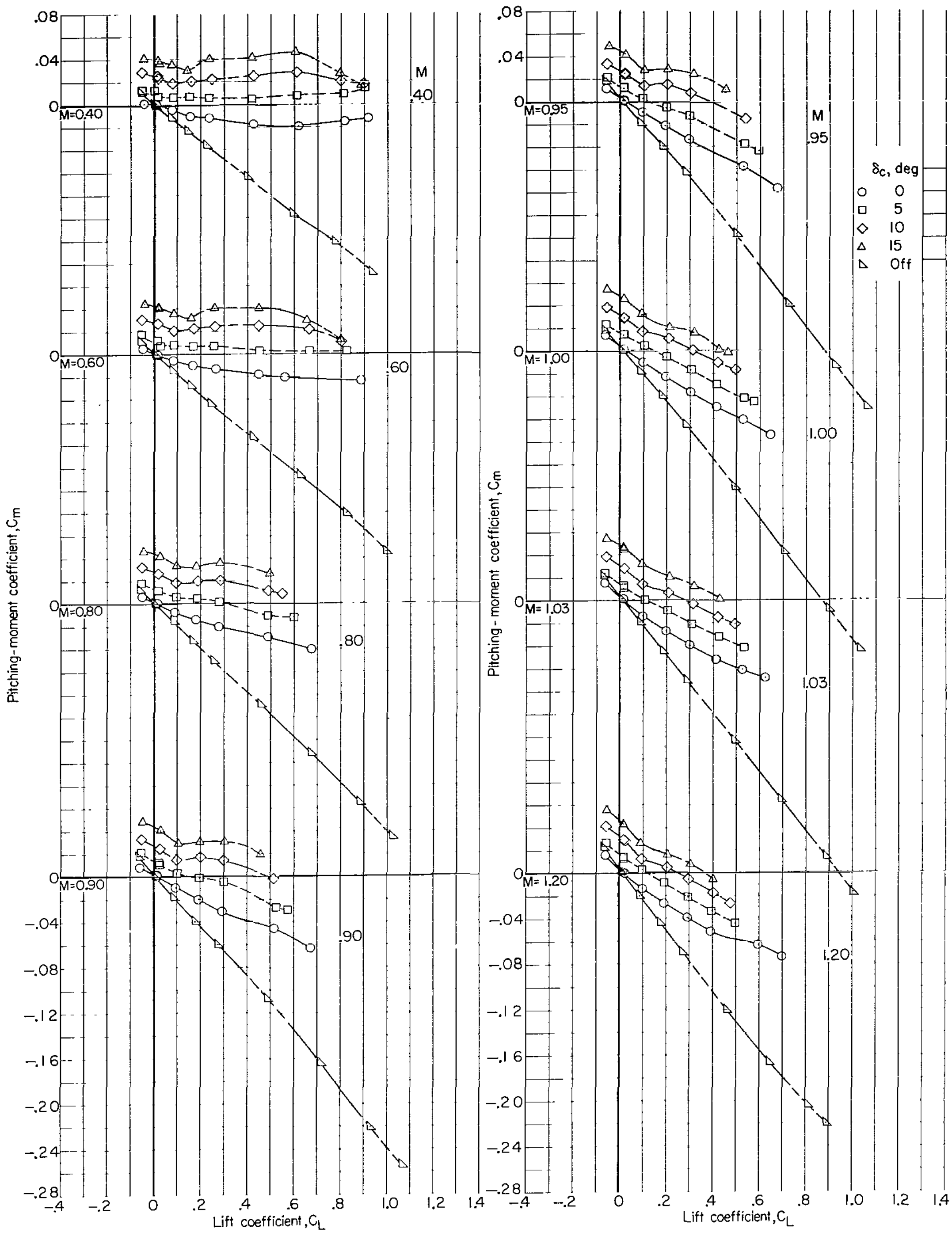

(c) Pitching-moment coefficient plotted against lift coefficient.

Figure 6.- Concluded.

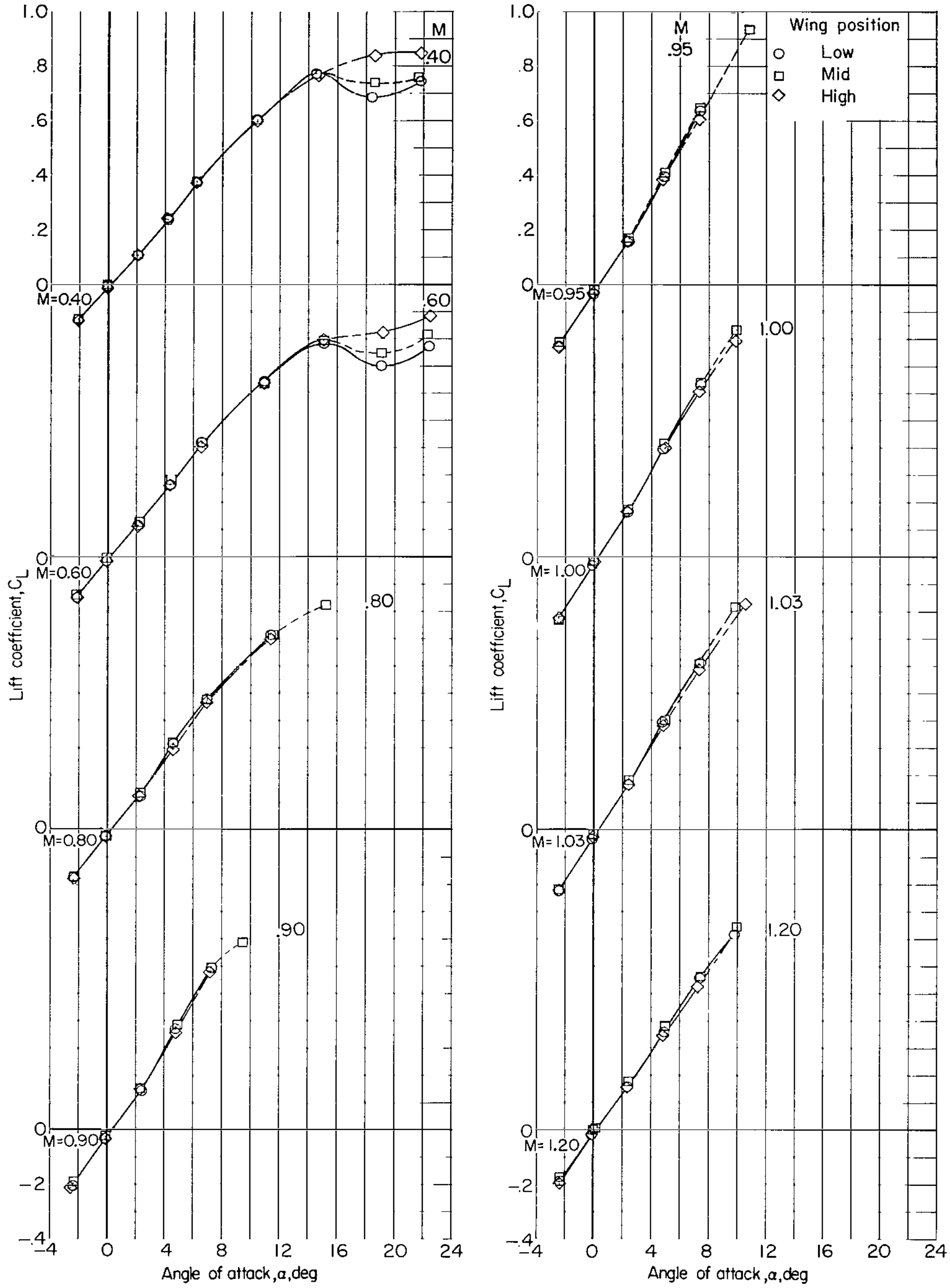

(a) Lift coefficient plotted against angle of attack. $\delta_c = 0^{\circ}$.

Figure 7.- Effects of wing vertical location on longitudinal aerodynamic characteristics of $B_4W_3C_2V_2$ configuration for canard deflection angles of 0° and 10°. $\delta_n = 0^{\circ}$; $\Gamma_c = 0^{\circ}$.

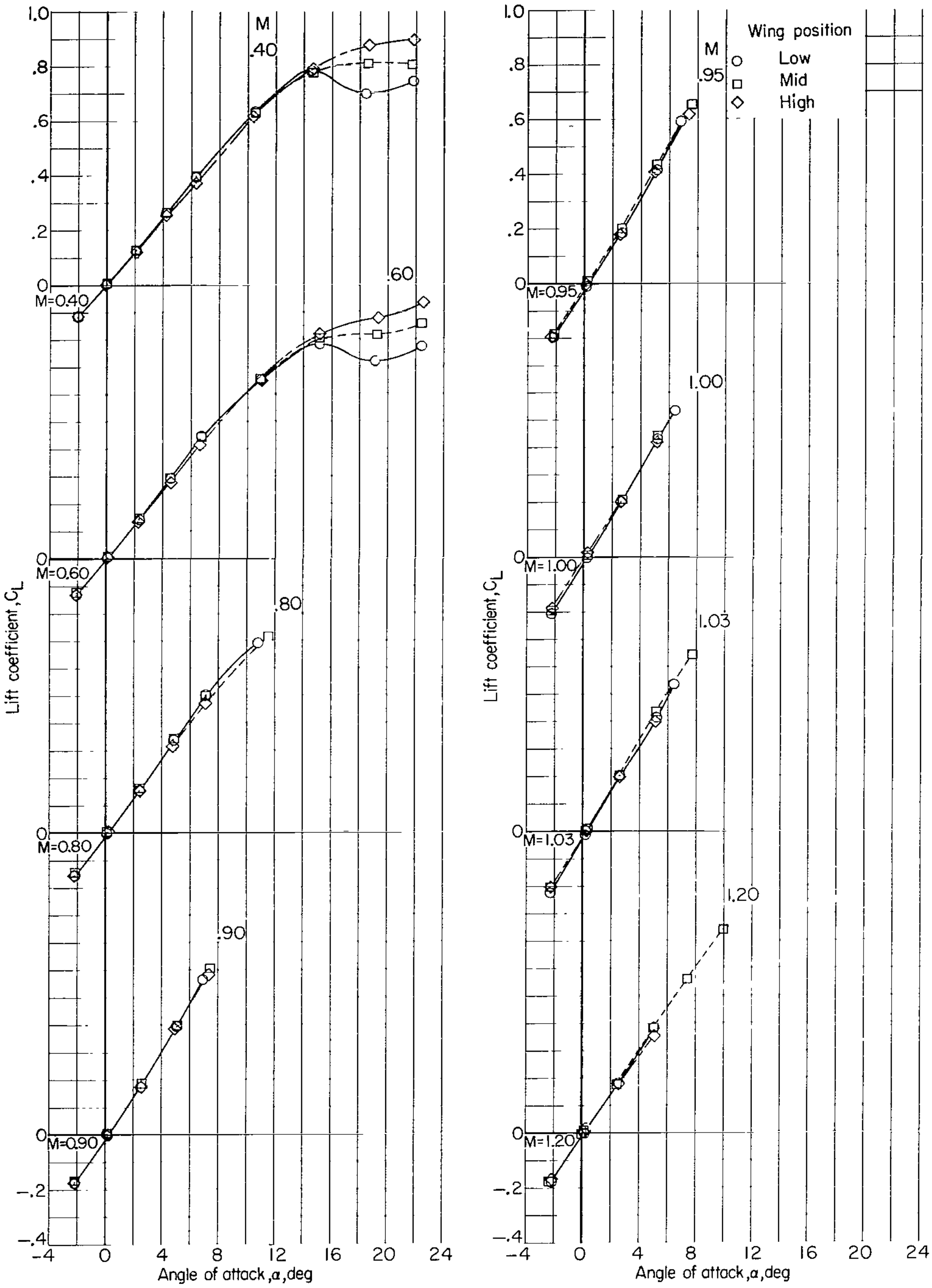

(b) Lift coefficient plotted against angle of attack. $\delta_c = 10^o$.

Figure 7.- Continued.

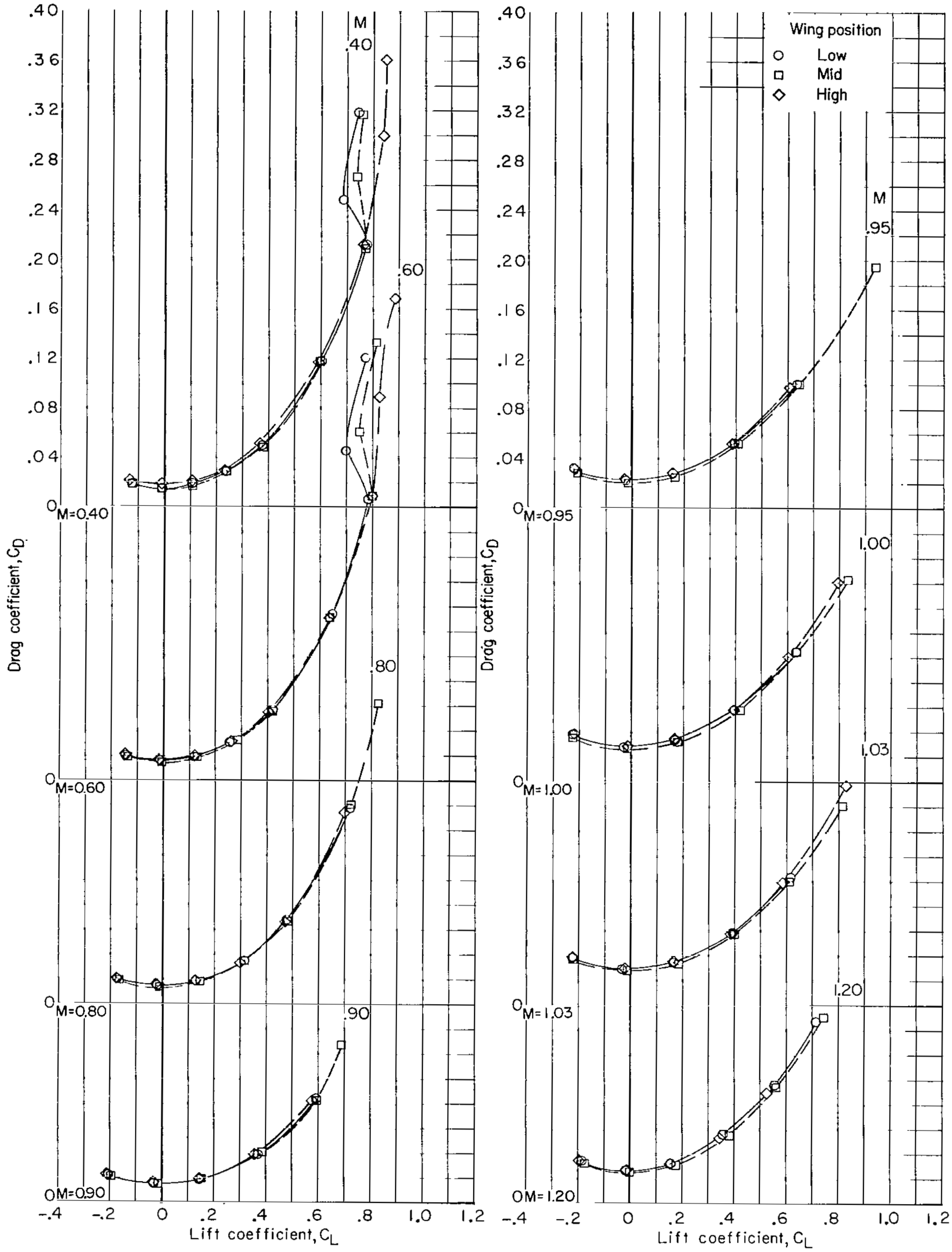

(c) Drag coefficient plotted against lift coefficient. $\delta_c = 0^o$.

Figure 7.- Continued.

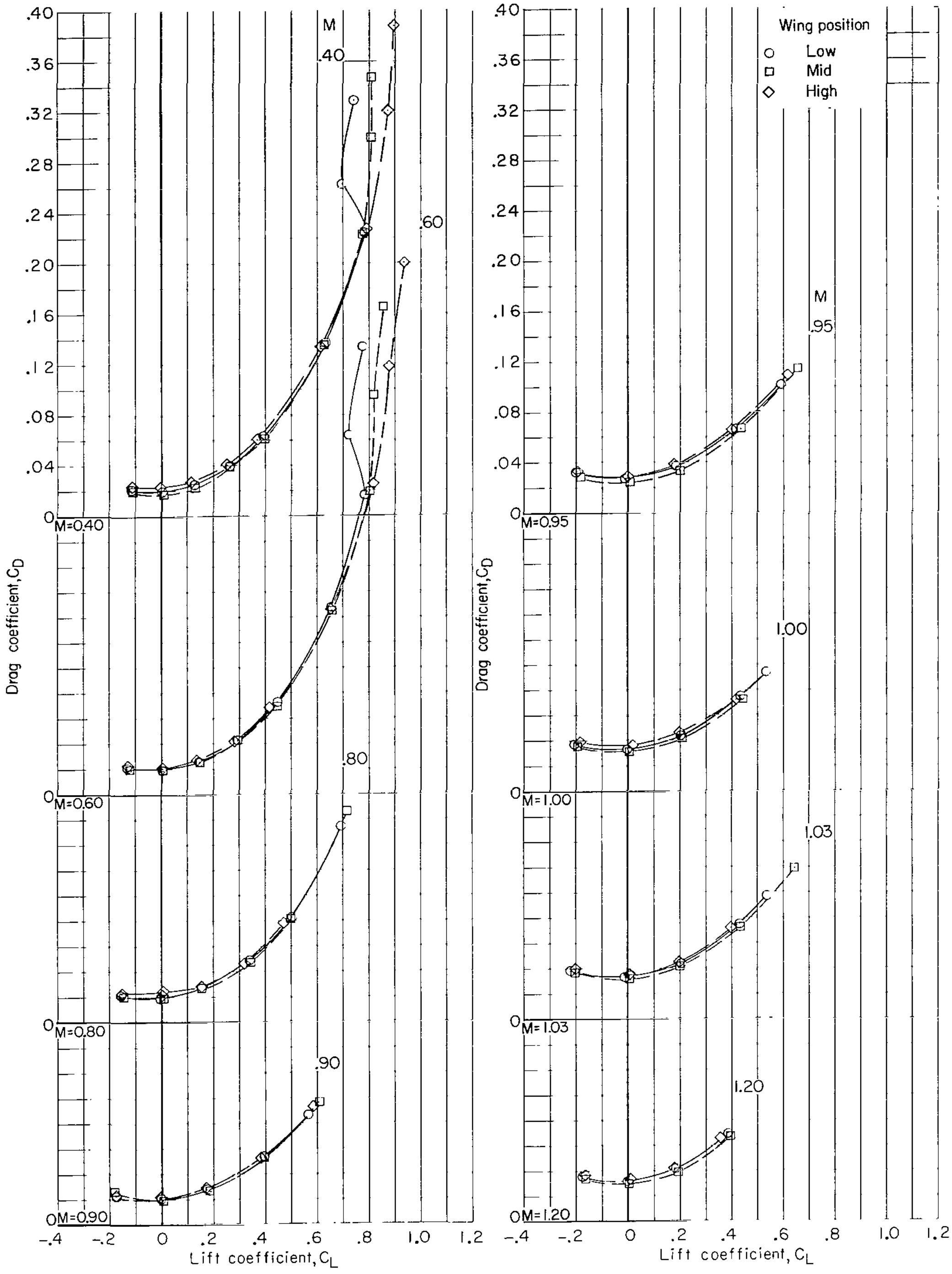

(d) Drag coefficient plotted against lift coefficient. $\delta_c = 10^{\circ}$.

Figure 7.- Continued.

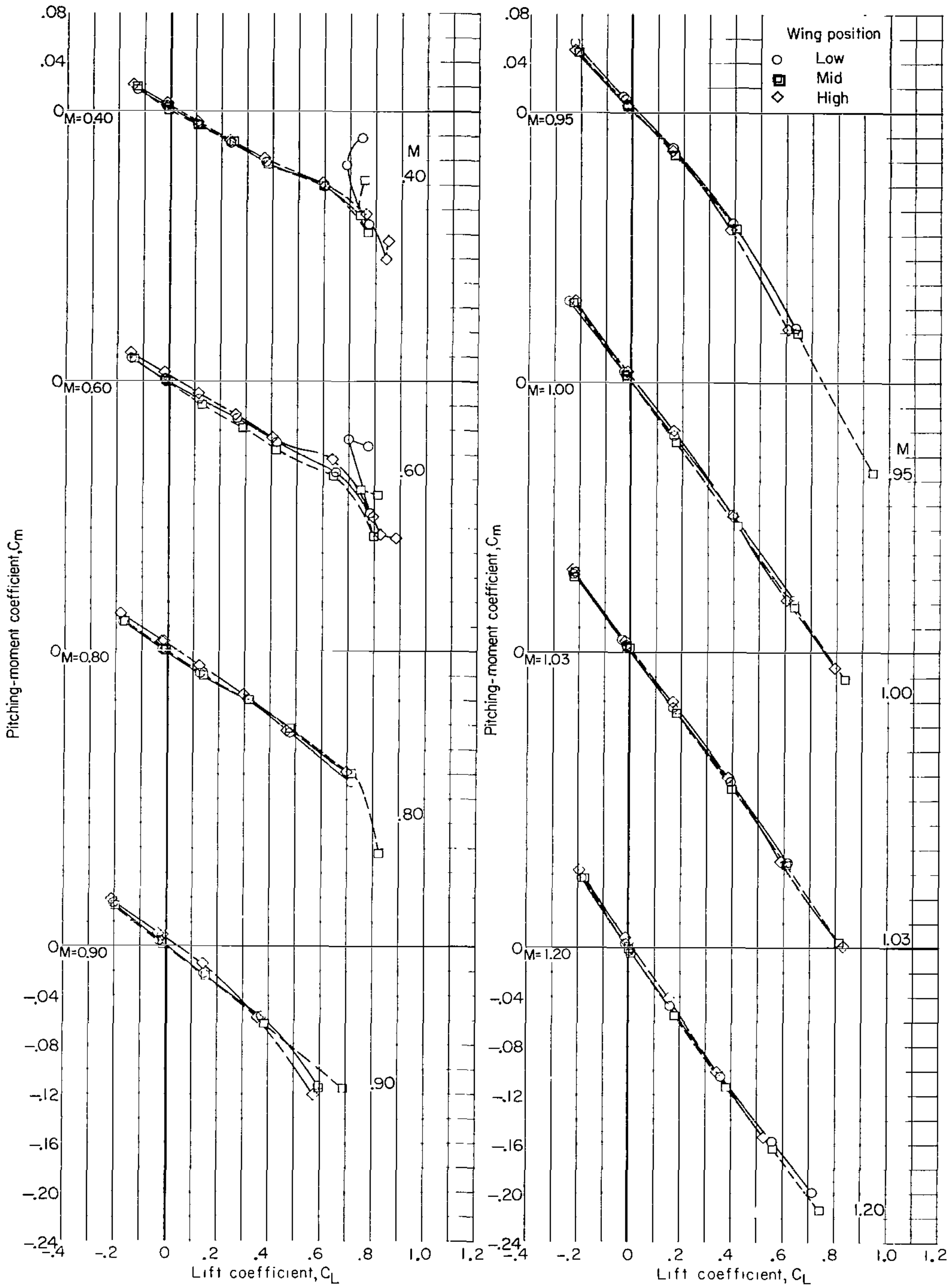

(e) Pitching-moment coefficient plotted against lift coefficient. $\delta_c = 0^o$.

Figure 7.- Continued.

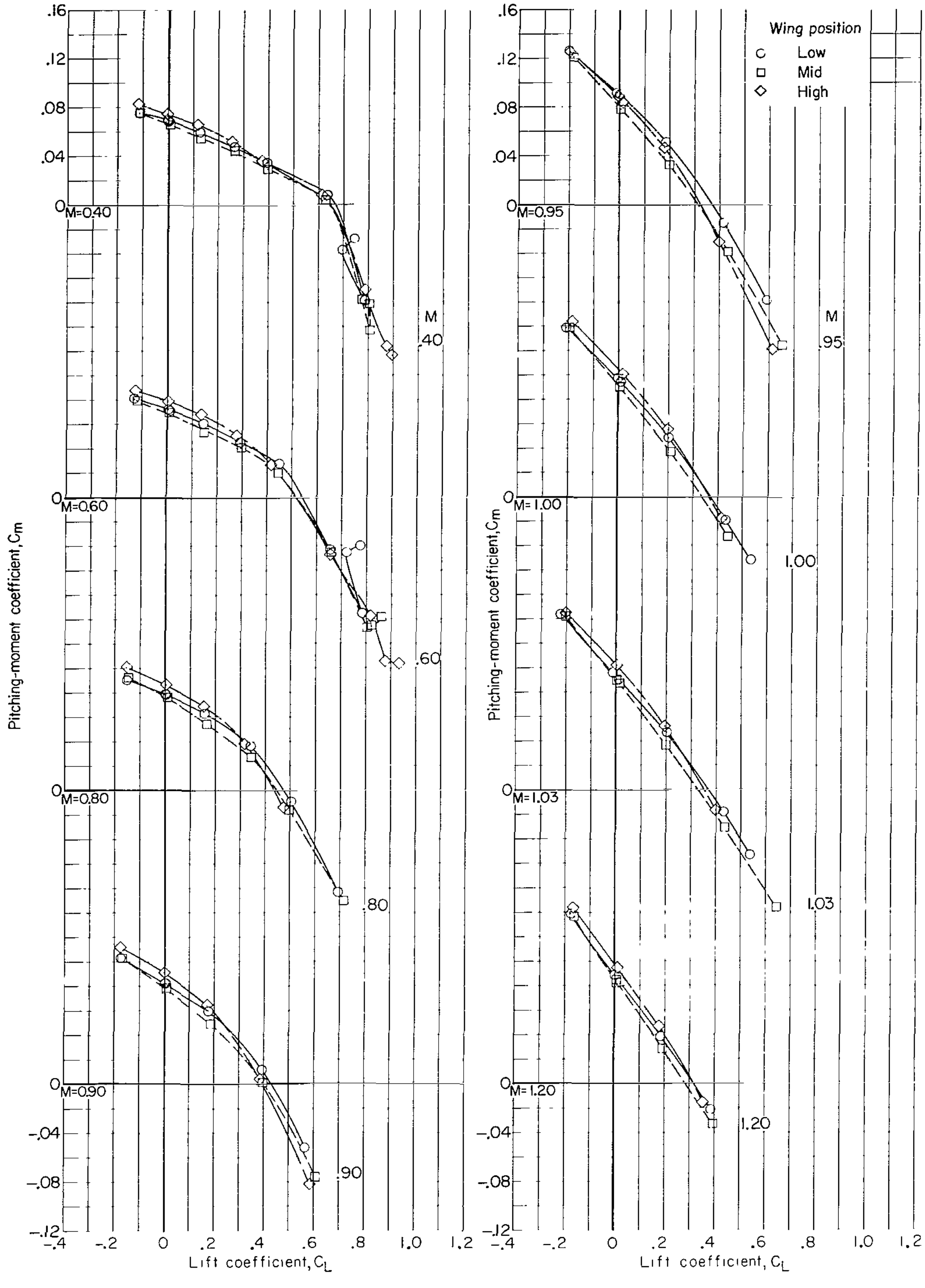

(f) Pitching-moment coefficient plotted against lift coefficient. $\delta_c = 10^\circ$.

Figure 7.- Concluded.

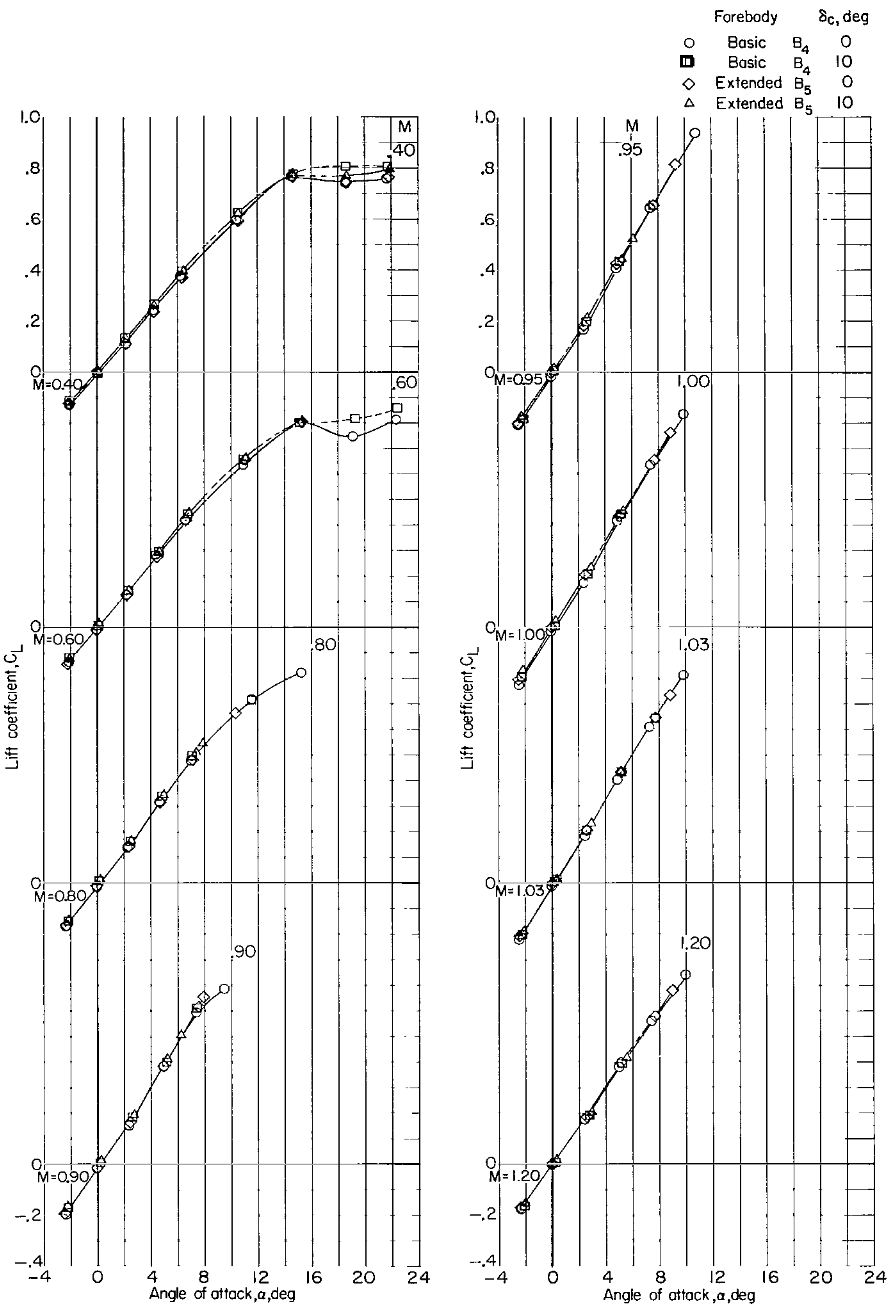

(a) Lift coefficient plotted against angle of attack.

Figure 8.- Effects of forebody length on longitudinal aerodynamic characteristics of $W_3C_2V_2$ midwing configuration for canard deflection angles of 0° and 10°. $\delta_n = 0^{\circ}$; $\Gamma_c = 0^{\circ}$.

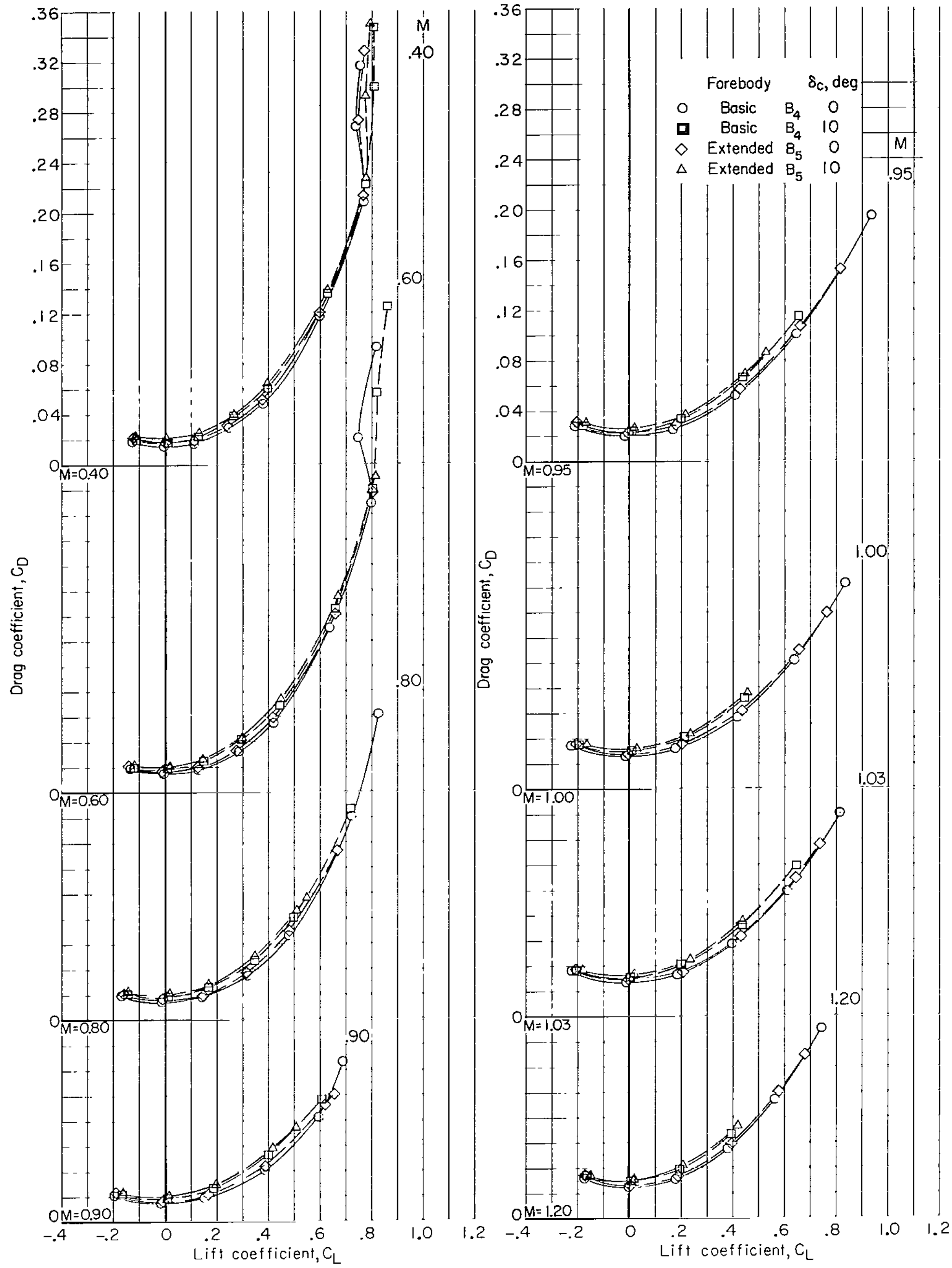

(b) Drag coefficient plotted against lift coefficient.

Figure 8.- Continued.

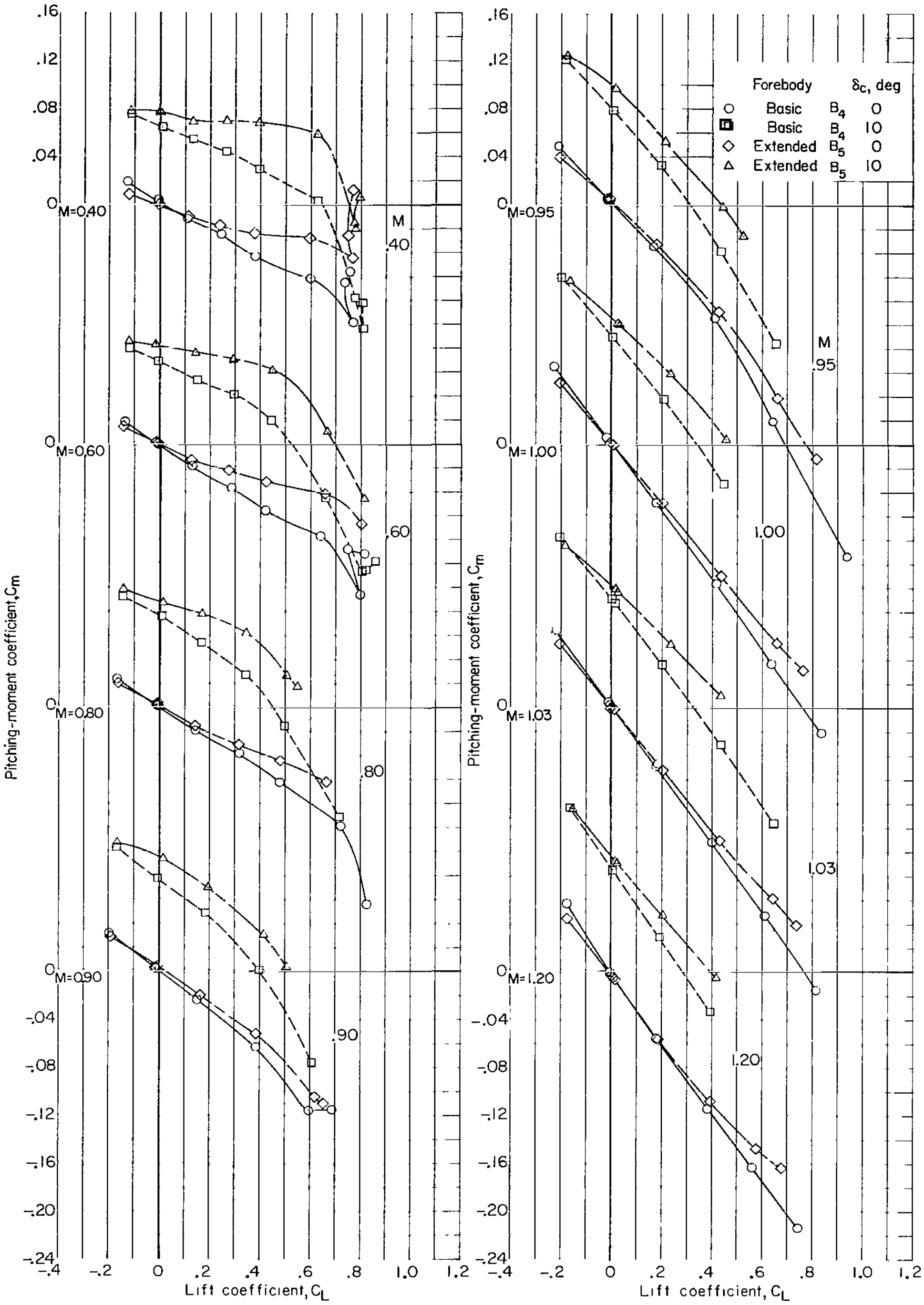

(c) Pitching-moment coefficients plotted against lift coefficient.

Figure 8.- Concluded.

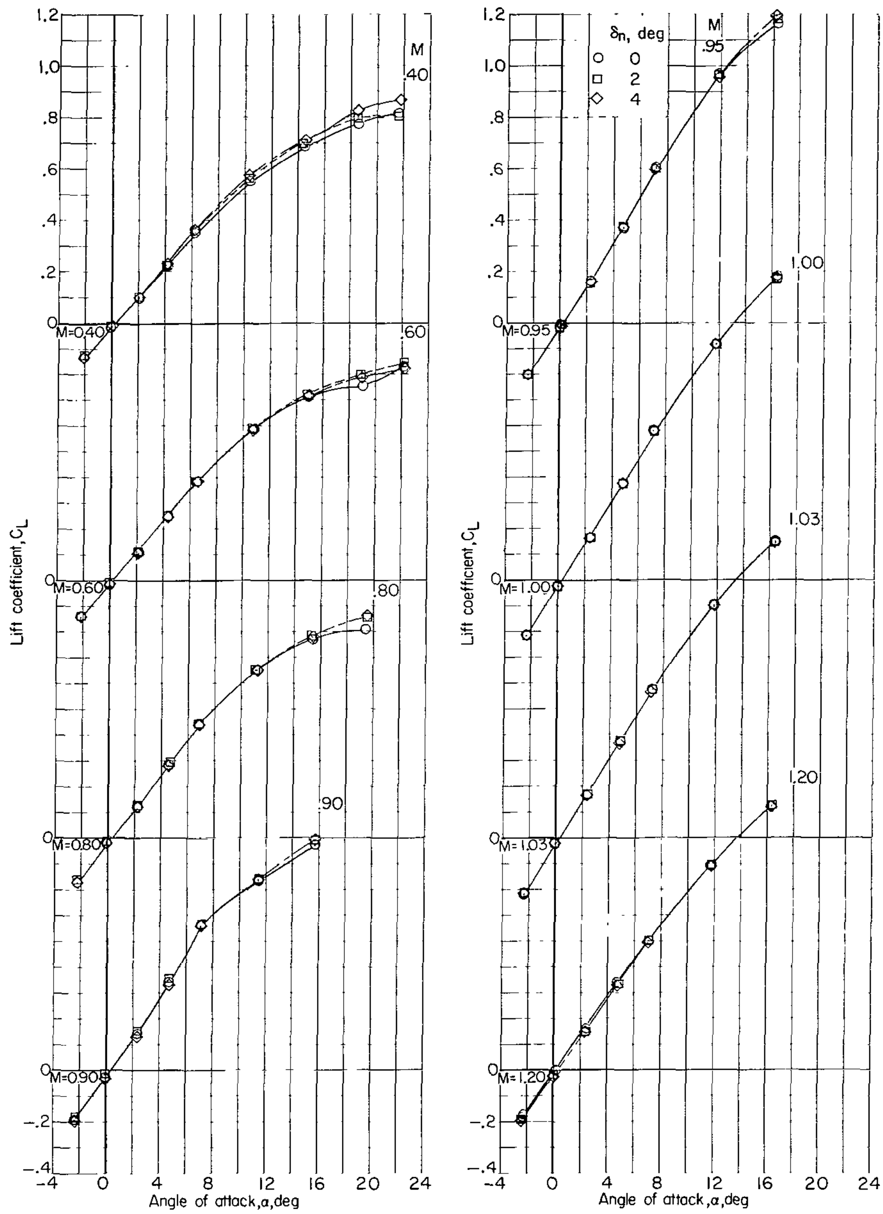

(a) Lift coefficient plotted against angle of attack.

Figure 9.- Effects of forebody deflection on longitudinal aerodynamic characteristics of $B_4W_3V_2$ high-wing configuration with canards off.

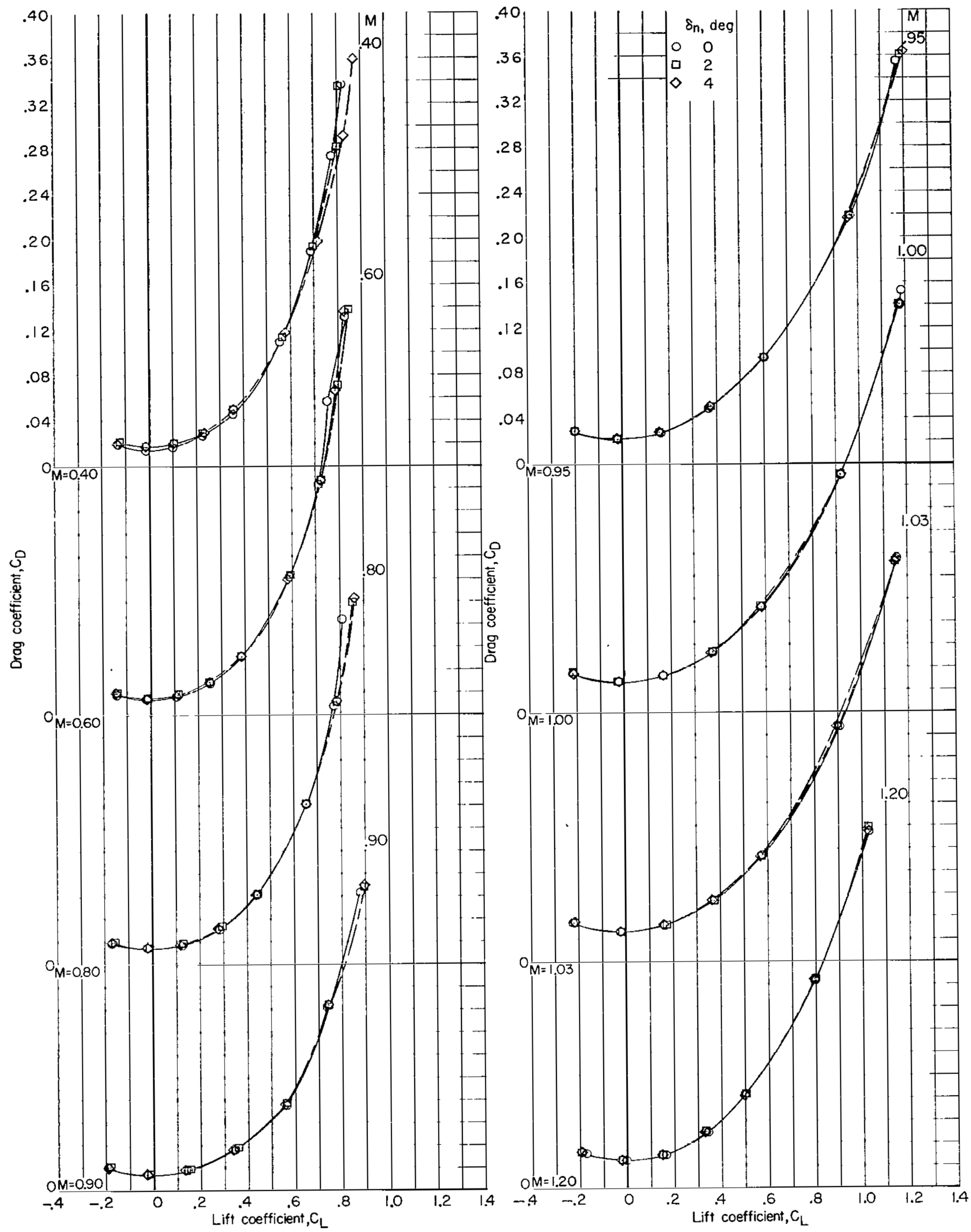

(b) Drag coefficient plotted against lift coefficient.

Figure 9.- Continued.

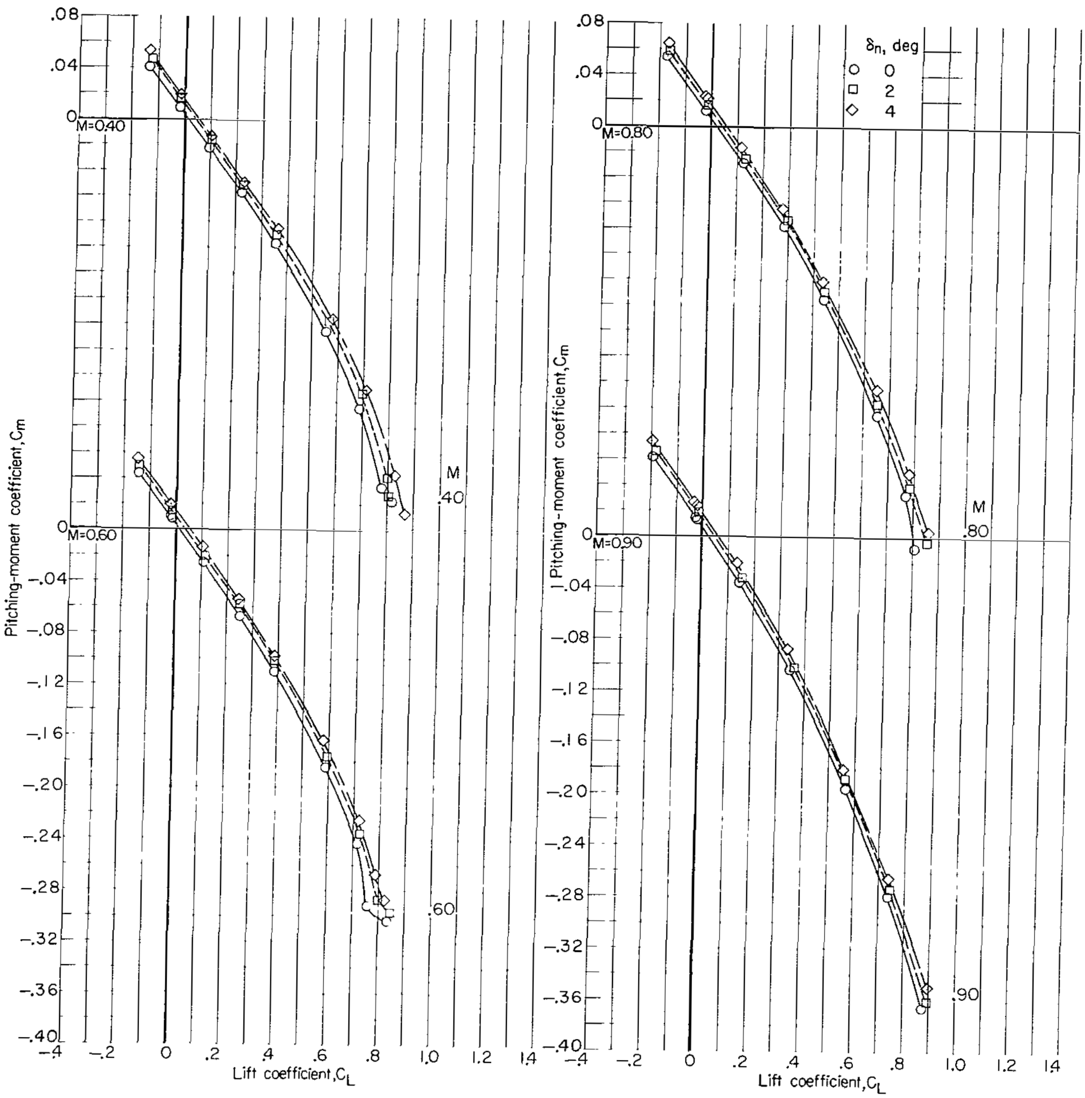

(c) Pitching-moment coefficient plotted against lift coefficient.

Figure 9.- Continued.

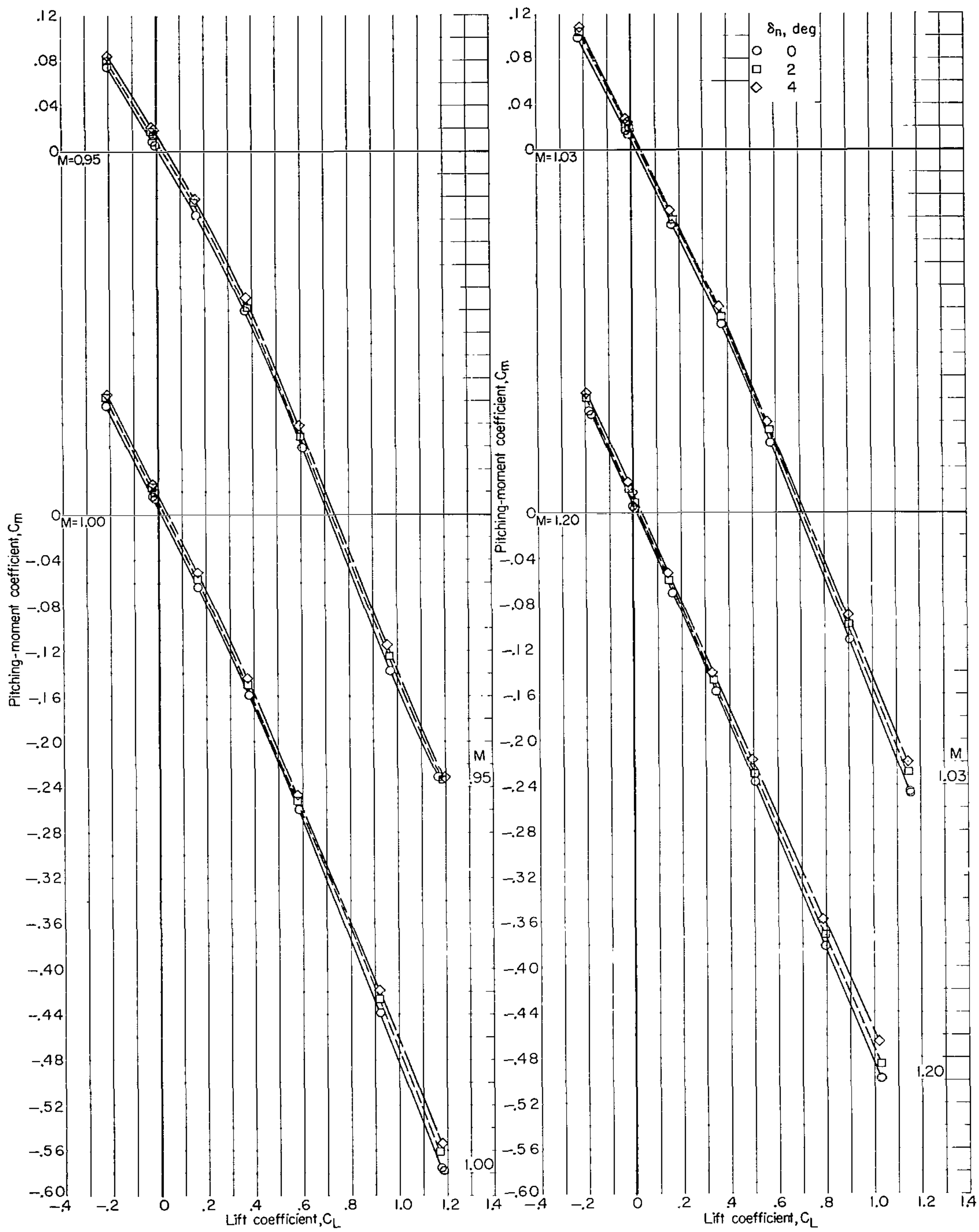

(c) Pitching-moment coefficient plotted against lift coefficient. Concluded.

Figure 9.- Concluded.

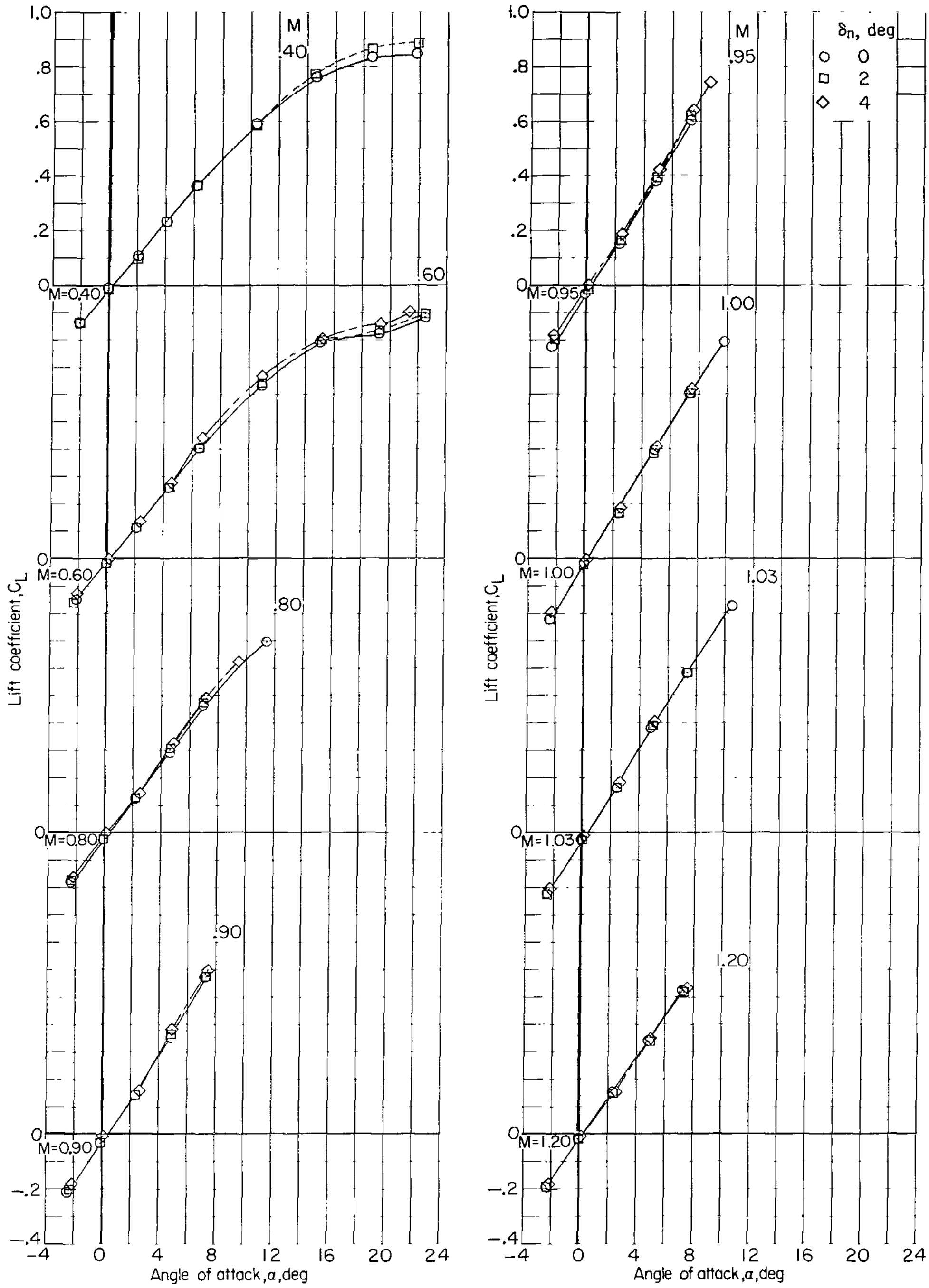

(a) Lift coefficient plotted against angle of attack. $\delta_c = 0^{\circ}$.

Figure 10.- Effects of forebody deflection on longitudinal aerodynamic characteristics of $B_4W_3C_2V_2$ high-wing configuration for canard deflection angles of 0° and 10°. $\Gamma_c = 0^{\circ}$.

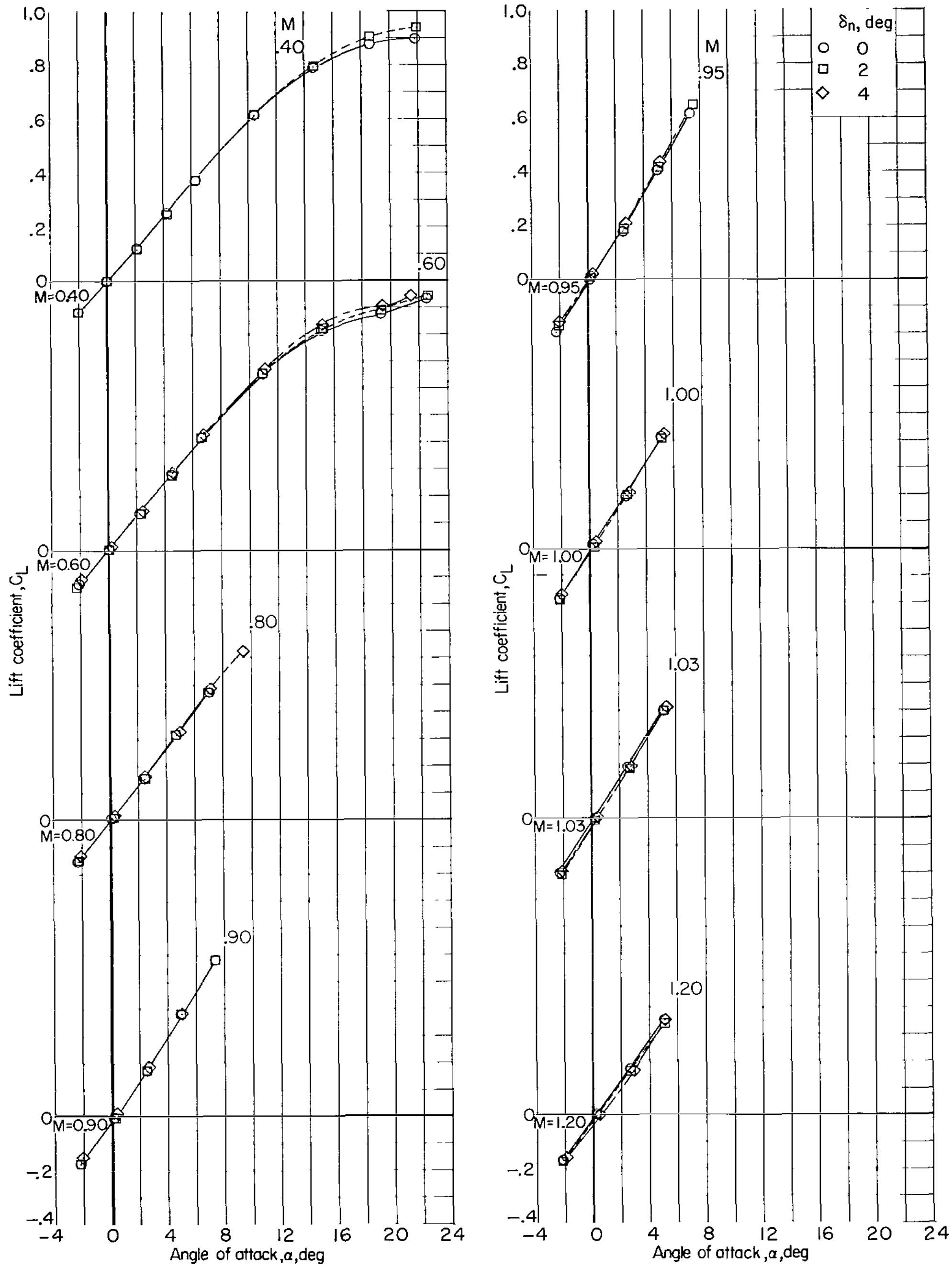

(b) Lift coefficient plotted against angle of attack. $\delta_c = 10^{\circ}$.

Figure 10.- Continued.

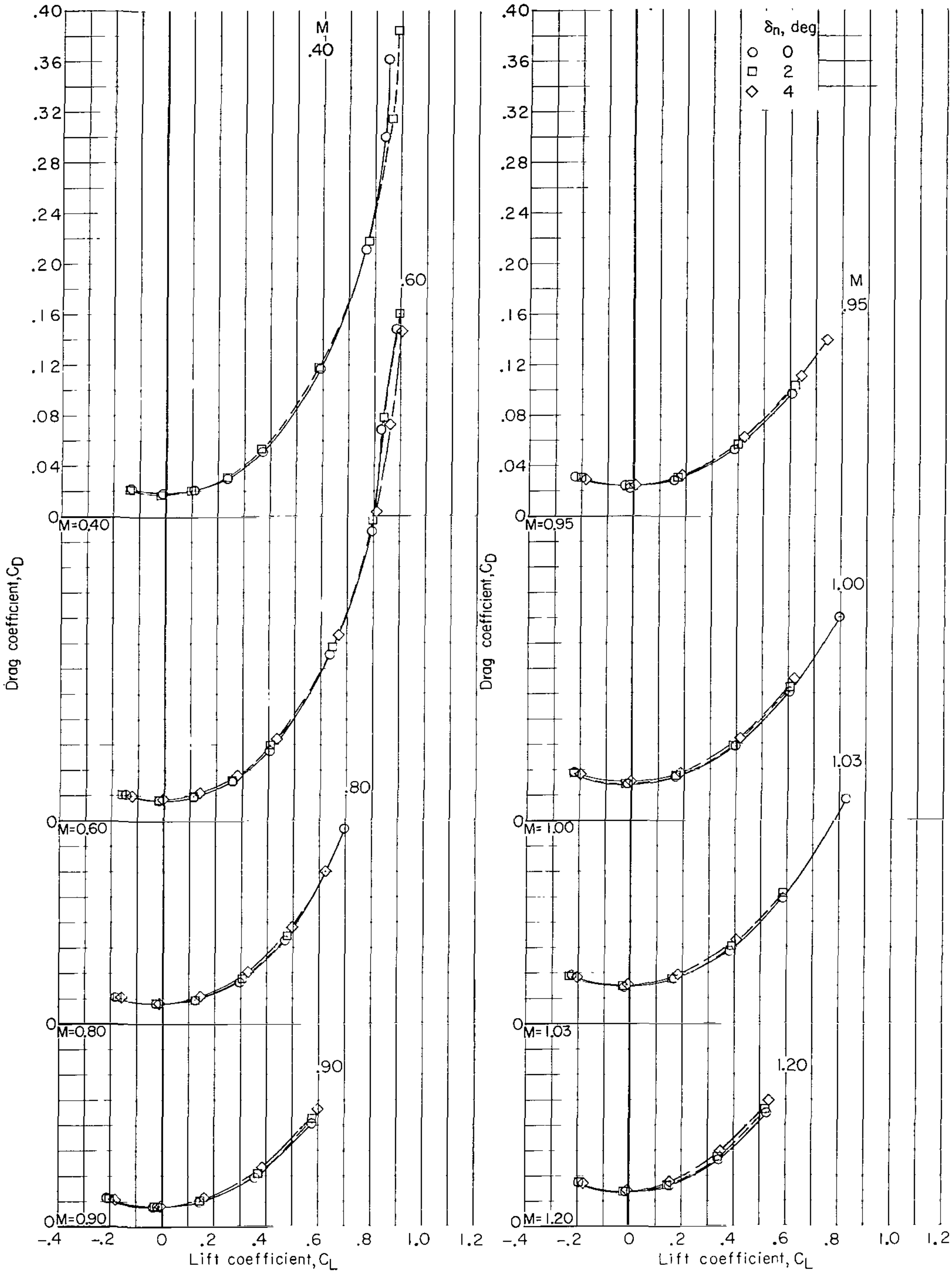

(c) Drag coefficient plotted against lift coefficient. $\delta_c = 0^o$.

Figure 10.- Continued.

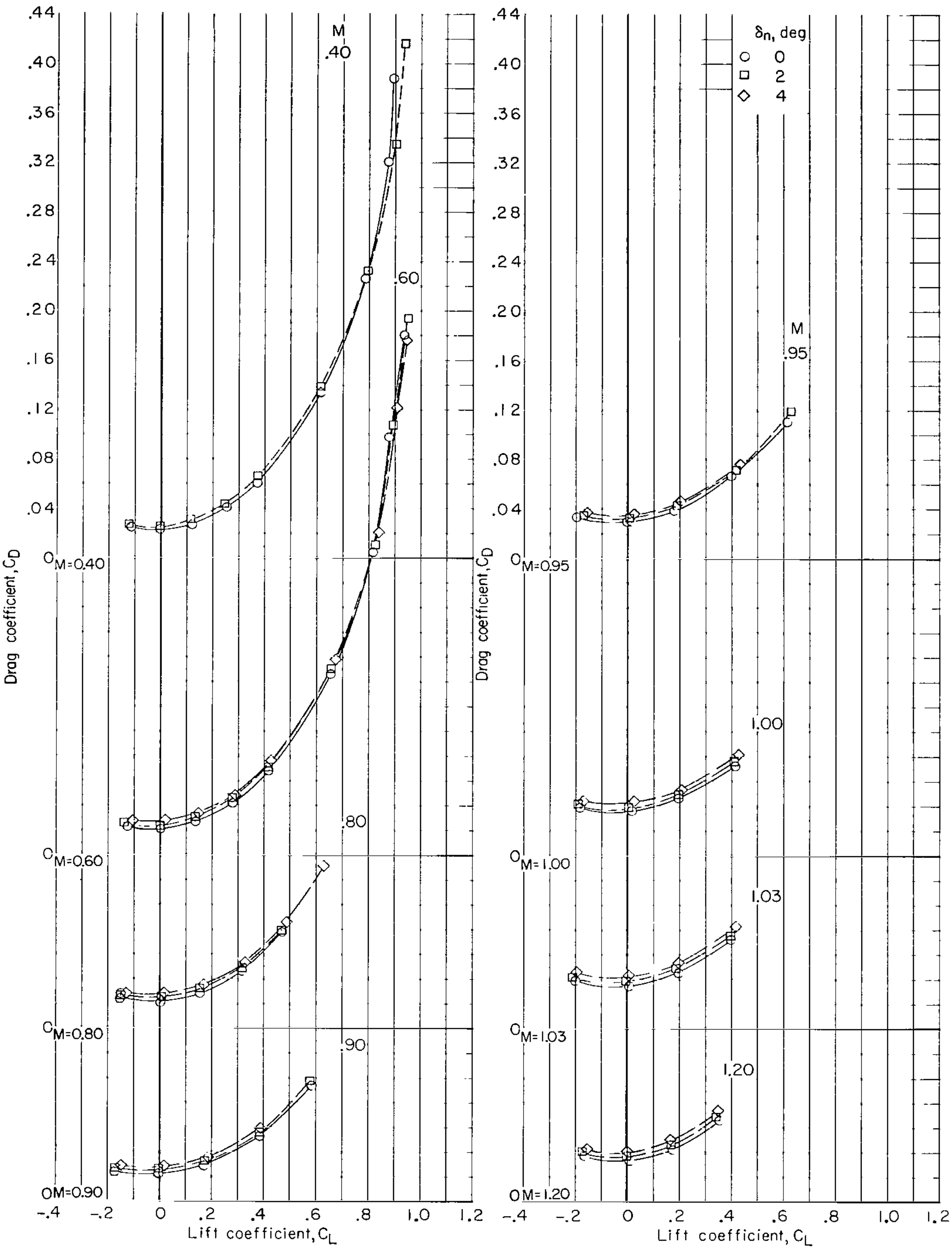

(d) Drag coefficient plotted against lift coefficient. $\delta_c = 10^{\circ}$.

Figure 10.- Continued.

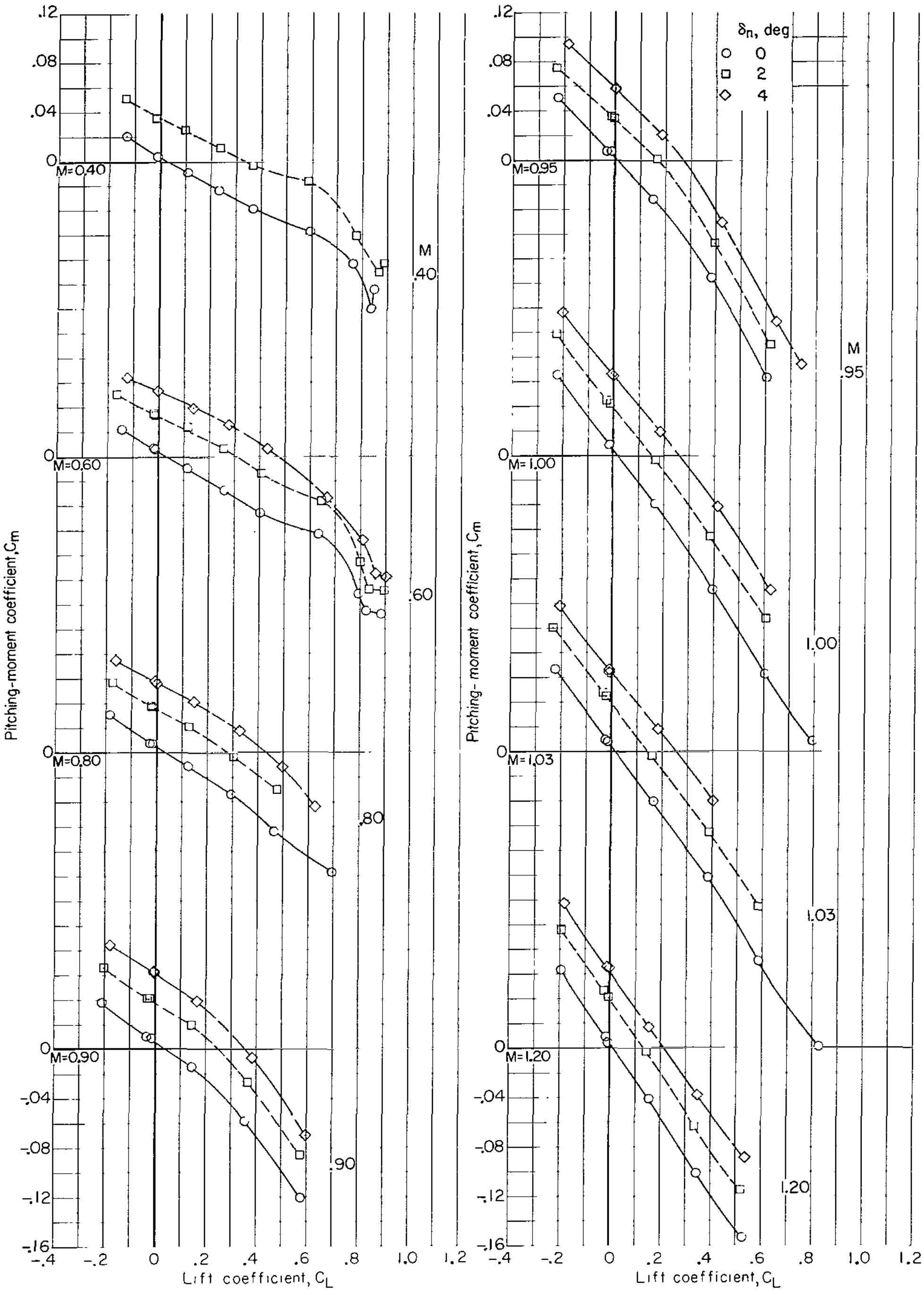

(e) Pitching-moment coefficient plotted against lift coefficient. $\delta_c = 0^{\circ}$.

Figure 10.- Continued.

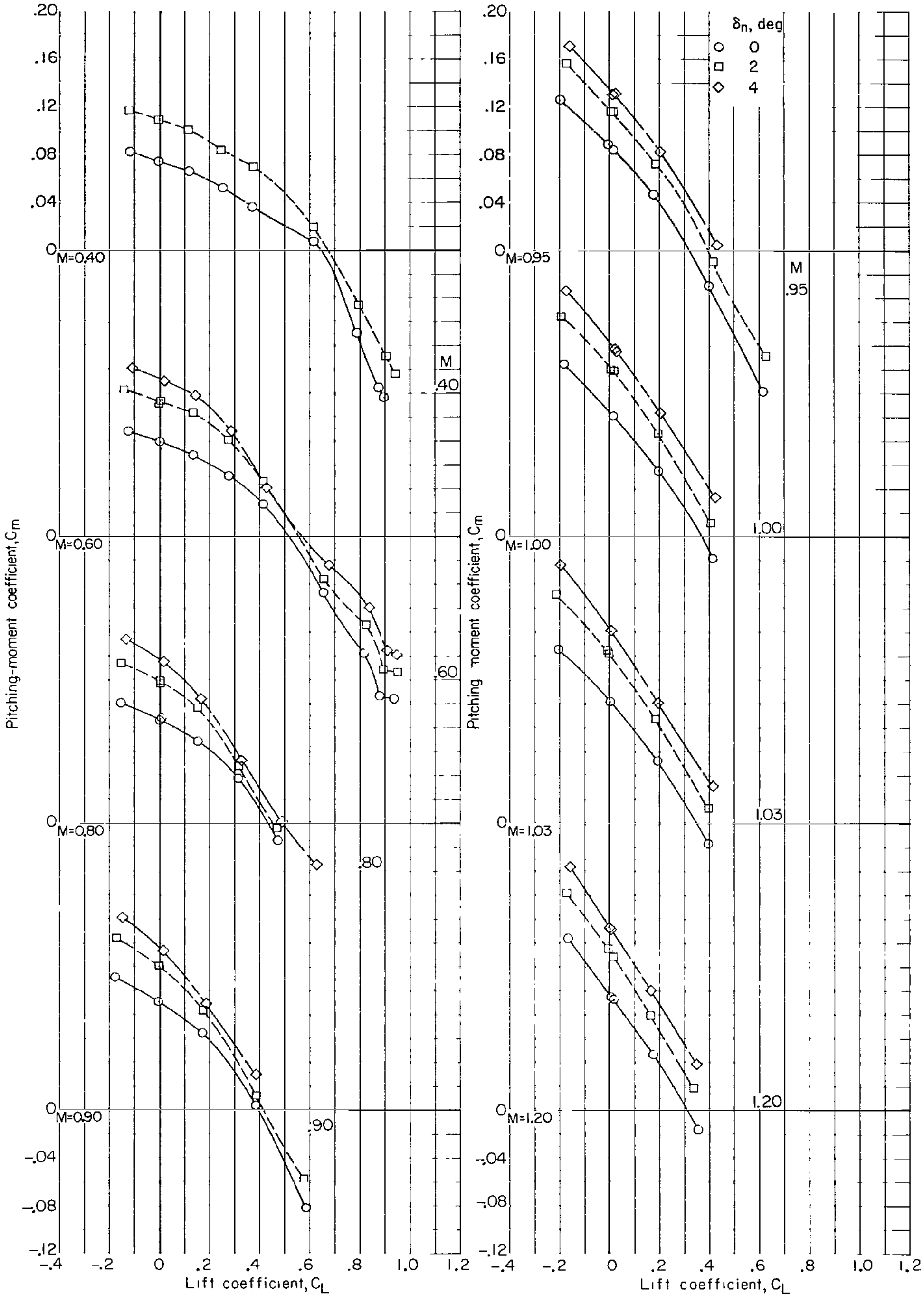

(f) Pitching-moment coefficient plotted against lift coefficient. $\delta_c = 10^{\circ}$.

Figure 10.- Concluded.

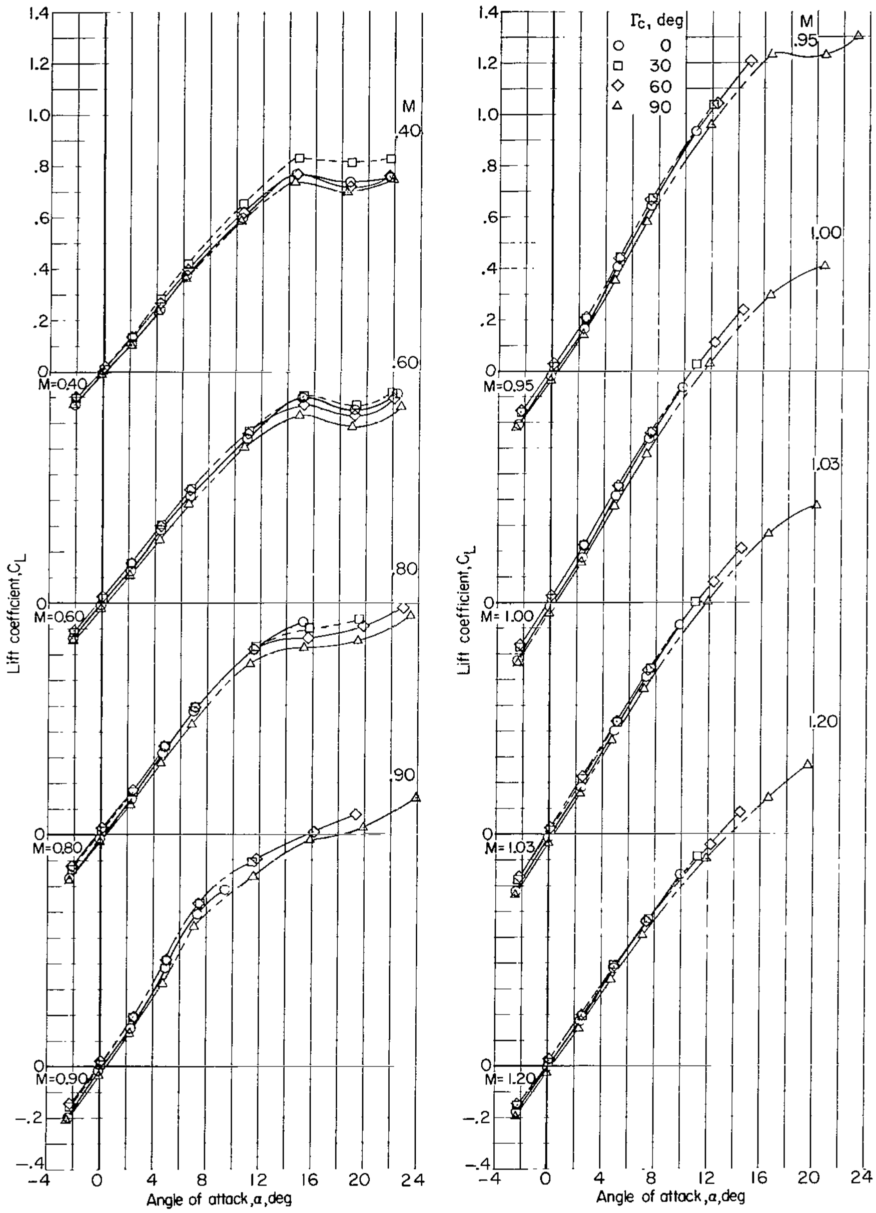

(a) Lift coefficient plotted against angle of attack.

Figure 11.- Effects of canard dihedral on longitudinal aerodynamic characteristics of $B_4W_3C_2V_2$ midwing configuration. $\delta_n = 0^{\circ}$; $\delta_c = 0^{\circ}$.

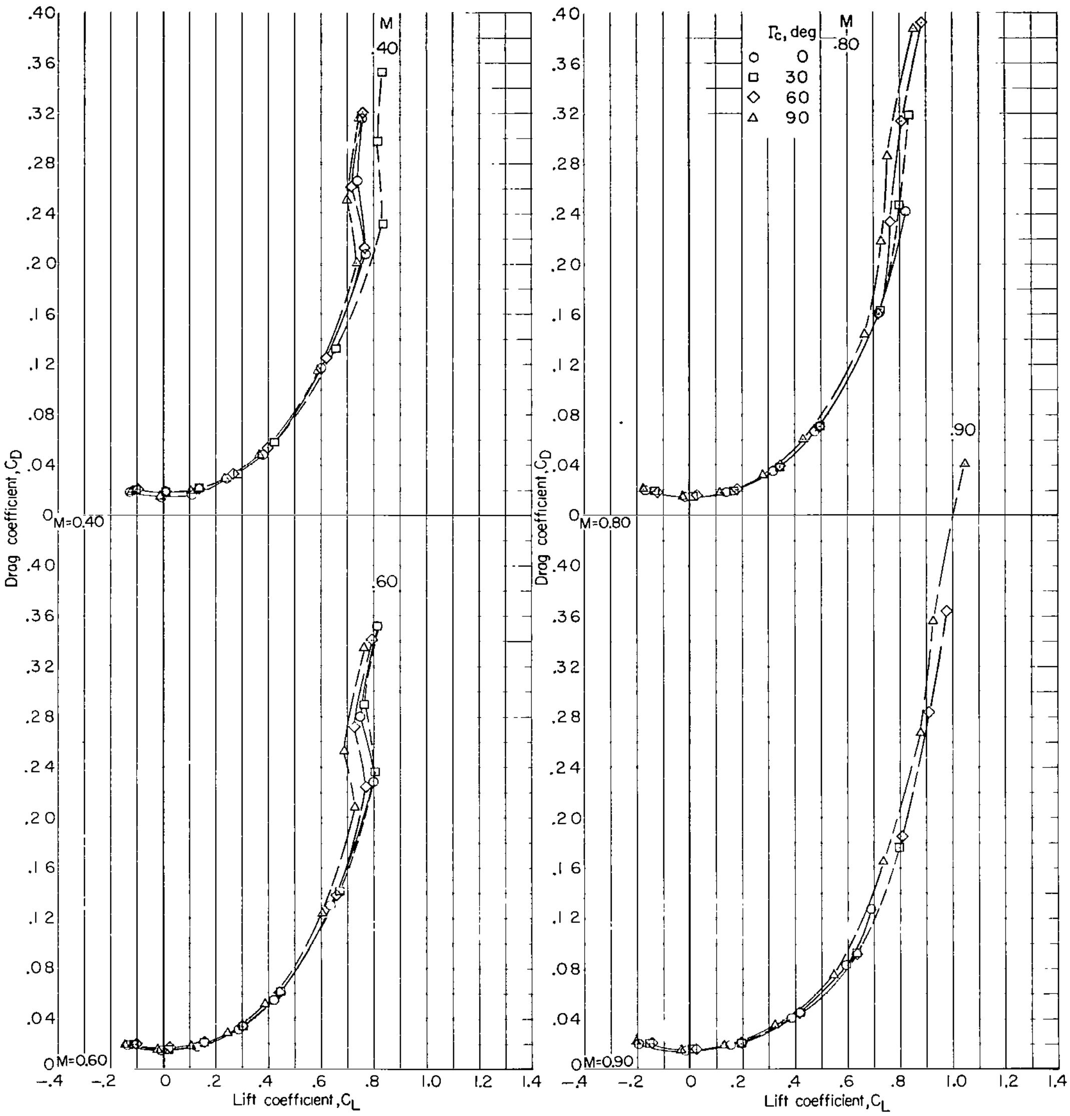

(b) Drag coefficient plotted against lift coefficient.

Figure 11.- Continued.

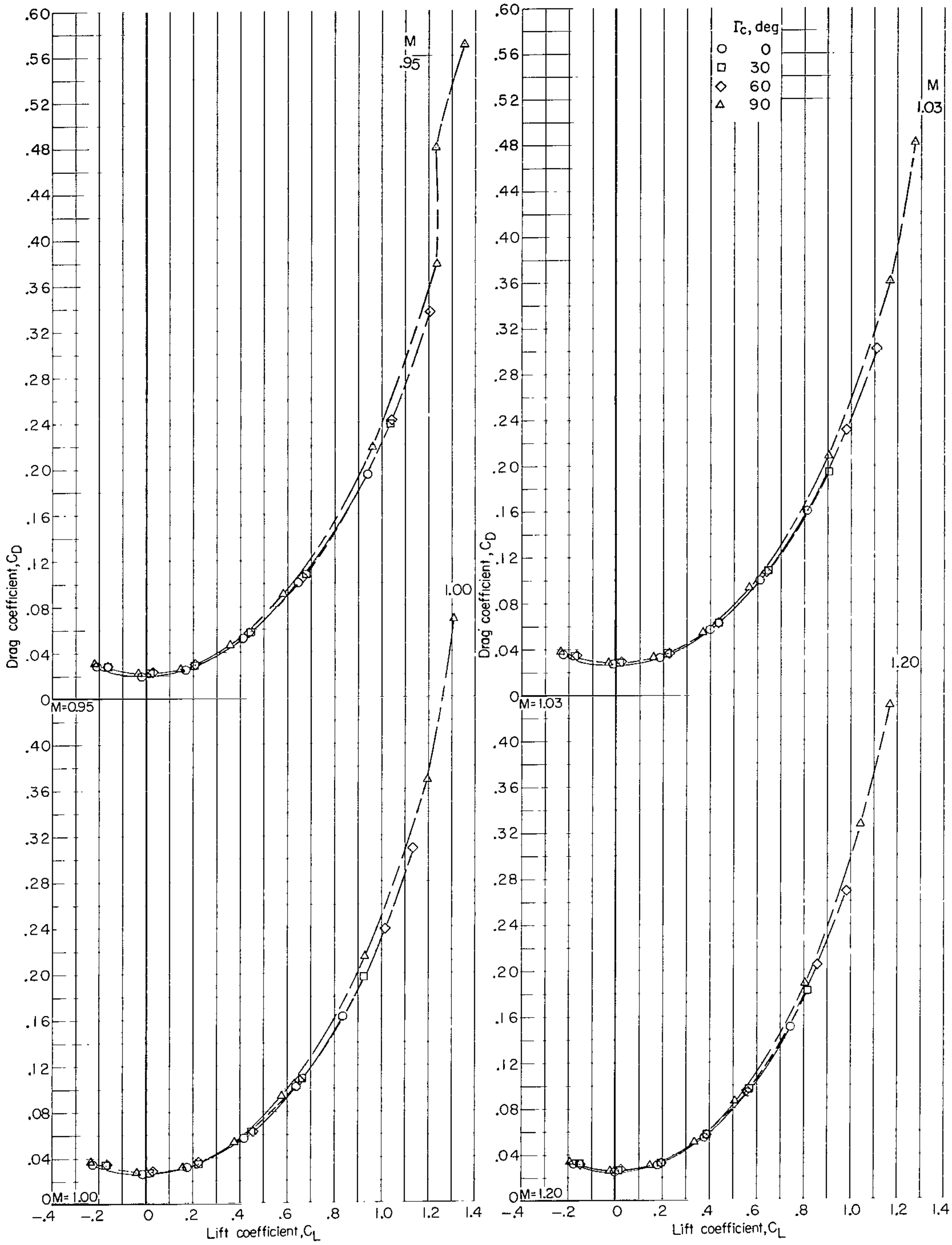

(b) Drag coefficient plotted against lift coefficient. Concluded.

Figure 11.- Continued.

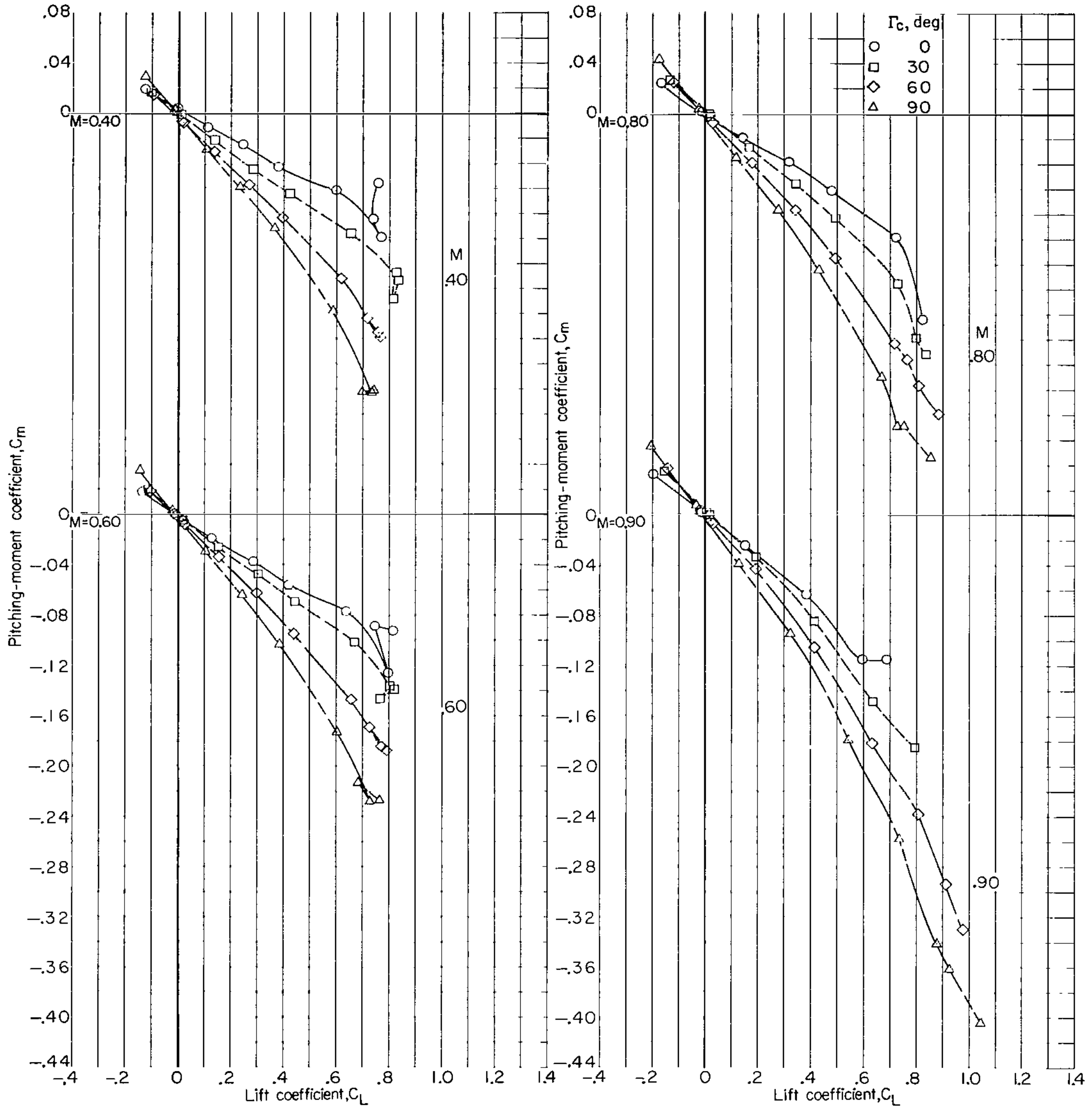

(c) Pitching-moment coefficient plotted against lift coefficient.

Figure 11.- Continued.

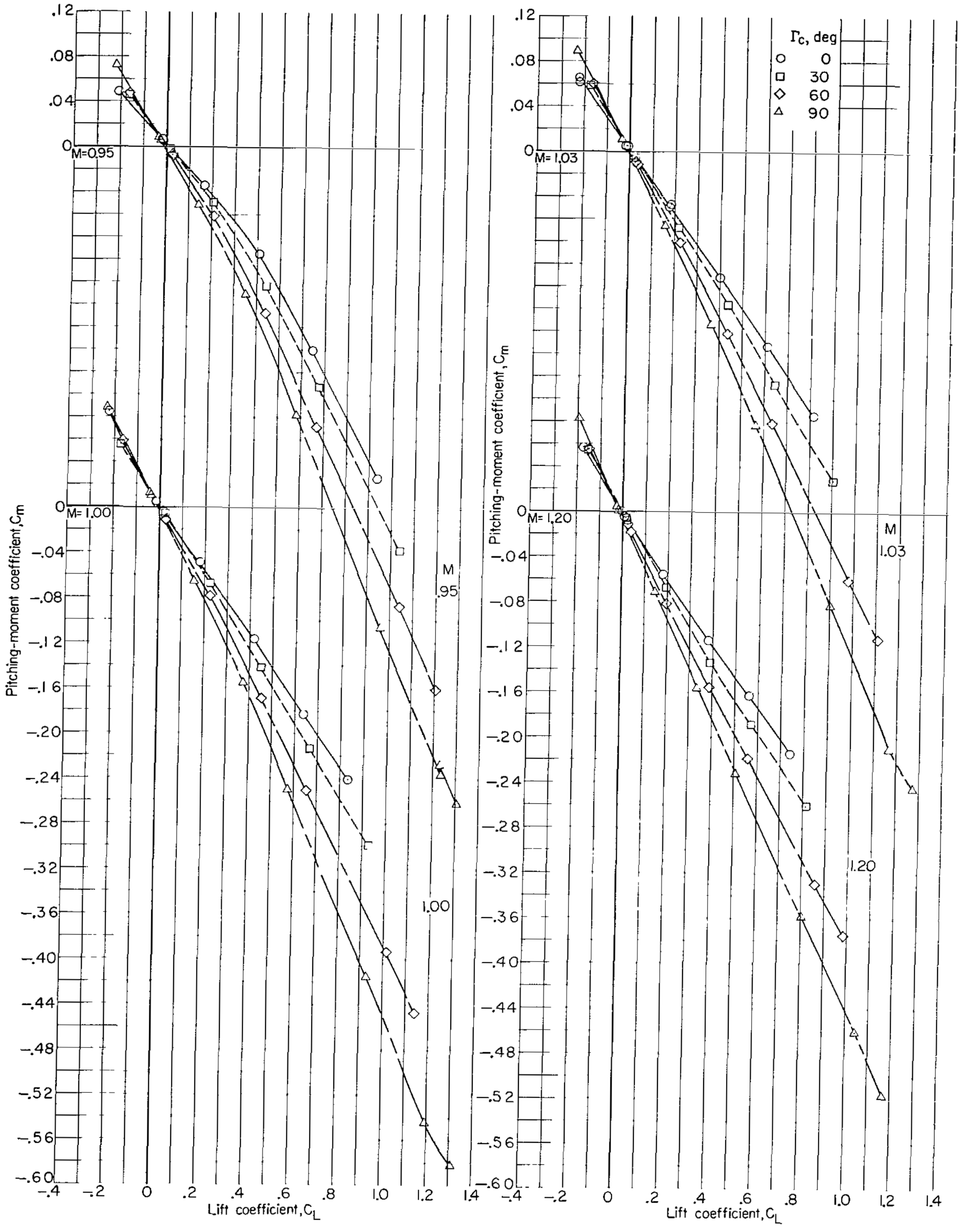

(c) Pitching-moment coefficient plotted against lift coefficient. Concluded.

Figure 11.- Concluded.

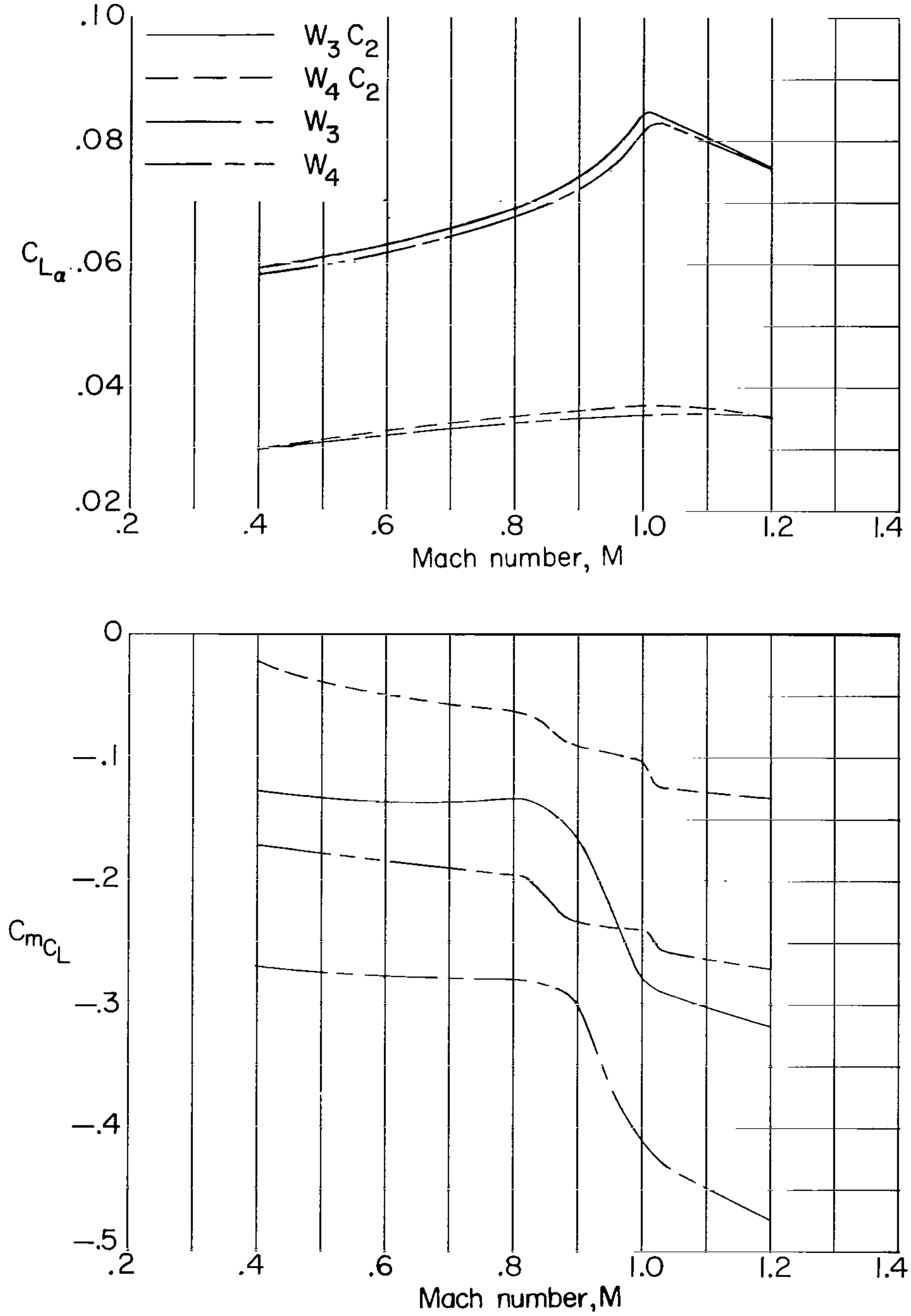

(a) C_{L_α} and $C_{m_{C_L}}$.

Figure 12.- Variation of longitudinal aerodynamic characteristics with Mach number for trapezoidal and delta midwing configurations with canards on and off. B_4V_2; $\delta_c = 0^\circ$; $\delta_n = 0^\circ$; $\Gamma_c = 0^\circ$.

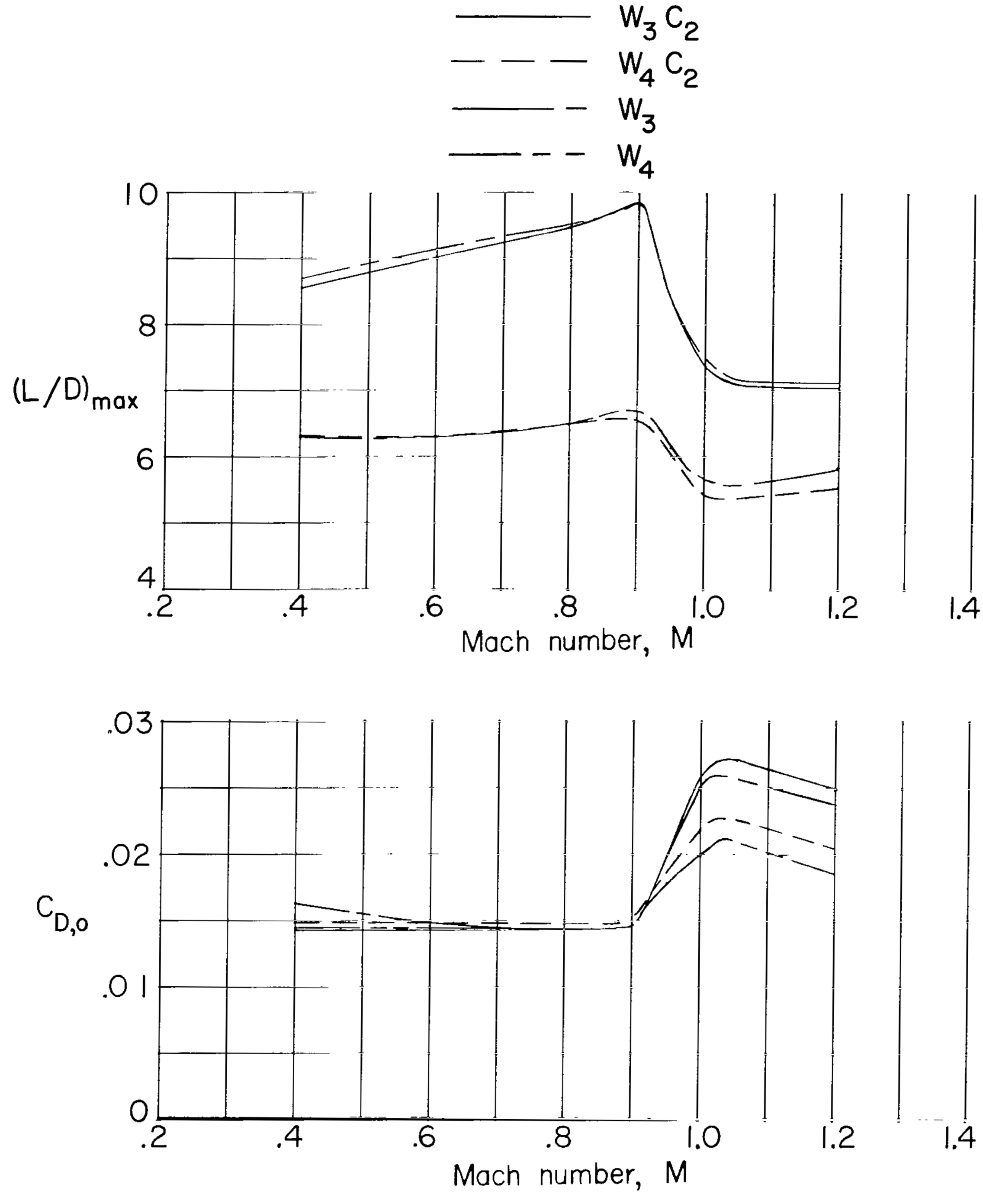

(b) $(L/D)_{max}$ and $C_{D,o}$.

Figure 12.- Concluded.

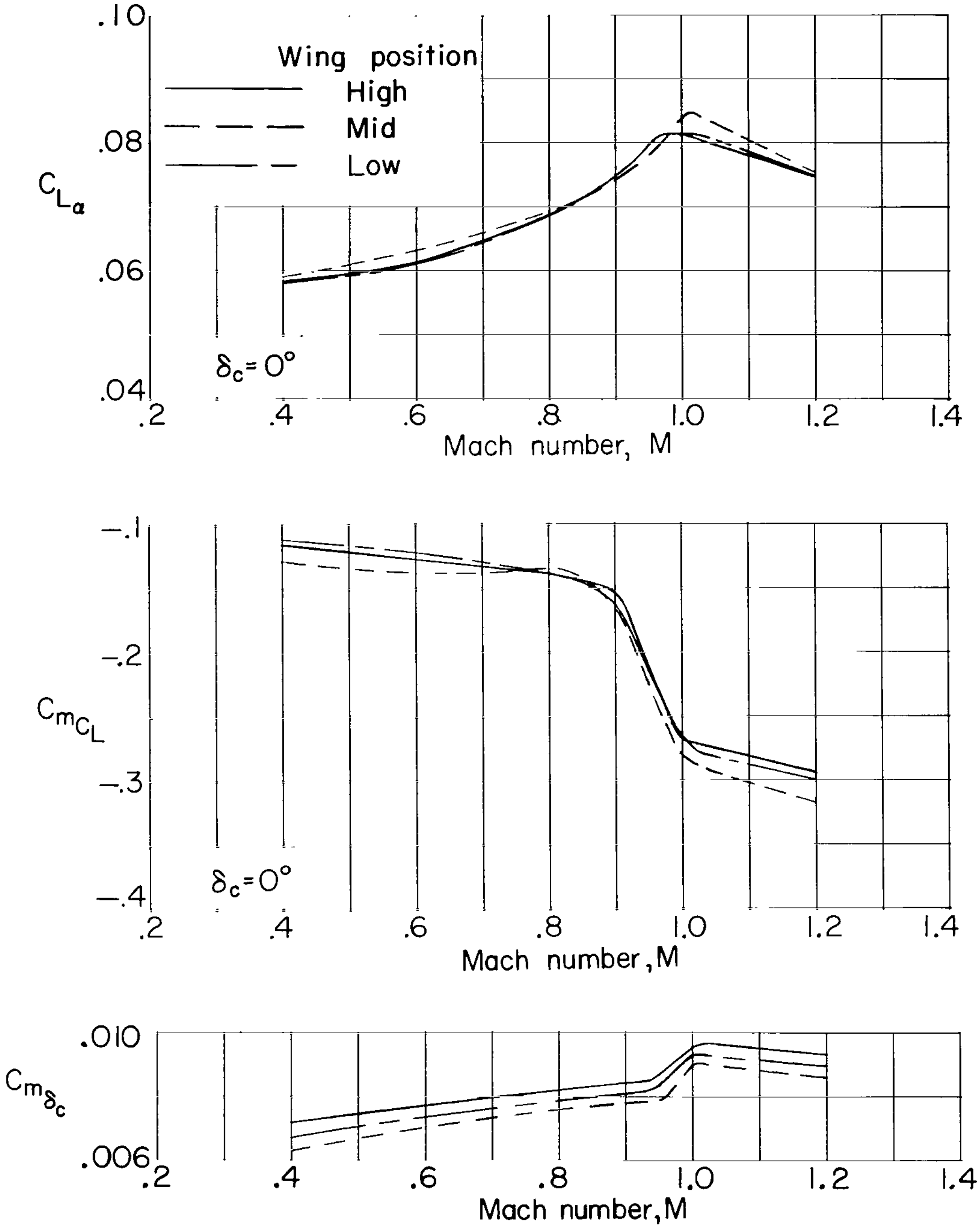

(a) C_{L_α}, $C_{m_{C_L}}$, and $C_{m_{\delta_c}}$.

Figure 13.- Variation of longitudinal aerodynamic characteristics with Mach number for various wing vertical locations. $B_4W_3C_2V_2$; $\delta_n = 0°$; $\Gamma_c = 0°$.

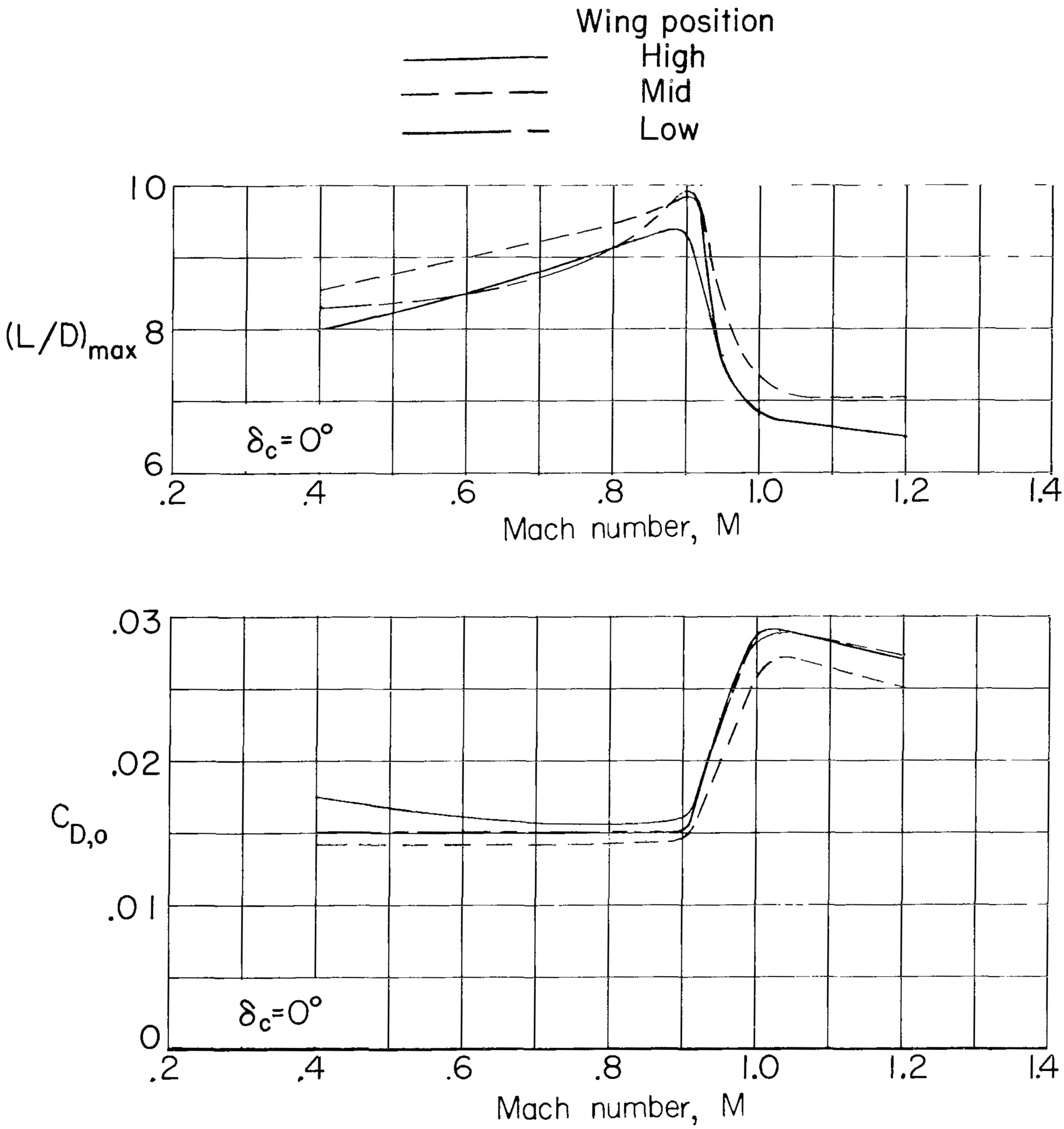

(b) $(L/D)_{max}$ and $C_{D,o}$.

Figure 13.- Concluded.

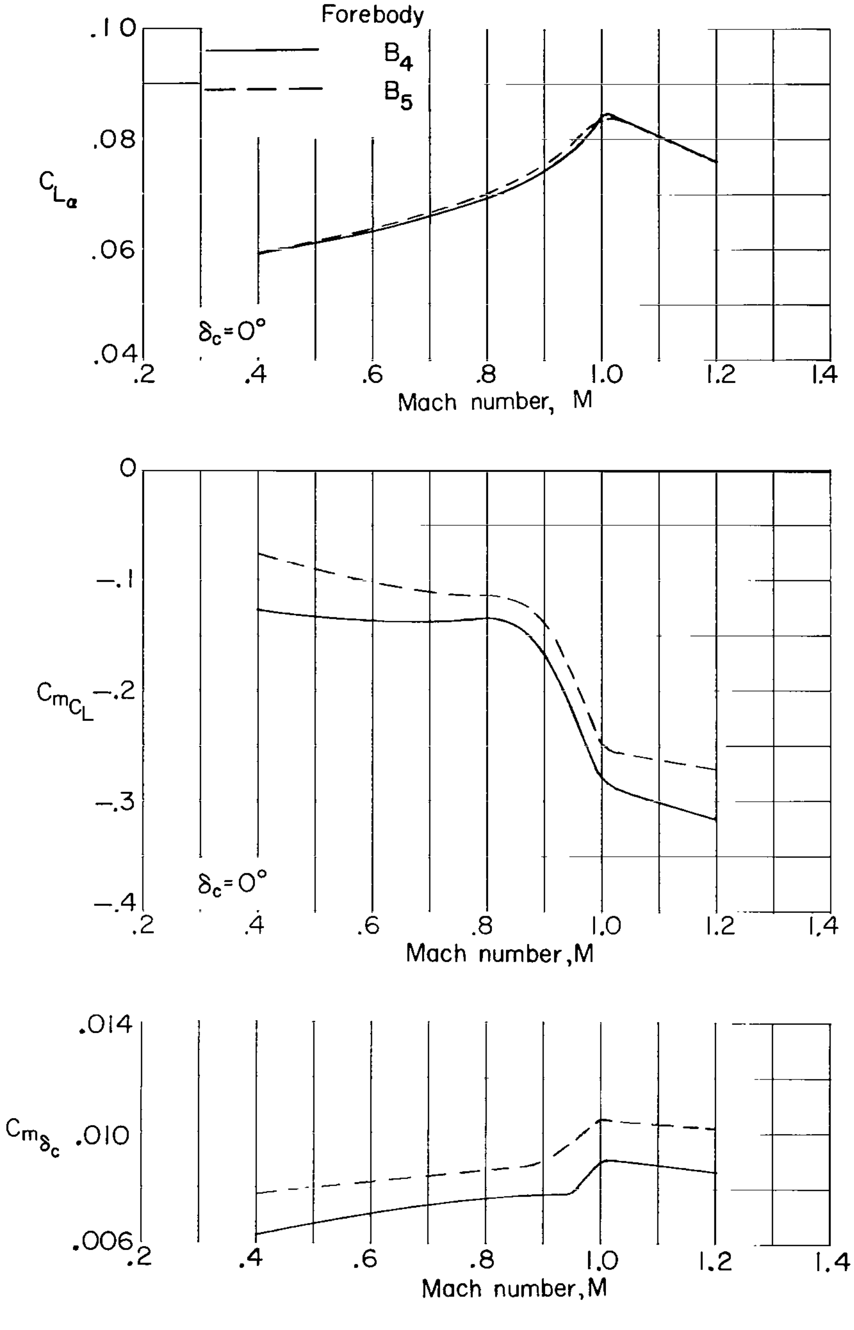

(a) C_{L_α}, $C_{m_{C_L}}$, and $C_{m_{\delta_c}}$.

Figure 14.- Variation of longitudinal aerodynamic characteristics with Mach number for various forebody lengths. Midwing $W_3C_2V_2$; $\delta_n = 0^{\circ}$; $\Gamma_c = 0^{\circ}$.

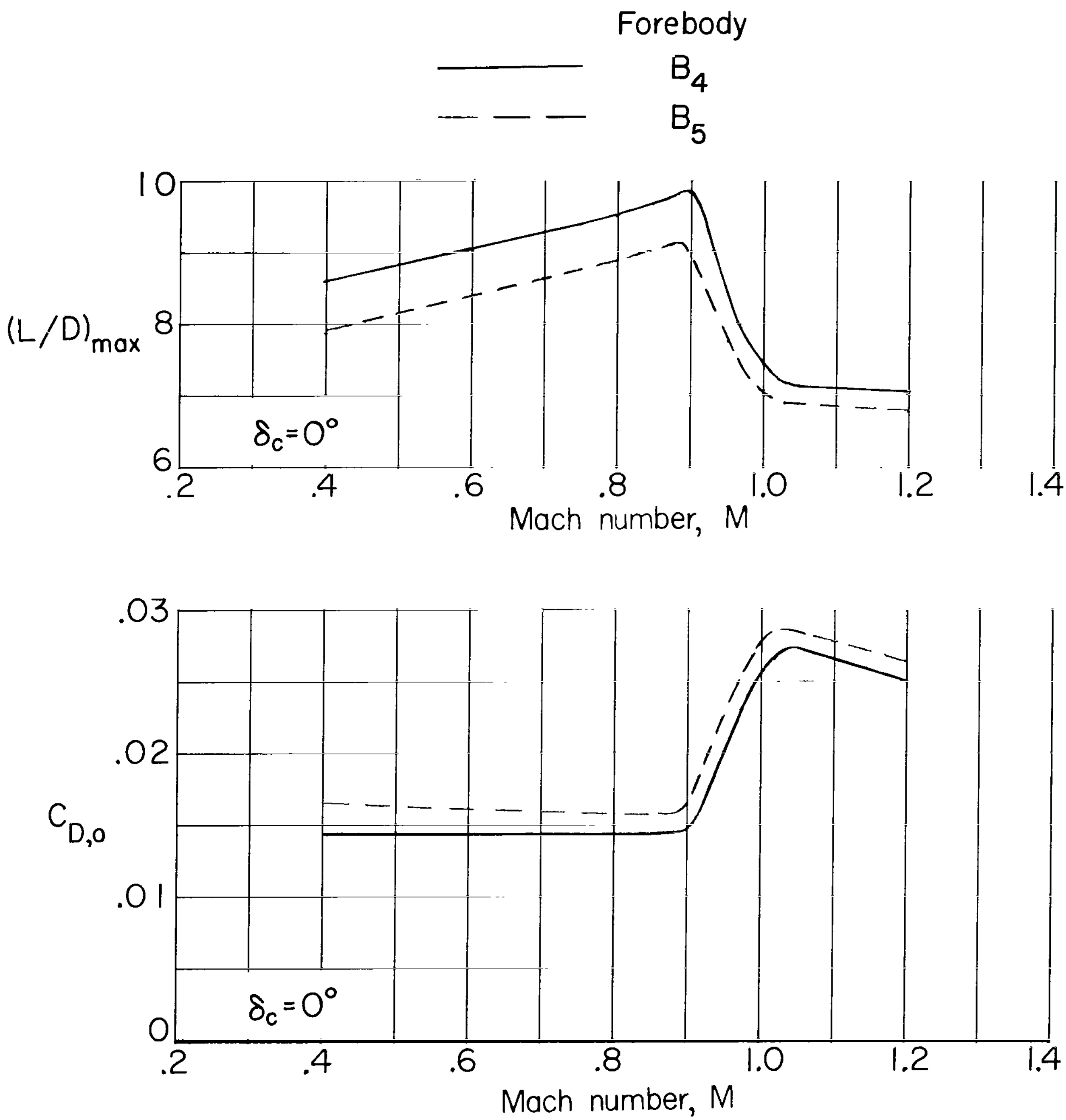

(b) $(L/D)_{max}$ and $C_{D,o}$.

Figure 14.- Concluded.

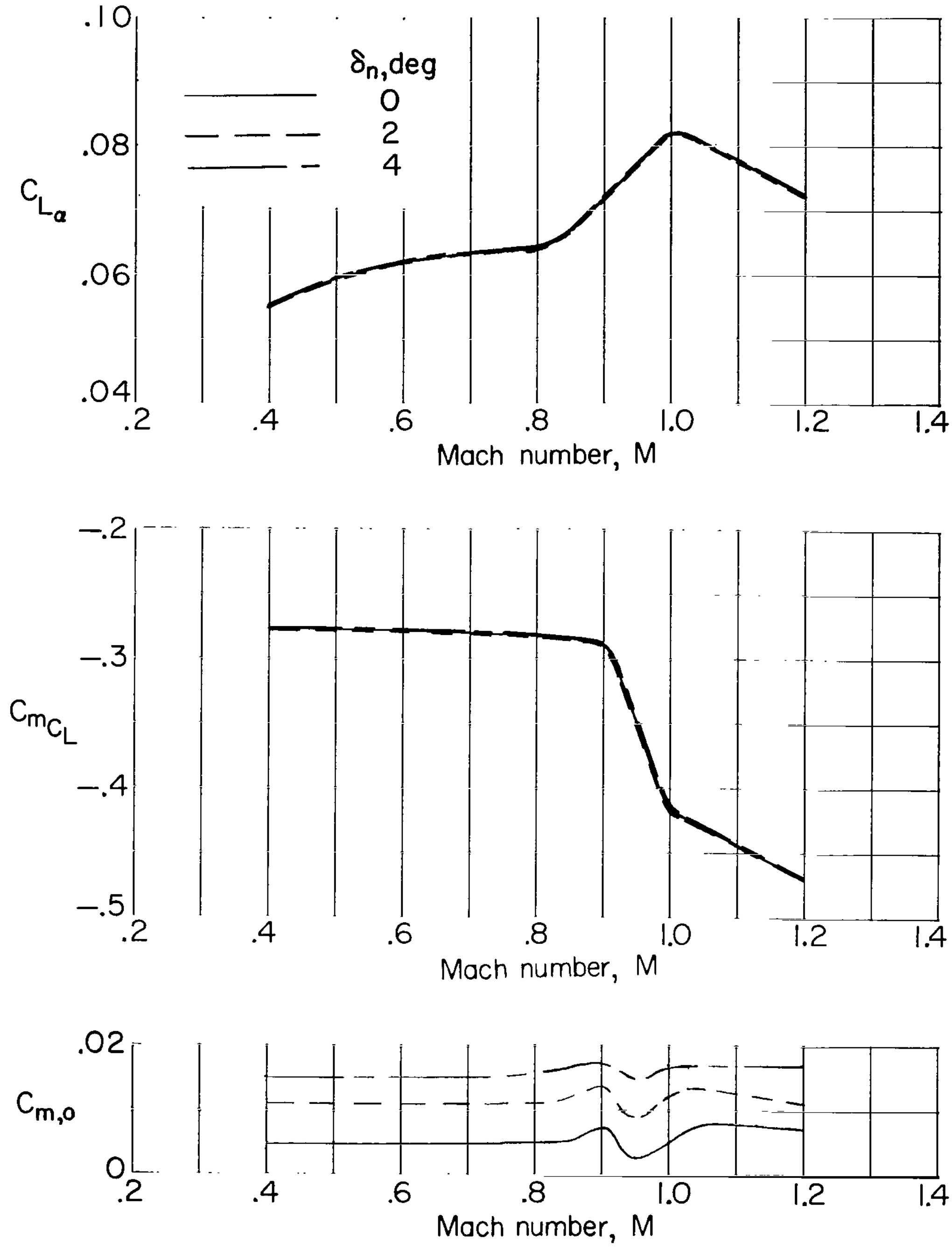

(a) C_{L_α}, $C_{m_{C_L}}$, and $C_{m,o}$.

Figure 15.- Variation of longitudinal aerodynamic characteristics with Mach number for various forebody deflections with canards off. High-wing $B_4W_3V_2$.

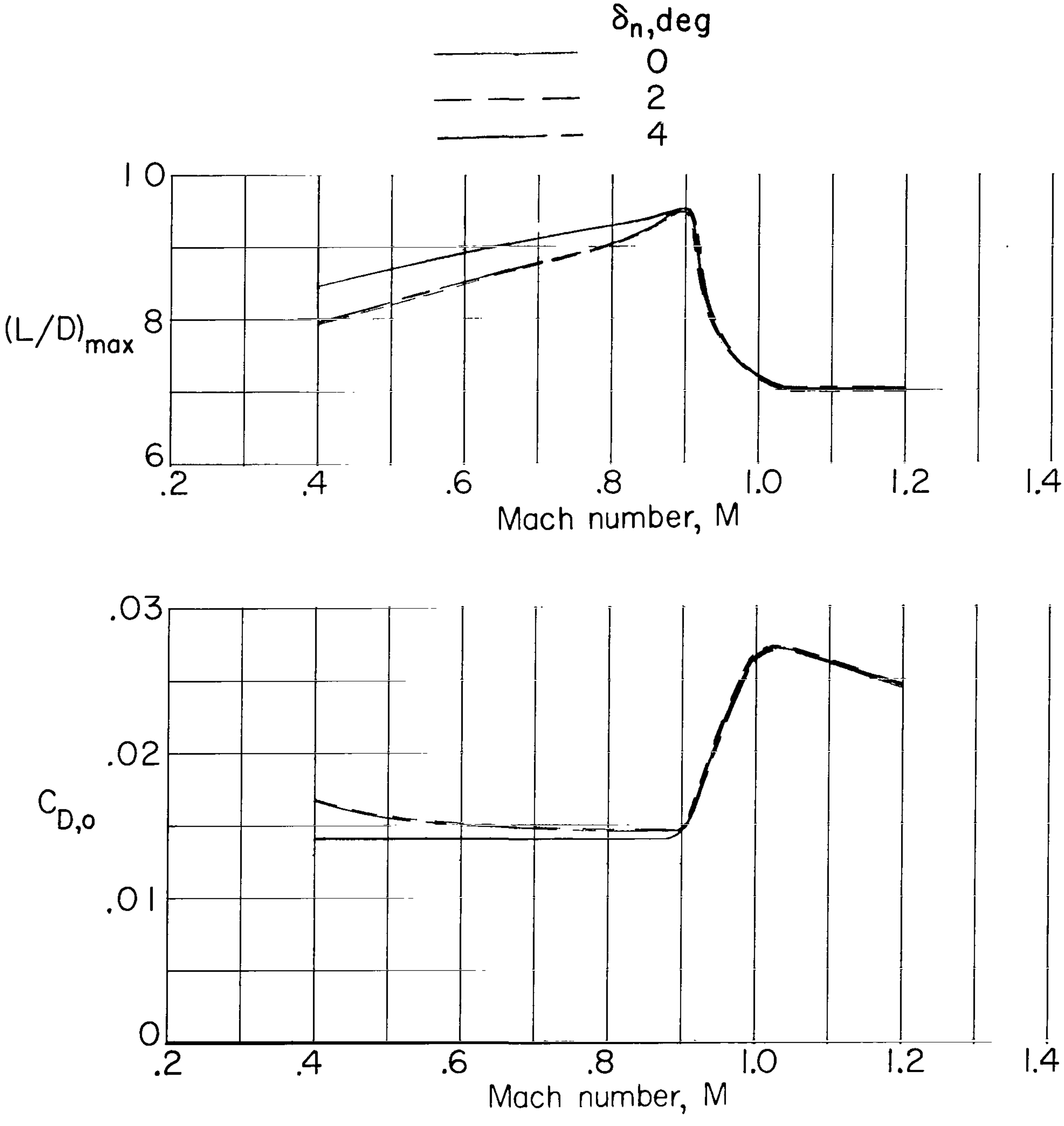

(b) $(L/D)_{max}$ and $C_{D,o}$.

Figure 15.- Concluded.

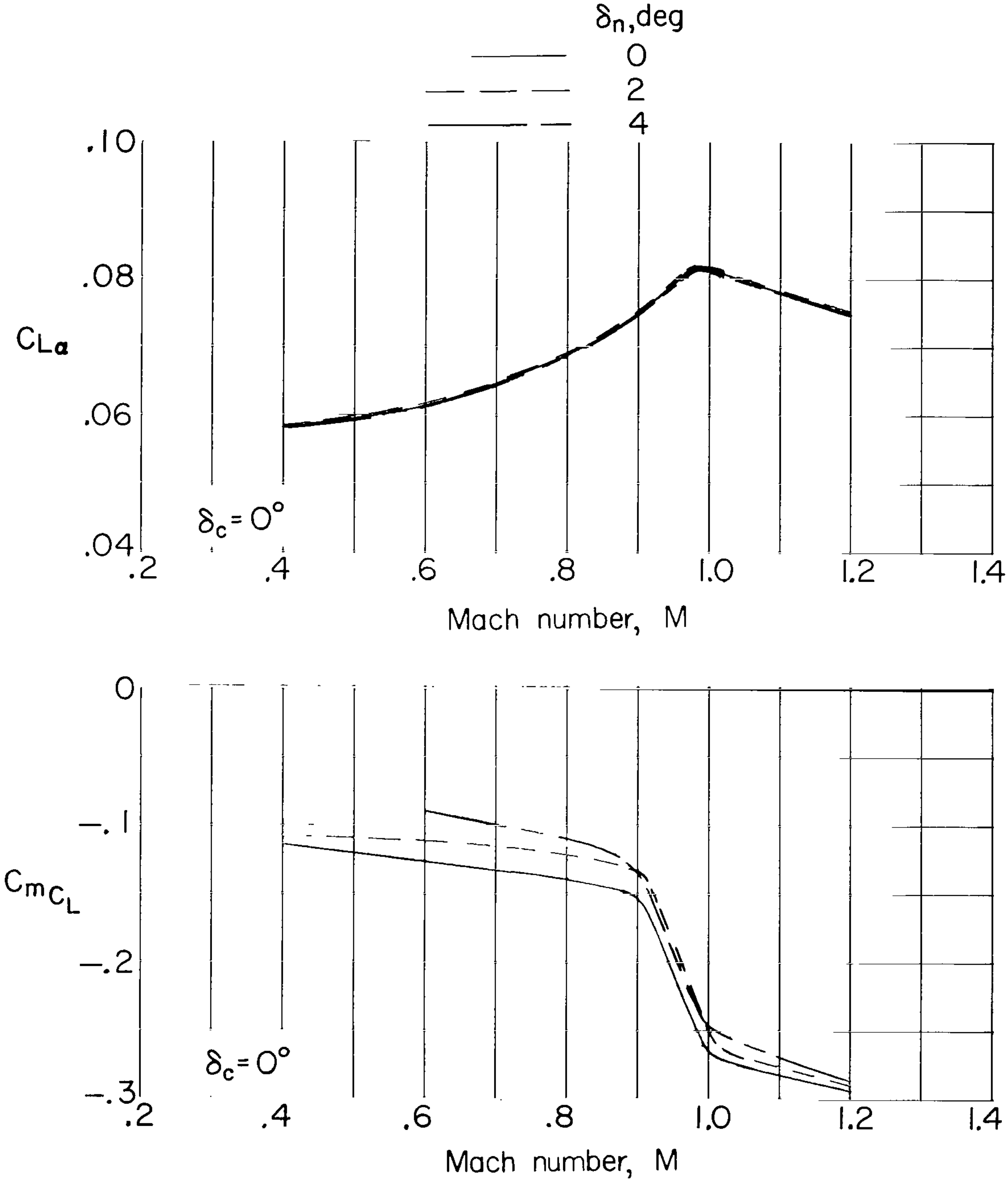

(a) C_{L_α} and $C_{m_{C_L}}$.

Figure 16.- Variation of longitudinal aerodynamic characteristics with Mach number for various forebody deflections with canards on. High-wing $B_4W_3C_2V_2$; $\Gamma_c = 0°$.

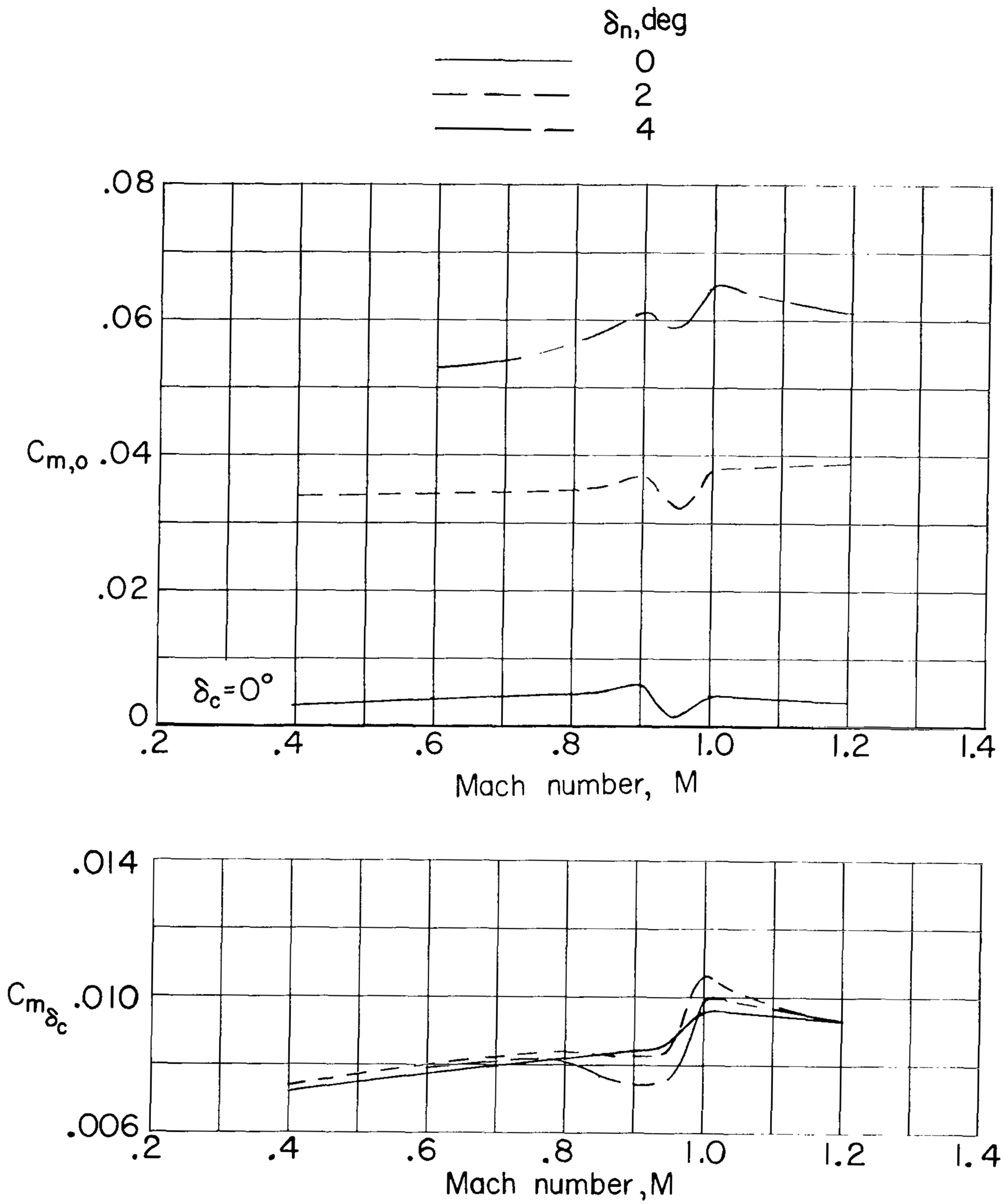

(b) $C_{m,o}$ and $C_{m_{\delta_c}}$.

Figure 16.- Continued.

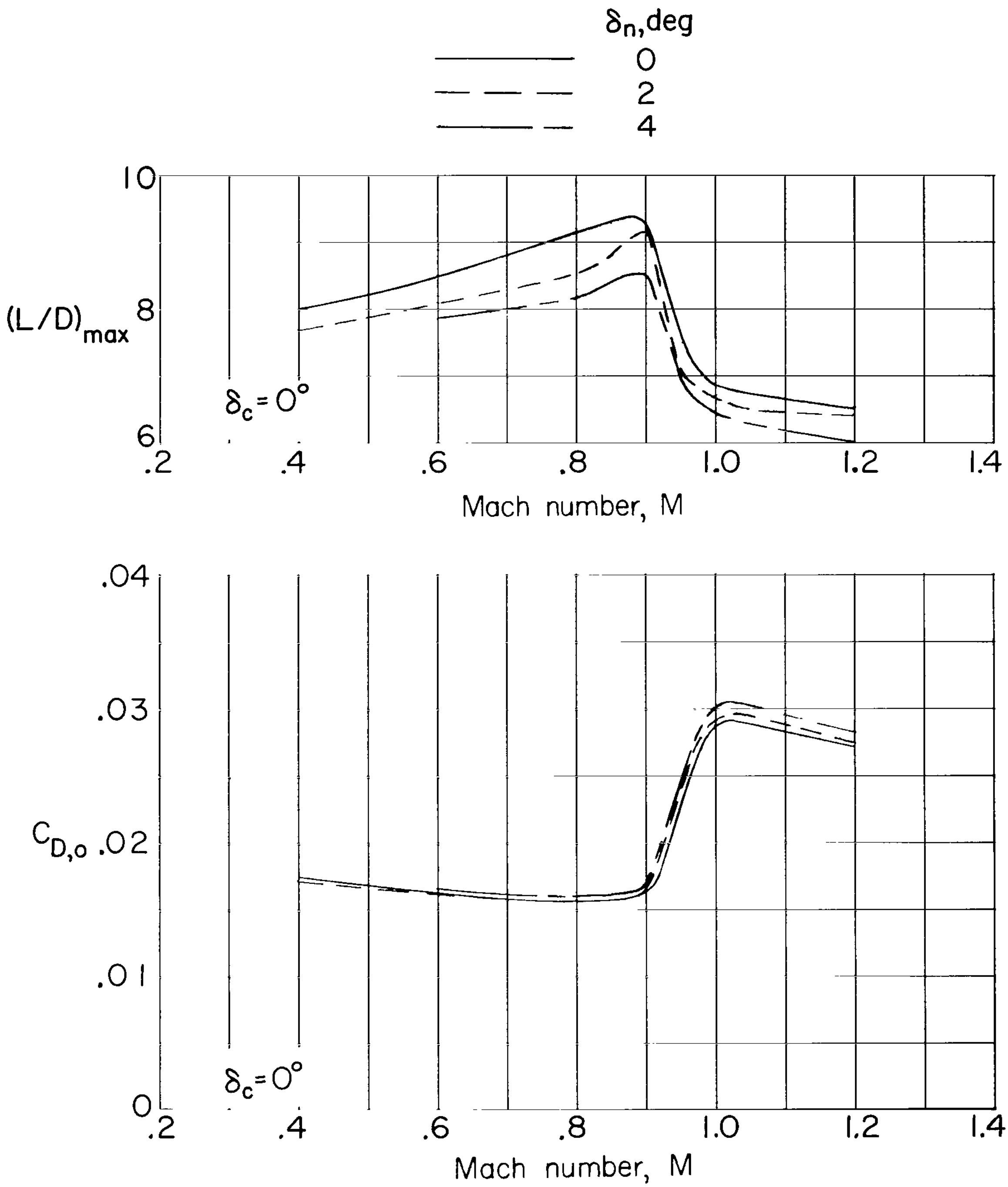

(c) $(L/D)_{max}$ and $C_{D,o}$.

Figure 16.- Concluded.

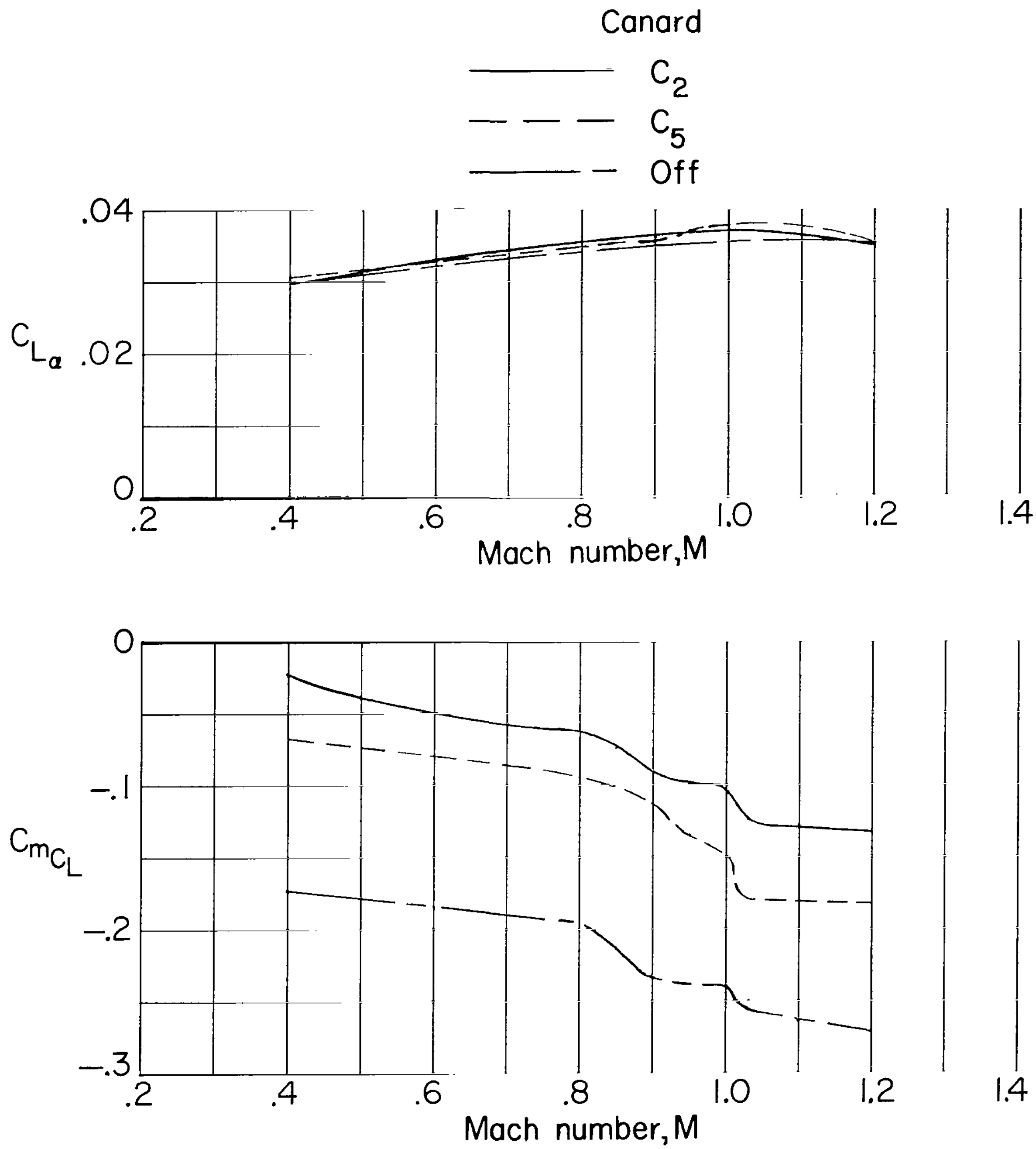

(a) C_{L_α} and $C_{m_{C_L}}$.

Figure 17.- Variation of longitudinal aerodynamic characteristics with Mach number for $B_4W_4V_2$ midwing configuration and for $B_4W_4V_2$ midwing configuration with delta and trapezoidal canards on. $\delta_c = 0^\circ$; $\delta_n = 0^\circ$; $\Gamma_c = 0^\circ$.

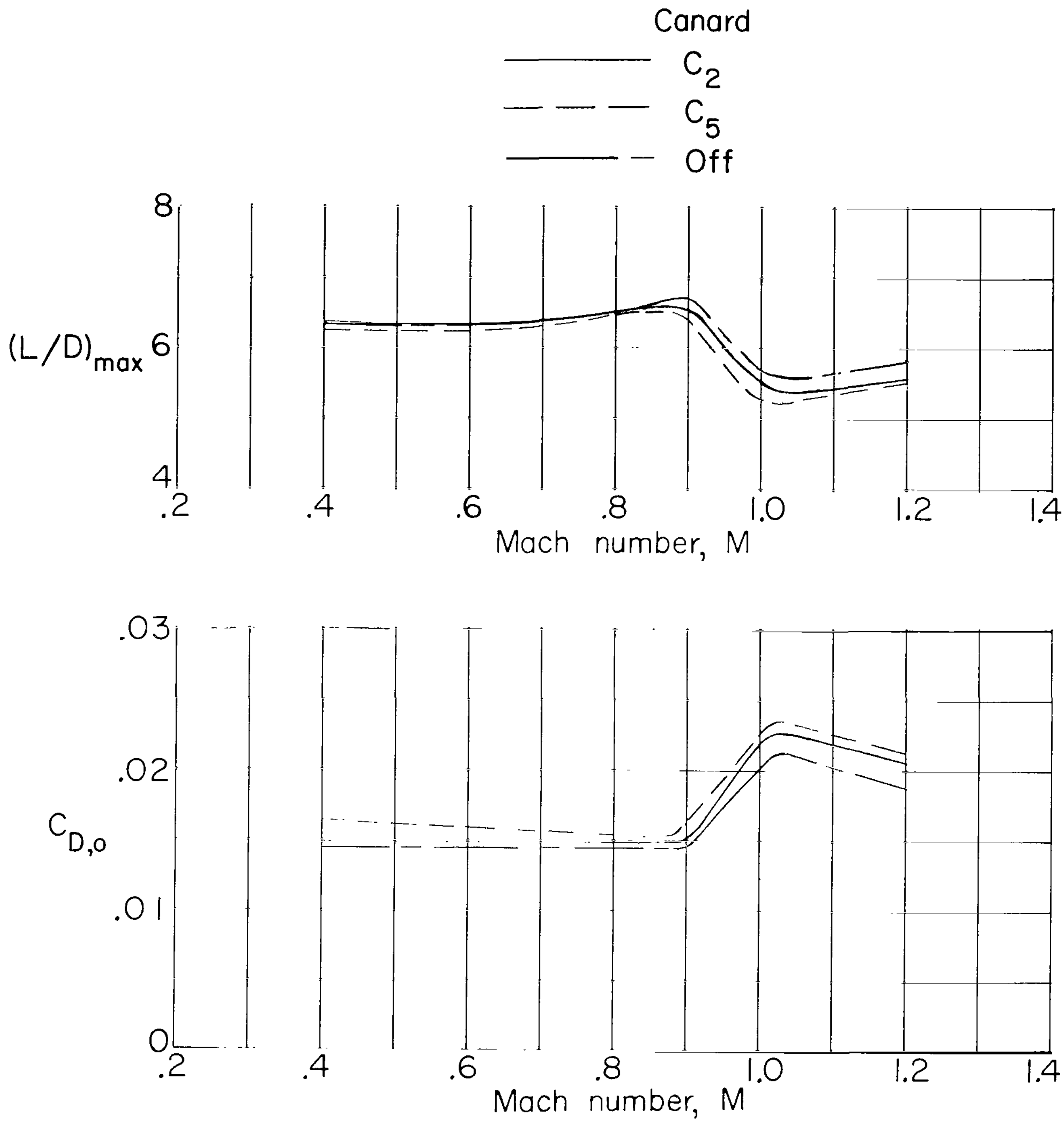

(b) $(L/D)_{max}$ and $C_{D,o}$.

Figure 17.- Concluded.

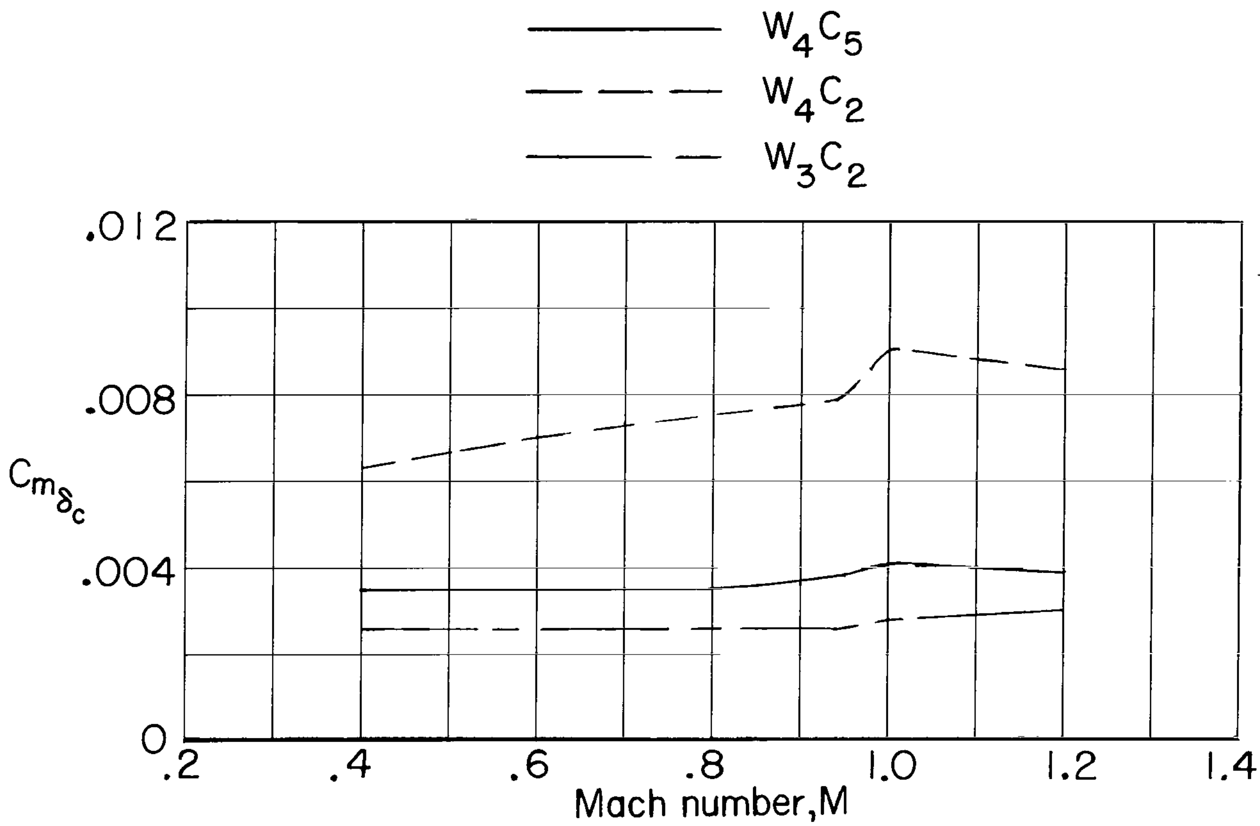

Figure 18.- Variation of canard pitching effectiveness parameter with Mach number for trapezoidal and delta midwing configurations. B_4V_2; $\delta_n = 0^{\circ}$; $\Gamma_c = 0^{\circ}$.

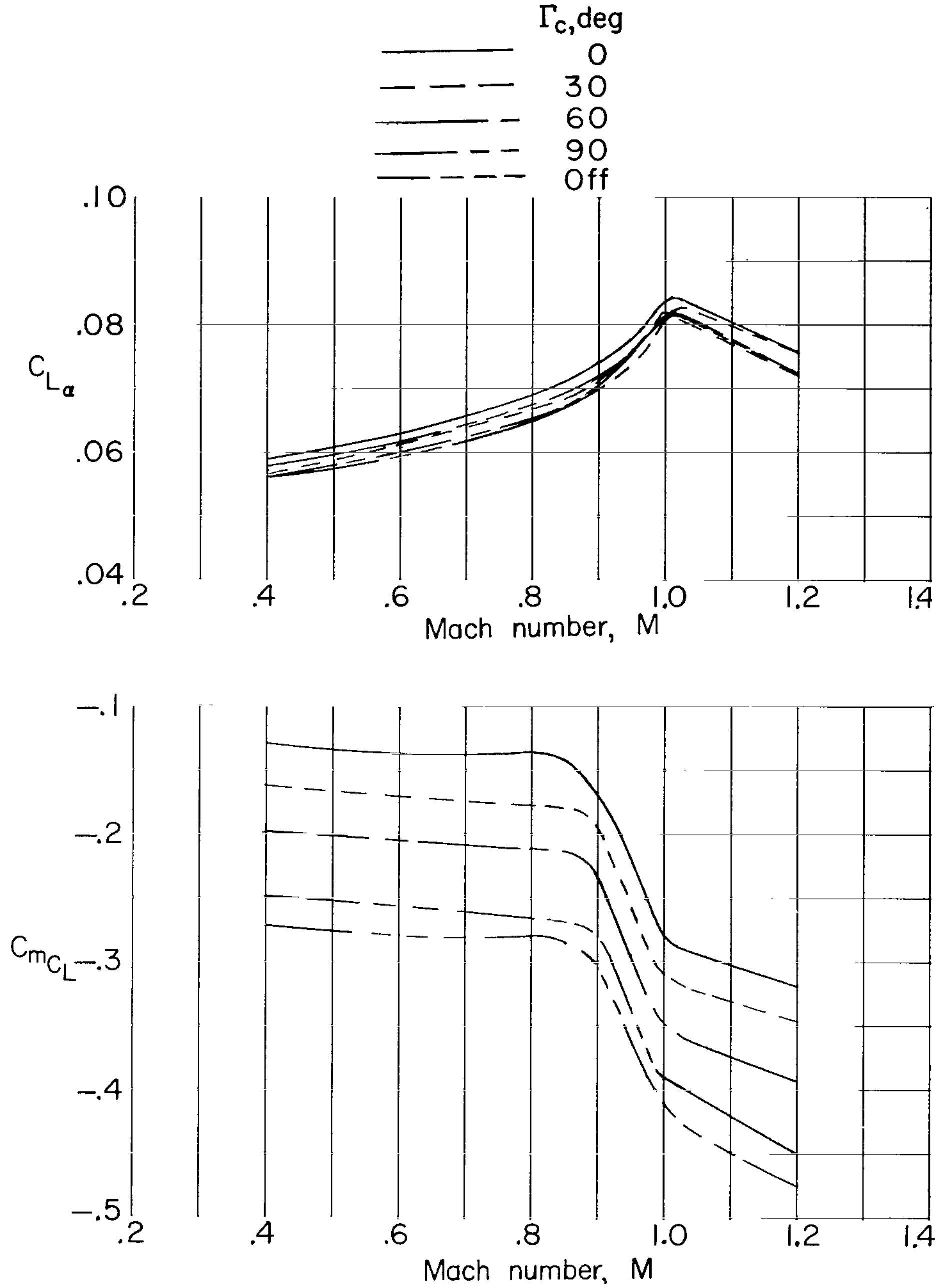

(a) C_{L_α} and $C_{m_{C_L}}$.

Figure 19.- Variation of longitudinal aerodynamic characteristics with Mach number for midwing $B_4W_3V_2$ configuration with canards off and with trapezoidal canards at various dihedral angles. $\delta_n = 0^\circ$; $\delta_c = 0^\circ$.

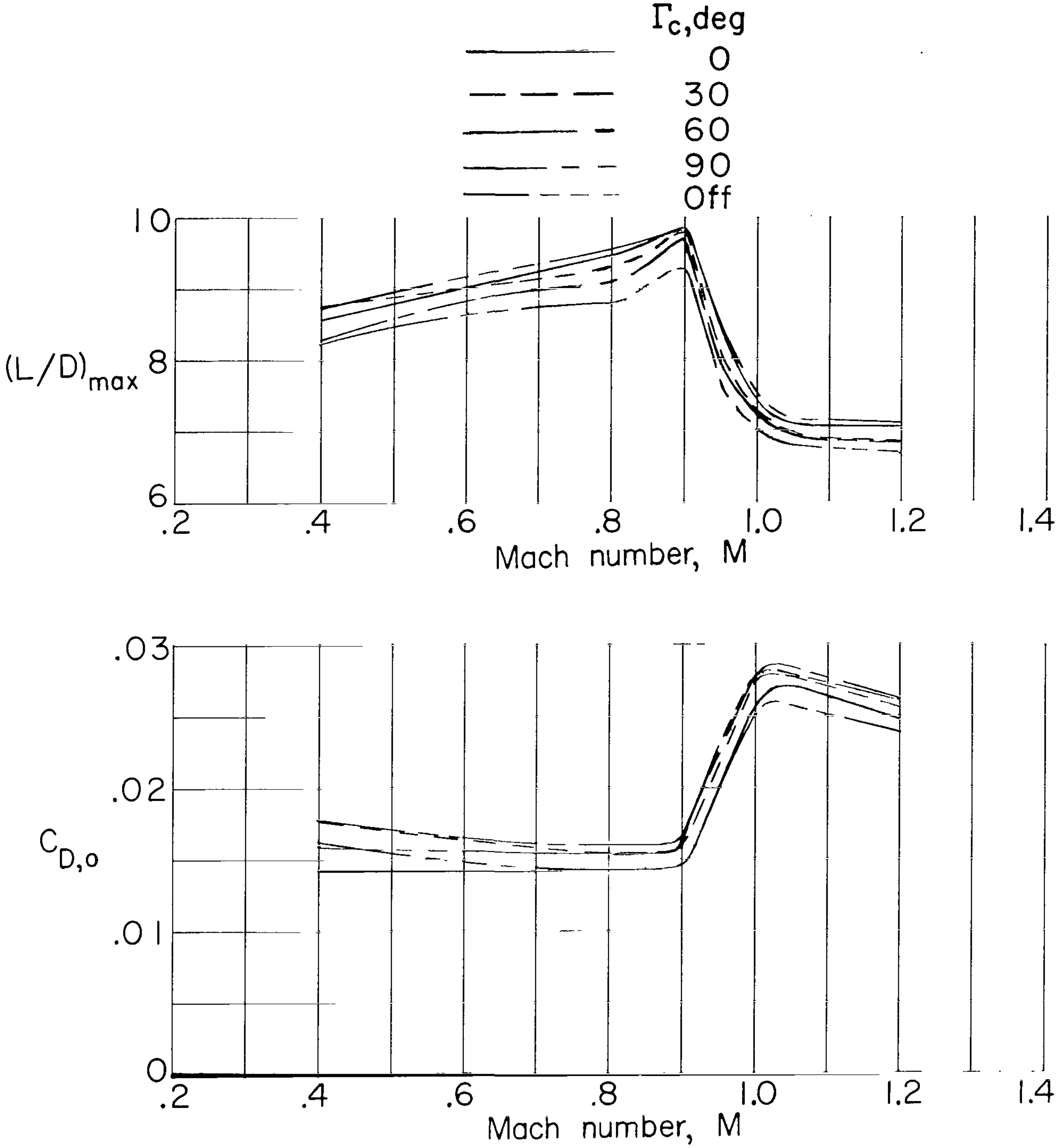

(b) $(L/D)_{max}$ and $C_{D,o}$.

Figure 19.- Concluded.

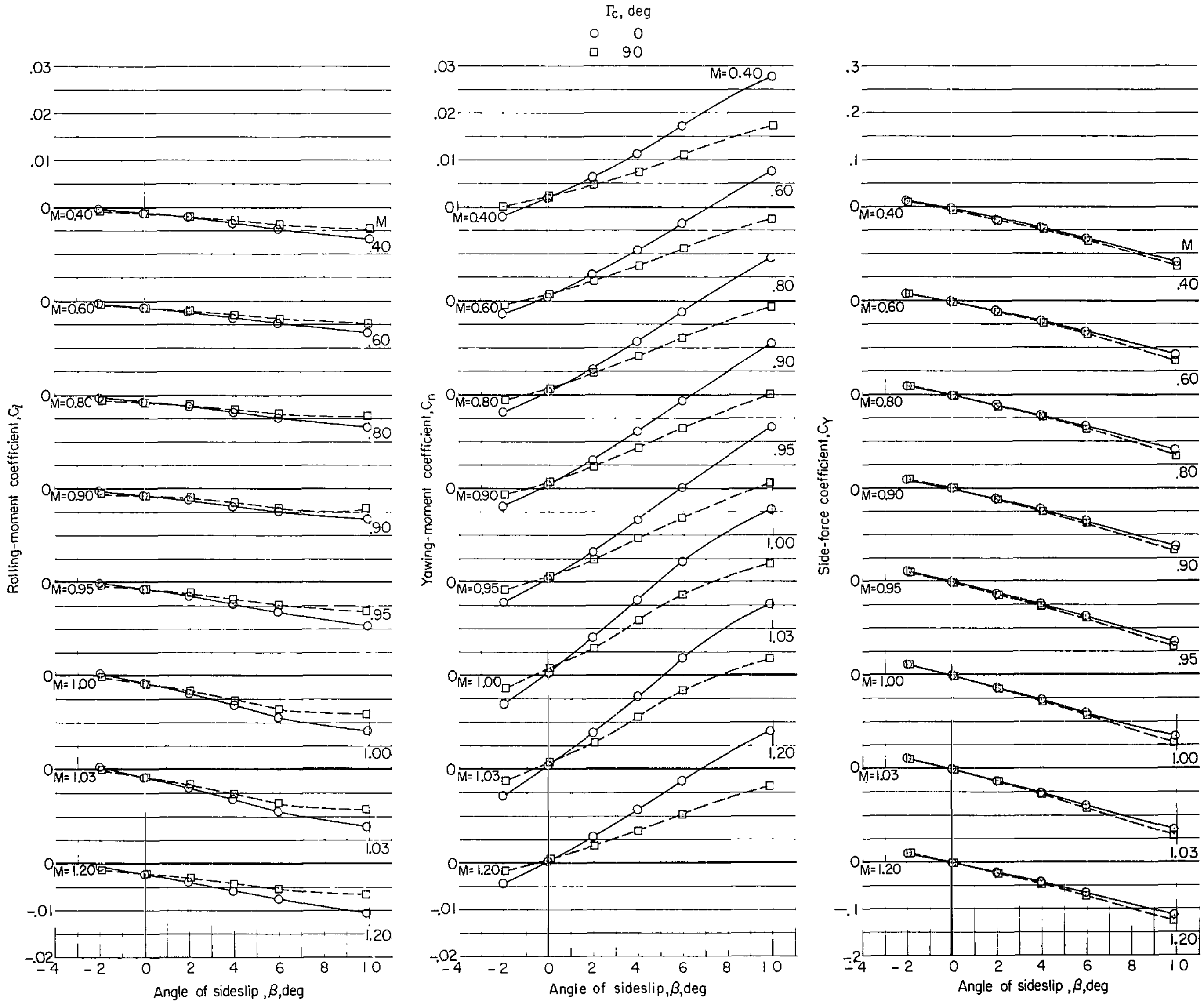

Figure 20.- Effect of canard dihedral on lateral aerodynamic characteristics of $B_4W_3C_2V_2$ midwing configuration. $\delta_n = 0^{\circ}$; $\delta_c = 0^{\circ}$; $\alpha = 0^{\circ}$.

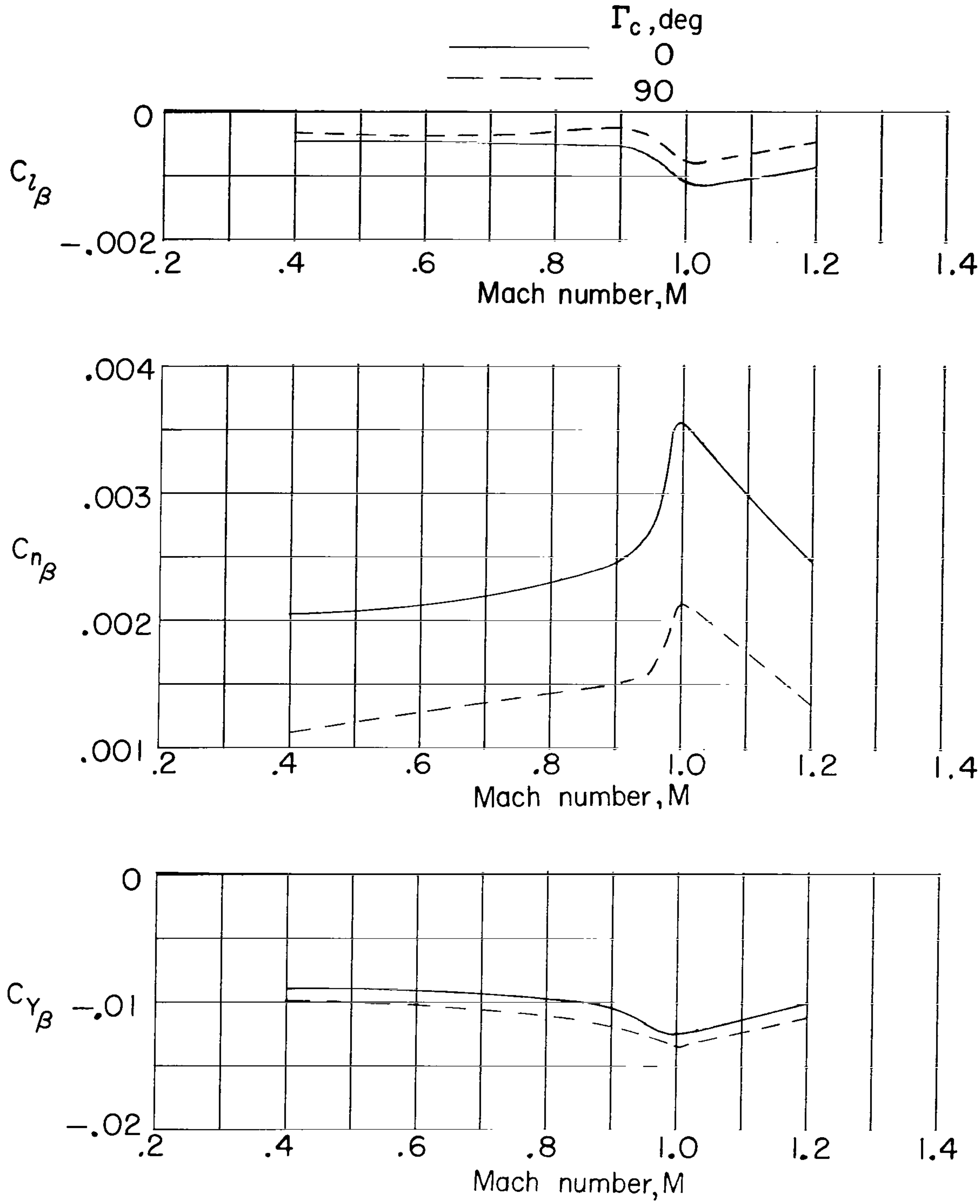

Figure 21.- Variation of lateral aerodynamic characteristics with Mach number for canard dihedral angles of 0° and 90°. Midwing $B_4W_3C_2V_2$; $\delta_n = 0^\circ$; $\delta_c = 0^\circ$; $\alpha = 0^\circ$.

NASA-Langley, 1964 L-3959